UNIVERSITY OF CALIFORNIA, MERCED

On The Size of Spherical Cows: How Body-Mass Influences the Existence and Coexistence of Mammalian Herbivores.

A dissertation submitted in partial fulfillment of the requirements
for the degree of Doctor of Philosophy
in

Quantitative and Systems Biology

by

Taran D. Rallings

Committee in charge:

Dr. Jessica Blois,Chair
Dr. Paul Smaldino
Dr. Jason Sexton
Dr. Justin Yeakel

2022

The dissertation of Taran D. Rallings, titled On The Size of Spherical Cows: How Body-Mass Influences the Existence and Coexistence of Mammalian Herbivores., is approved, and it is acceptable in quality and form for publication.

(Dr. Justin Yeakel) Principal Adviser	Date
(Dr. Jessica Blois) Committee Chair	Date
(Dr. Paul Smaldino) Committee Member	Date
(Dr. Jason Sexton) Committee Member	Date

University of California, Merced

2022

For Anna, whose love and support gave me the strength to get here.

And for Annette, my mother, for without her unyielding passion for education, none of this would have been possible.

Acknowledgments

Acknowledgements are a difficult thing for a project of this size. A finished dissertation rides on the back of a lifetime of support, opportunity, and struggle. It is in many ways harder to write a satisfactory acknowledgements section than it is to write the actual dissertation. I will abandon completeness and accept that, no matter how I write this, there will be important people and experiences that go unacknowledged.

An enormous thank you to Justin, whose mentorship and persistent tolerance for my ridiculousness is a big reason that I've actually made it through. There are a lot of environments in which I would not have flourished so successfully and I am grateful for the experience.

I am deeply indebted to Jessica, Paul, and Jay for being amazing committee members and mentors. Each of you has genuinely helped shape me as a scientist. Thank you, Jessica, for giving me so much guidance in grounding my work ecology and paleontology. Thank you, Paul, for the foundation and insights in how to think about models and the their place in science. And thank you, Jay, for always reminding me that I'm not an engineer, actually, and to keep my eye on the questions.

Thank you to the La Brea Food Webs team and project for insights, opportunities, and funding to work on such an exciting project. La Brea was my first exposure to Cenozoic paleontology as a child and it was a great pleasure to participate.

Lab members are incredible unsung heroes of the graduate experience. Irina, Ritu, and Megha all made big contributions to how I think about the work. More importantly, they helped keep me sane in otherwise trying times.

I must thank Philip Rallings, my father, for teaching me the that confidence emerges from competence, for sharing his passion for the natural world, and for instilling in me the vital link between motion and sanity.

Alan and Jean deserve a huge thank you for their incredible generosity. Letting me stay

with them on their beautiful farm at Tennersfield while I wrote this dissertation made an enormous difference. Their herd of longhorns, including Cannonball the bull, were a vital audience for my thoughts and practicing my defense.

I want to thank my students for giving me so many positive experiences, funny stories, and opportunities for growth. I never imagined I would enjoy teaching as much as I do.

Bill Mills, for encouraging me to undertake this absurd process and for convincing me that graduation is simply an issue of "holding the hot coal".

Purpose Secondary School, which took me in after I was expelled from two normal high schools, provided me the opportunity to pivot my life away from the early grave I was headed for. I am incredibly thankful for the patience and compassion they showed me. I don't think I would have ever graduated high school without them.

I have had a host of teachers over the years, many in non-academic areas, who have had a big impact on how I think about character, labour, and the world, all of whom deserve thanks. Mary O'Connor, for giving me my first taste of academic life and instilling in me a persistent interest in the role of metabolism in ecology. Tim Smith, for building my confidence to do hard things and showing me my fragility so that it could be overcome. Loki Jörgenson, for teaching me that the way out is through. Sally Otto for inspiring me to theory and modelling. Many others go unnamed.

I owe debts of gratitude to the struggles - to the pandemic, to living in a foreign country, to the ADHD, and to the basic grueling reality of getting through a PhD program. I have grown more through these battles than I could ever have hoped and I am now a more skilled wrestler of my own mind than I had dreamt was possible.

Taran D. Rallings

Education

University of California, Merced, Merced, California, USA

Ph.D. Quantitative and Systems Biology **Aug 2016 - Present**

- Dissertation Topic: "On The Size of Spherical Cows: How Body-Mass Influences the Existence and Coexistence of Mammalian Herbivores"
- Advisor: Dr. Justin D. Yeakel, Quantitative Ecological Dynamics Lab Academic Committee member:Dr. Jessica Blois, Dr. Paul Smaldino, Dr. Jason Sexton

University of British Columbia, Vancouver, British Columbia,, Canada

B.S. Integrated Sciences (Ecology and Mathematics) **Aug 2012 - Aug 2014**

Langara College, Vancouver, British Columbia,, Canada

Science Transfer - Biology and Mathematics **Aug 2010 - Jul 2012**

Jack Mountain Bushcraft, Ashland, Maine, USA

Spring Semester - field ecology and wilderness guiding **Apr 2009 - May 2009**

In Preparation

Dissertation Projects

Taran Rallings, Chris Kempes, Justin Yeakel. **On the Dynamics of Mortality and the Ephemeral Nature of Mammalian Megafauna**

Taran Rallings, Chris Kempes, Justin Yeakel. **Body Size and Competition Drive the Structure and Dynamics of Mammalian Herbivore Communities**

Taran Rallings, Chris Kempes, Justin Yeakel. **The Dynamics of Competition Constrain and Explain Macroevolutionary Trends Among Mammalian Communities Across the Cenozoic**

Awards

- Quantitative and Systems Biology *Remote Teaching and Research Fellowship* (2021)
- Quantitative and Systems Biology *Summer Research Fellowship* (2018)
- Quantitative and Systems Biology *Fee and Tuition Award* (2017)
- Quantitative and Systems Biology *Graduate Group Recruitment Fellowship* (2016)
- Xerox Canada *Arts and Sciences Scholarship* (2010)

Presentations

- Gordon Research Conference on Plant-Herbivore Interactions (Poster). 2019.
  Predicting the diets of herbivorous mammals from plant-herbivore trait interactions.
  T.D. Rallings, U. Bhat, J. Blois, J.D. Yeakel
- Society of Vertebrate Paleontology (Poster). 2017.
  Mapping mammalian morphological traits to diets with machine learning.
  T.D. Rallings, H. Duran, J.D. Yeakel

Research Experience

University of California, Merced, Merced, California, USA

Graduate Research Assistant - La Brea Food Webs **May 2018 - Dec 2019**
Dr. Justin D. Yeakel

University of British Columbia, Kelowna, British Columbia, Canada

Research Assistant - Complex Environmental Systems Lab **May 2014 - Aug 2014**
Dr. Lael Parrott

University of British Columbia, Vancouver, British Columbia, Canada

Research Assistant - Marine Ecology Research Group **May 2013 - Apr 2014**
Dr. Mary O'Connor

Teaching Experience

University of California, Merced, Merced, California, USA

Teaching Assistant - Natural Sciences

For each position I independently led weekly discussion sessions with a lecturing component, held office hours to assist students with work, and graded course work.

- Calculus II - Integral Calculus **Sum 2020 - Spr 2022**
- Calculus I - Differential Calculus **Fall 2016, Spr 2020**
- Natural History of Dinosaurs **Spr 2018**
- Statistics for Scientific Data Analysis **Fall 2017**
- Fundamentals of Ecology **Spr 2017**

University of California, Merced, Merced, California, USA

Guest Lectures - Natural Sciences

- Ecological Dynamics (graduate) - The mathematics of herbivory **Fall 2019**
- Paleoecology (mixed) - The science of rewilding **Spr 2019**
- Fundamentals of Ecology (undergraduate) - Predator-prey models **Spr 2018**

Jack Mountain Bushcraft, Ashland, Maine, USA

Teaching Assistant - Jack Mountain Bushcraft School **June, 2012**

- Assisted instruction in field ecology and bushcraft techniques

Complementary Education

National Science Foundation - Research Traineeship

Intelligent Adaptive Systems **Jan 2017 - Aug 2019**

Interdisciplinary Computational Graduate Education **Dec 2016 - April 2017**

Service

Data and Analytical Science at the University of California, Merced

Club President **Sept 2017- Aug 2018**

Abstract

The fundamental constraints governing the flow of energy through consumer-resource systems ultimately determines the structure and dynamics of food webs. As this is true generally, it is also true for plant-herbivore systems, where herbivores must compete with each other to obtain sufficient caloric return. Because diverse herbivore communities are composed of species spanning a large range in body sizes, the different life histories imposed by these body sizes, the different effects of mortalities upon them, and the different effects these species have on their resources interact in complex ways, perhaps playing a role in determining the conditions for coexistence. This dissertation describes a complex of ways in which herbivore body size governs the existence and coexistence of populations over three scales of inquiry: pair-wise consumer resource dynamics, adaptive food-webs, and food-webs in environmental and historical contexts.

Firstly, we construct a minimal consumer-resource dynamic system where the vital rates determining life history attributes are established on process-based energetic trade-offs. For this system, we derive the timescales associated with four alternative sources of mortality for terrestrial mammals: starvation from resource limitation, mortality associated with aging, consumption by specialist to generalist predators, and mortality introduced by subsidized harvest. The incorporation of these allometric relationships into the consumer-resource system illuminates central constraints that may contribute to the structure of mammalian communities. Our framework reveals that while starvation largely impacts smaller-bodied species, external predation and subsidized harvest primarily influence larger-bodied species. Finally, we predict the harvest pressure required to induce mass-specific extinctions as well as the predator-prey mass ratios at which dynamic instabilities form that may limit the feasibility of megaherbivore populations

Secondly, we expand the minimal consumer-resource model of Chapter 1 into an n-dimensional plant-herbivore food web model, and where foraging behaviors are adaptive.

In addition, we explore three alternative relationships between body-mass and diet-breadth: that of increasing breadth with mass, decreasing breadth with mass, and a non-linear relationship with high diet breadth for large and small herbivores. Our results demonstrate that our approach accurately captures macroecological patterns such as Damuth's Law. We observe that the negative mass-breadth relationship maximizes herbivore survival, while the competitive dynamics of plant-herbivore systems heavily favours larger consumers, with smaller consumers adaptively avoiding competitive overlap to enable persistence. Finally, communities with high levels of dietary overlap, where small consumers cannot escape predation, display consistently reduced richness.

Thirdly, we investigate mammalian herbivore body-mass distributions through the allometric, adaptive, plant-herbivore food-webs of Chapter 2 over two broad environmental axes: closed vs open environments and humid vs arid environments. The incorporation of diverse historical mass-distributions with environmental scenarios provides insight into the relationship between distribution structure and community stability. Our framework demonstrates that broad separation in body-mass increases community stability. It shows that large gaps in body-size can reverse the normally positive mass-fitness relationship. It shows that the distinction between humid and arid environments does not alter the patterns of herbivore competition that govern community stability. Finally, the distinction between closed and open environments can substantially alter competitive outcomes as closed environments can provide more opportunities for niche partitioning by smaller herbivores.

Contents

List of Tables

List of Figures

Chapter 1

Introduction

I began this PhD with a couple of concrete objectives. As a 'mature' student, I wanted to make sure I had the technical skills for gainful employment outside of the academy and I wanted to make some sort of contribution to using food-web modelling for paleoecology and conservation. I iterated through quite a number of different projects and plans for meeting those goals. The problem space I whittled myself down to was the mysteries of plant-herbivore interactions. The work presented here is an extension (or perhaps a kind of prequel) to my earlier attempts to unravel the the ways in which food-webs are constructed so that they can be anticipated.

There are two major reasons this issue of predicting food-webs is of interest. One motivation is primarily scientific, to be able to accurately reconstruct ecosystems from the past. Food-webs are not physical objects that are preserved in a fossil record. A food-web is an abstraction. It's a type of model we use to draw a border around the movement of energy through trophic interactions. To understand food-webs of the past we need mappings from observable things like fossils to the network of trophic interactions that we call a food-web. Part of this is accomplished through understanding how the physical traits of consumers interact with the traits of plants to create the landscapes of profitability that that lead to diets. These trait-to-diet mappings are also what we need for the second major motivation, predicting the rewiring of food-webs in the future. Responding to climate change and restoring ecosystems both require a strong predictive capacity. We need to know how existing ecosystems are likely to change with shifts in climate in order to accurately triage and manage them. Restoring ecosystems through reintroduction regimes, like rewilding, requires a similar capacity to predict the effects of species introductions. The necessity of

food-web prediction for both climate change adaptation and ecosystem restoration makes the issue a significant scientific bottleneck in our ability to meet the needs of the future.

The question I started with was "How do you predict the structure of food-webs from traits available in the fossil record?". It turned out that while we can do quite a bit of this for predator-prey interactions, herbivory is a high-dimensional problem [11] and there is too much undiscovered country to dive right in to the deep-end. In the details: mouths and dentition meet plant structure and defenses [12], physiology meets toxins [13], nutrients meet the complex bio-chemical reactors that are mammal guts [14], and so on. These are the entanglements on the banks of herbivory that make the modeler's spherical cows into something like actual cows. The details are scientifically interesting and vitally important to our ability to predict food-web structure in the ways that I had originally intended. Unfortunately, we do not understand enough of the basic dynamics of herbivore body-mass to do justice to the those weedy nuances. The question I arrived at is "How does body-mass influence the structure and dynamics of terrestrial mammalian herbivore communities?" and so, despite all of my efforts to the contrary, this is a dissertation about the size of spherical cows.

Herbivore body-mass is understood in the way a shaken puzzle box is understood. Empirical researchers have done some amazing work compiling quantitative relationships like metabolic rate [15], chewing rate [16], and fecal particle size [17] that all scale with mass. What has been lacking is a coherent assembly of these rates, with sufficient metabolic detail, into a consumer-resource system that could be built up to understand complex dynamics. The model from the Justin Yeakel's work on starvation dynamics [18] serves as the foundation for the work that I have done here because it is one of the few models that tackles herbivory at, what I believe to be, an appropriate resolution for building towards a predictive food-web ecology.

Resolution is a pernicious problem in scientific modelling. The journey from a good question to identifying the right scale of model for an answer can be a difficult one. The tendency in studies of herbivory is to either model at very fine scales, like partitioning sward-height [19] or guts-as-chemical-reactors [14], or to model at very broad scales, like lumping all plants into a single resource pool [20]. If the goal is to predict the structure of a future (or past) food-web, the fine-scale model cannot generalize far beyond its original use case and the broad-scale model lacks the detail to say much of anything about internal system dynamics. I think the greatest success of the work presented here is in striking a

balance that allows us to partition communities along the foundational trait (body-mass) but to do so in a way that generalizes, allows us to ask big questions, and is well suited for adding additional layers of hairy detail.

The three chapters of research that follow this introduction all deal with the same foundational model of how energy flows from a plant resource population into a mammalian herbivore population, as modulated by the body-mass of the herbivore species. The work picks up right where Justin Yeakel's starvation dynamics work [18] leaves off. We first collapse the 3D starvation system into a 2D consumer-resource system and then build from an exploration of the 2D system all the way up to the dynamics of plant-herbivore food-webs in specific historical contexts.

In chapter 2, we articulate the 2D consumer-resource system and ask, how do different assumptions about the nature of mortality interact with body-size to influence population density? We find important differences in which mortalities are major threats to small herbivores or large herbivores. Findings that highlight the importance of clarifying our assumptions about allometric scaling in mortality.

In chapter 3, we expand the 2D system into an n-dimensional plant-herbivore food-web and ask, how does body-size structure herbivore competition? This is accomplished by exploring the relationship between body-size, diet-breadth, and adaptive foraging behavior. We find a strong pattern of competitive superiority in large-bodied herbivores that highlights the necessity of dietary partitioning over body-size to achieve co-existence.

In chapter 4, we ask how does environmental context influence our expectations of the outcome of herbivore competition? We do this through the addition of historical body-mass distributions from throughout the Cenozoic as well as some simple assumptions about the how environmental context structures the plant community. We find that the details of a body-mass distribution can alter, or even reverse, normal relationships between mass and persistence as well as finding major impacts from the evolution and expansion of open environments through the Cenozoic.

This is a detailed study of how the first layer of biological realism forms the foundation for plant-herbivore interactions and governs the survival of mammalian herbivores more broadly. As a whole, it is the work I wish I had access to when I started in 2016. The model is a scaffolding for all of that wonderful detail we need to define realistic communities and I have at least another six years worth of questions I could ask about it. I hope you find it, and our results, half as intriguing as I do.

Chapter 2

On the Dynamics of Mortality and the Ephemeral Nature of Mammalian Megafauna

2.1 Abstract

The vital rates constraining energy flow through consumer-resource interactions largely vary as a function of body size. These allometric relationships govern the dynamics of populations, and the energetic constraints induced by different sources of mortality influence small- to large-bodied species in different ways. Here we derive the timescales associated with four alternative sources of mortality for terrestrial mammals: starvation from resource limitation, mortality associated with aging, consumption by specialist to generalist predators, and mortality introduced by subsidized harvest. The incorporation of these allometric relationships into a minimal consumer-resource dynamic system illuminates central constraints that may contribute to the structure of mammalian communities. Our framework reveals that while starvation largely impacts smaller-bodied species, the allometry of senescence is expected to be more difficult to observe. In contrast, external predation and subsidized harvest primarily influence larger-bodied species. The inclusion of predation mortality reveals mass thresholds of mammalian herbivores at which dynamic instabilities limit the feasibility of megaherbivore populations. Moreover, we show how these thresholds vary with predator-prey mass ratios, a relationship that is little understood within terrestrial systems. Finally,

we predict the harvest pressure required to induce mass-specific extinction, and compare these values to estimates from episodes of both paleontological and historical megafaunal exploitation.

2.2 Introduction

Consumer-resource interactions are the fundamental unit from which complex food webs arise [21]. In such dynamics the rates governing transitions of biomass and energy from one species to another are largely determined by body sizes [22]. Specifically, the allometric relationships between consumer body mass and metabolic rate constrain energetic assimilation [23], storage [24], and growth [25], all of which govern the dynamics of populations [18, 26–28]. Because allometrically-constrained models of population dynamics apply generally across large taxonomic clades, they are useful for examining dynamic constraints that may contribute to community structure across macroevolutionary timescales [18, 29]. Furthermore, examination of community dynamics at these scales enables the investigation of extinct communities where body size distributions were different than those in contemporary ecosystems [4, 30, 31].

The dynamics of populations represent an energetic balance between reproduction and mortality [32]. While reproduction is typically predictable from allometric scaling relationships [33], mortality has a variety of forms that do not all scale similarly. Mortality originates from both internal and external drivers, where the former depends on an organism's internal state to initiate death. For example, senescence and starvation involve physiological states that change with respect to clock time, metabolic rate, and resource depletion [18, 34]. In contrast, external drivers of mortality consist of an outside force that induces death more independently of an organism's internal state, such as mortality due to natural predation or subsidized anthropogenic harvest. Often mortality occurs through correlations between internal and external drivers, where for example, the starvation state of prey may alter the success rates of predators [35]. While virtually all primary consumer populations must deal with the effects of resource limitation, aging, and predation, the effects of harvesting are uniquely limited to those species serving as resources for human populations [36].

How do different sources of mortality impact the dynamics of mammalian populations? Here we construct a general consumer-resource framework to examine mammalian herbivore populations as a function of consumer body size M_C, as well as size-dependent vulnerability

to different internal and external pressures. Our approach integrates relationships governing specific physiology and assimilation timescales from a process-based energetic perspective [25]. Our model is low-dimensional and compact, [18] but due to it's close connection to fundamental energetic mechanism it is also capable of reproducing observed large-scale empirical patterns of mammalian communities. We begin by describing our approach, reproducing key macroecological relationships such as Damuth's law [1], and then examining how changes to energetic parameters impact these predictions. We then derive timescales associated with four sources of mortality experienced by mammalian consumers: *i*) natural mortality, *ii*) starvation mortality, *iii*) natural predation, and *iv*) subsidized anthropogenic harvesting. By examining each source of mortality in turn, our framework illuminates central constraints governing mass-specific behaviors, strategies, and risks experienced by mammalian consumers.

Our results reveal four key insights into the constraints structuring mammalian communities. First, our allometric consumer-resource system accurately captures both the central tendency and variability of Damuth's law, suggesting that the included vital rates accurately capture mass-specific dynamics. Second, our results demonstrate that natural and starvation mortality deferentially impact small mammals, confirming expectations, and point to why the allometric effects of senescence are difficult to observe in nature. Third, we detail the differences in how mortality from specialist or generalist predators induce population instabilities for large-bodied herbivores. We also show that the body size at which these instabilities occur is dependent on the prevailing predator-prey mass ratios (PPMRs). Finally, we evaluate the harvest pressure required to induce mass-specific extinction, and show that our predictions are comparable to estimates of both paleontological and historical exploitation of mammalian megafauna.

2.3 Allometric Consumer-Resource Model

We model a consumer-resource interaction, where the resource R (g/m^2) grows logistically with intrinsic growth rate α to a carrying capacity k, and declines due to consumption by an herbivore consumer population C (g/m^2) (Eq. 2.3). Consumed resources govern both consumer somatic maintenance and reproduction. The rate of consumption to fuel somatic maintenance is given by ρ, and is independent of resource density, as these are invariant requirements of the consumer population [18]. In contrast, the rate of consumption to fuel

reproduction is proportional to resource density and is given by $\lambda_C(R)/Y_C$, where $\lambda_{\mathrm{C}}(R)$ is the consumer growth rate and Y_{C} is the consumer yield coefficient, or the grams of consumer produced per gram of resource consumed. As in DeLong & Vasseur [37], the consumer's growth rate $\lambda_C(R)$ follows Michaelis-Menton (Type II) kinetics as a function of the resource density R, where the maximum growth is $\lambda_{\mathrm{C}}^{\max}$ and the resource half-saturation density is $\hat{k} = k/2$, such that

$$\lambda_{\mathrm{C}}(R) = \lambda_{\mathrm{C}}^{\max}\left(\frac{R}{\hat{k}+R}\right). \tag{2.1}$$

While the consumer population density grows at rate $\lambda_{\mathrm{C}}(R)$, we assume for now that consumer mortality is a function of both natural mortality μ and starvation $\sigma(R)$, where the rate of starvation

$$\sigma(R) = \sigma^{\max}\left(1-\frac{R}{k}\right) \tag{2.2}$$

increases as resources become scarce. In this context, $\sigma^{\max}$ is the maximal rate of starvation that occurs when the environment is devoid of resources. The full system describing resource and consumer dynamics is given by

$$\begin{aligned}\frac{\mathrm{d}}{\mathrm{dt}}C &= \lambda_{\mathrm{C}}(R)C - (\mu+\sigma(R)+...)\,C,\\ \frac{\mathrm{d}}{\mathrm{dt}}R &= \alpha R\left(1-\frac{R}{k}\right) - \left(\frac{\lambda_{\mathrm{C}}(R)}{Y_{\mathrm{C}}}+\rho\right)C,\end{aligned} \tag{2.3}$$

where the '...' denotes where additional mortality terms, described later, will be included. The dynamic outcomes of this system of equations include two trivial steady states at $(R^* = 0, C^* = 0)$ and $(R^* = k, C^* = 0)$, and one internal steady state where both the consumer and resource population coexist. Because the internal steady state cannot be concisely written, we do not report it here. See Table 2.1 for a description of parameters.

The rate laws describing resource consumption as well as consumer growth and mortality all vary as a function of consumer body mass M_C, where the consumer is assumed to be a mammalian herbivore, and the resource is an unspecified primary producer with characteristic growth rate α, carrying capacity k, and energy density E_d. We approach the derivation of vital rates with respect to consumer mass by solving for multiple timescales associated with ontogenetic growth, maintenance, and expenditure. The growth of an individual consumer from birth mass $m = m_0$ to its reproductive size $m = 0.95M_C$ is given by the solution to the general balance condition $B_0 m^{\eta} = E_m\dot{m} + B_m m$, where E_m is the energy

needed to synthesize a unit of biomass, B_m is the metabolic rate to support an existing unit of biomass, and the metabolic exponent $\eta = 3/4$ [25]. From this balance condition, the time required for an organism starting from mass m_1 to reach mass m_2 follows

$$\tau(m_1, m_2) = \ln\left(\frac{1-(m_1/M_C)^{1-\eta}}{1-(m_2/M_C)^{1-\eta}}\right)\frac{M_C^{1-\eta}}{a(1-\eta)} \tag{2.4}$$

where $a = B_0/E_m$. From this general equation, we calculate the timescale of reproduction for an herbivore consumer of mass M_C as $t_\lambda = \tau(m_0, 0.95M_C)$, such that the reproductive rate is $\lambda_C^{\max} = \ln(\nu)/t_\lambda$, where $\nu = 2$ is the set number of offspring per reproductive cycle [18, 38]. The consumer yield coefficient is given by $Y_C = M_C E_d/B_\lambda$ (g consumer per g resource), where B_λ is the lifetime energy use required to reach maturity $B_\lambda = \int_0^{t_\lambda} B_0 m(t)^\eta \mathrm{d}t$, and the maintenance rate is given by $\rho = B_0 M_C^\eta / M_C E_d$ [18].

To determine the rate of mortality from starvation, we calculate the time required for an organism to metabolize its endogenous energetic stores, estimated from its cumulative fat and muscle mass, where the remaining mass is given by $M_C^{\text{starve}} = M_C - (M_C^{\text{fat}} + M_C^{\text{musc}})$ (see Table 2.1). During starvation, we assume that an organism burns its existing endogenous stores as its sole energy source, where the balance condition is altered to $\dot{m}E'_m = -B_m m$, where E'_m is the amount of energy stored in a unit of biomass (differing from the amount of energy used to synthesize a unit of biomass E_m). The starvation timescale is then given by

$$t_{\sigma^{\max}} = -\frac{M_C^{1-\eta}}{a'}\ln(M_C^{\text{starve}}/M_C), \tag{2.5}$$

where $a' = B_0/E'_m$, such that the starvation rate is the $\sigma^{\max} = 1/t_{\sigma^{\max}}$.

To determine the rate of mortality from aging, we note that population cohorts experience two primary sources of natural mortality: the initial cohort mortality rate q_0 and the annual rate of increase in mortality as the cohort ages, or the actuarial aging rate, q_a over lifetime t_ℓ. We begin by assuming that the number of survivors over time follows a Gompertz relationship [18, 33] from which we can derive the average rate of natural mortality

$$\mu = \frac{q_0}{q_a t_\ell}\big(\exp(q_a t_\ell) - 1\big). \tag{2.6}$$

The three parameters (q_0, q_a, t_ℓ) each have well-documented allometric relationships for terrestrial mammals, such that natural mortality can be written as a function of consumer mass $\mu(M_C)$ (see Supplementary Materials Appendix I).

We emphasize that while the sizes of physiological biomass compartments are obtained from empirically-measured relationships, the rates determining biomass flux are derived from process-based energetic relationships. Together, the allometric rate laws and the dynamic system presented in Eq. 2.3 allow us to assess the dynamics of consumer-resource systems for mammalian herbivores spanning the observed range of terrestrial body sizes, from the smallest (the Etruscan shrew at roughly 1 g) to the largest (the Oligocene paraceratheres and Miocene deinotheres at ca. $1.5 - 1.74 \times 10^7$ g) [39]. We next examine how this minimal framework is well-suited to provide general insight into several key allometric constraints that contribute to the functioning and limitations of terrestrial mammalian communities.

Table 2.1: Model parameters and values/units

Definition	Parameter	Value/Units
Resource		
density	R	g/m^2
reproduction rate	α	1/s
carrying capacity	k	g/m^2
Consumer		
density	C	g/m^2
body mass	M_C	g
body mass theshold	$M_C^\dagger$	g
theoretical max	$C^{\max}$	g/m^2
timescale of growth from m_1 to m_2	$\tau(m_1, m_2)$	s
reproduction rate	$\lambda_C^{\max}$	1/s
yield coefficient	Y_C	(g/m^2 C)/(g/m^2 R)
maintenance rate	ρ	1/s
natural mortality rate	μ	1/s
starvation rate	σ	1/s
harvest rate	h	1/s
Predator		
steady state intercept	P_0	8.62×10^{-4} inds/m^2 [40]
steady state density	P^*	$P_0 M_P^{-0.88}$ inds/m^2 [40]
body mass	M_P	g
body mass theshold	$M_P^\dagger$	g
theoretical max	$P^{\max}$	g/m^2
growth rate	$\lambda_P^{\max}$	1/s
yield coefficient	Y_P	(g/m^2 P)/(g/m^2 C)
specialization	f	(0,1)
Prop. change starvation rate	χ_s	(-0.99,1)
PPMR intercept	v_0	1.18×10^5 g
PPMR slope	v_1	0.19
Prop. change PPMR intercept	χ_{int}	(-0.99,2)
Prop. change PPMR slope	χ_{slope}	(-0.99,2)
Extinction-inducing harvest rate	$h^\dagger$	1/s
Extinction-inducing harvest pressure	$\psi^\dagger$	inds/yr/A_{CA}
Post-harvest fraction consumer density	ϵ	0.01

2.4 Results and Discussion

2.4.1 Recovering Damuth's mass-density relationship

Our consumer-resource system is related to the nutritional state model (NSM) proposed in Yeakel et al. [18], where an explicit starvation dynamic was incorporated by separating the consumer population density into 'full' and 'hungry' states. Here we eliminate the transition between full and hungry states. Because the timescales of transitioning between full and hungry states are short relative to those of reproduction, we have only sacrificed a modest degree of physiological realism to enable analytical expression of steady states with additional sources of mortality. After substituting allometric relationships into the rate laws in Eq. 4.3, we observe that the internal steady state of the consumer is very close to observations of mammalian densities in natural systems, thereby approximating Damuth's Law (blue line in Fig. 2.1). Compared to the NSM [18], and similar to DeLong & Vasseur [41], we observe slightly exaggerated densities for small-bodied consumers, though within the observed range of variation. This overestimate is not observed when explicit starvation and recovery are included [18], suggesting these dynamics play an important role in depressing the populations of smaller-bodied species. The allometric consumer-resource model provides an approximation to the mass-density relationship observed among terrestrial herbivorous mammals [1]. Incorporating observed variations in measured values for α and k reveals strong alignment between model predictions and the observed variability of densities across mammalian clades (Fig. 2.1). We examine the effects of variation for other vital rates in Supplementary Materials Appendix II.

2.4.2 Natural mortality and starvation have an out-sized impact on smaller consumers

We first consider two internal sources of mortality: that due to the effects of aging, where mortality changes with an organism's temporal state, and that due to starvation, where mortality scales with an organism's energetic state. An immediate insight into this system's constraints can be gained by examining how the rates of consumer mortality compare to reproduction, with the expectation that stability requires mortality rates to be lower than reproductive rates (Fig. 2.2A). We observe that natural mortality, which accounts for both initial cohort mortality and actuarial mortality, is much lower and projects a steeper slope over M_C than the maximal reproductive rate (Fig. 2.2B), with a scaling $\propto M_C^{-0.56}$

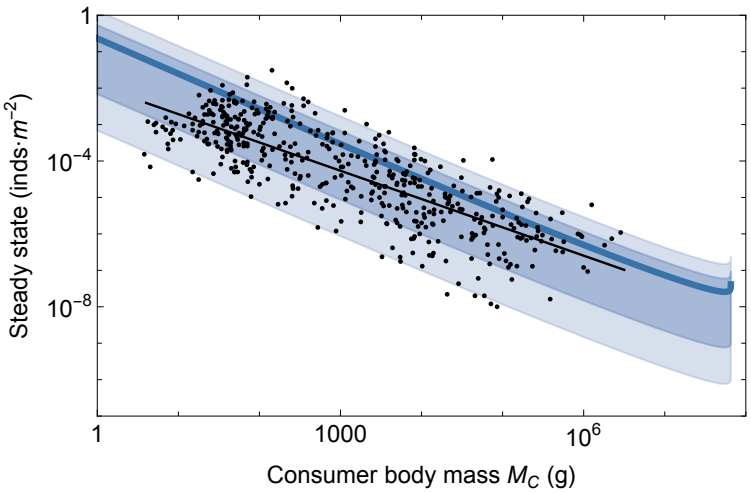

Figure 2.1: Model predictions of mammalian steady states (inds $\cdot$ m^{-2}) as a function of herbivore consumer body mass M_C (thick blue line) compared to observational data from Damuth [1] (black points). Variation in steady state densities is captured by allowing the plant resource growth rate to vary as $\alpha = 2.81 \times 10^{-10} : 2.19 \times 10^{-8}$ s^{-1} (dark blue shaded region), and both α and the plant resource carrying capacity to vary as $k = 2.3 : 34$ kg/m^2 (light blue shaded region). See Supplementary Materials Appendix II for details.

[42]. While the calculated value of μ is nearly one order of magnitude below the rate of reproduction $\lambda_C^{\max}$, a steeper slope implies that increases in μ will disproportionately harm smaller organisms.

To understand the effect of changes to $\mu(M_C)$ on consumer steady states, we examine variations in the principle components of μ: initial cohort mortality q_0 and actuarial mortality q_a. The initial cohort mortality represents the mortality experienced by a cohort prior to accruing effects from age. We observe that the mortality rate changes proportionally with q_0 independent of consumer mass, where the ratio $\mu/\lambda_C^{\max} < 1$ even with respect to large increases in q_0 unless q_a is similarly magnified (Fig. 2.2A,B). For survivorship mortality to approach the rate of reproduction ($\mu/\lambda_C^{\max} = 1$), where perceptible declines in population densities result, the initial cohort mortality must increase by roughly an order of magnitude (shaded region in Fig. 2.2C). Due to the steepness of the scaling of μ relative to $\lambda_C^{\max}$, this effect is felt exclusively by small-bodied organisms.

Actuarial mortality, q_a, represents the cumulative effects of aging, or senescence, across the organism's expected lifetime. We observe that as q_a increases, the magnitude of mortality increases disproportionately (Fig. 2.2B), while the slope of $\mu(M_C)$ becomes more

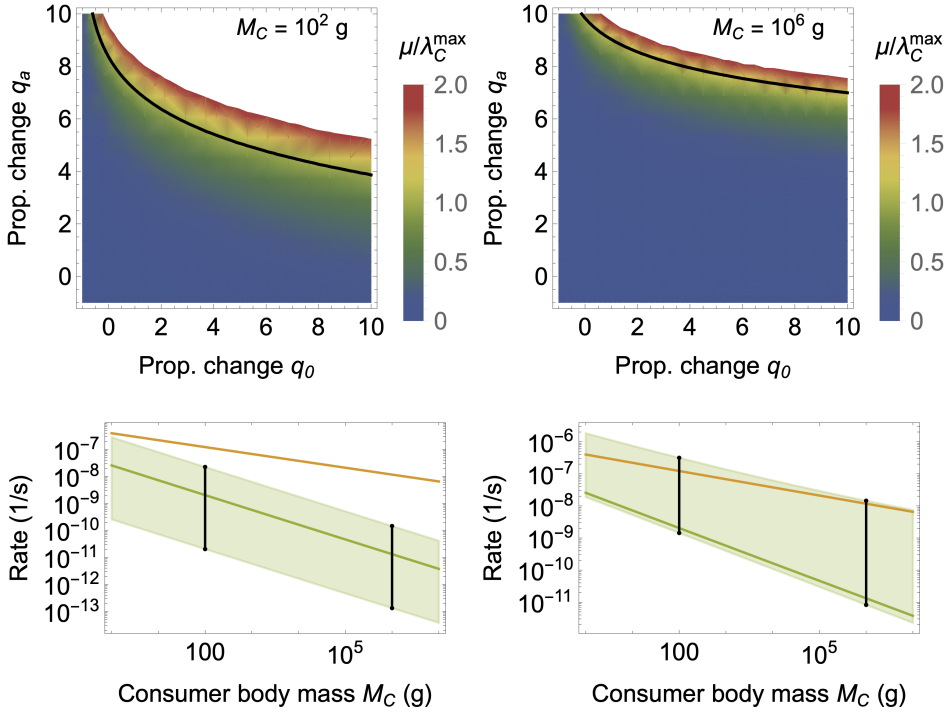

Figure 2.2: Changes in natural mortality as a function of initial cohort mortality q_0, and actuarial aging, q_a for two different consumer body masses, M_c. The ratio reproduction $\lambda_C^{\max}$ to natural mortality μ for a mammalian herbivore of (a) $M_C = 10^2$ g and (b) $M_C = 10^6$ g, across proportional changes to the initial cohort mortality rate q_0 and the actuarial aging rate q_a. The black contour denotes $\mu/\lambda = 1$. (c,d) Natural mortality μ (green) relative to reproduction $\lambda_C^{\max}$ (orange) as a function of consumer body mass M_C. The range of variation (light green shaded region) shows proportional changes to the (c) cohort mortality rate q_0 and the (d) actuarial aging rate q_a from -0.99 to 10.

shallow (Fig. 2.2D), primarily due to the cumulative nature of senescence magnifying its effects across the longer lifetimes of larger mammals. As such, an increase in q_a overwhelms the reproduction of mammals such that $\mu/\lambda_C^{\max} > 1$ compared to a similar proportional increase in q_0, resulting in population instability (Fig. 2.2B). The extinction risk imposed by senescence has been explored across mammalian taxa, and while some life history characteristics such as the inter-birth interval appear to correlate strongly with these risks, the role of body size is notably ambiguous [34]. Though our model – which considers averaged effects across terrestrial mammals – predicts that the risks of increased actuarial mortality are disproportionately felt by smaller size-classes, we also show that μ increasingly resembles $\lambda_C^{\max}$ with increasing q_a (the top border of the shaded region in Fig. 2.2D). This increased similarity implies that relatively small variations in other demographic processes or interactions may have potentially large and destabilizing effects on population size that cannot be predicted from body size, a potential source for the noted ambiguity of allometry and actuarial extinction risk [34].

While the temporal state of an organism is unidirectional and linear, other internal states, such as an organism's energetic state, fluctuate nonlinearly over time. In this case, the rate of starvation is low when resources become plentiful ($R \to k$) and increases to $\sigma^{\max}$ as resources become scarce ($R \to 0$). Because organisms metabolize their fat and muscle tissue during starvation, and die from starvation when these energetic stores are metabolized, the timescale of starvation varies with the amount of endogenous energetic stores an organism carries. Larger organisms carry a larger proportion of body mass as fat [24], such that they are more protected from the effects of short-term resource limitation [43]. We observe this effect by modifying the starvation rate and examining how the steady state population size is altered. We introduce variation to the rate of starvation as $\sigma(R)\cdot(1+\chi_s)$, such that the relative change in the steady state ΔC_s^* introduced by the modified rate is calculated as

$$\Delta C_s^* = \frac{C^*(M_C|\sigma(R)\cdot(1+\chi_s)) - C^*(M_C|\sigma(R))}{C^*(M_C|\sigma(R))}, \tag{2.7}$$

where positive values indicate a relative gain in steady state densities from the proportional change χ_s, and negative values indicate a relative loss (Fig. 2.3). We observe that, while all mammals benefit from reduced starvation rates ($\chi_s < 0$), smaller-bodied mammals benefit to a much greater extent, and this effect tapers off with increasing body mass. Because fat biomass scales super-linearly with body mass, the populations of larger consumers are more

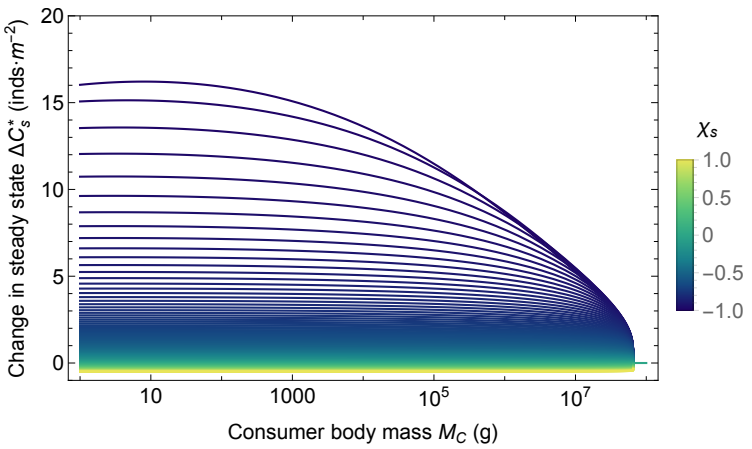

Figure 2.3: The relative change in consumer steady state ΔC_s^* as a function of consumer body mass M_C given an altered rate of starvation $\sigma(R) \cdot (1 + \chi_s)$ across the proportional change $\chi_s \in (-0.99, 1)$ (see Eq. 2.7). Declining ΔC_s^* with increasing body mass for lower values of χ_s mean that smaller organisms benefit more from reductions in the rate of starvation.

resilient to the effects of starvation, whereas those of smaller consumers are more prone.

An organism's rate of starvation emerges from two governing forces – the amount of energy storage and the rate of its use – and as such can be be manipulated both physiologically and behaviorally. For instance, behaviorally supplementing endogenous fat stores with exogenous caches magnifies an individual's energetic stores [44], whereas physiologically-mediated responses to starvation risk such as torpor can introduce significant temporal delays to the effects of resource scarcity [45]. In both cases the time required to pass from a replenished to a starved state is effectively increased, lowering the rate of starvation. The predicted benefits of such adaptations to mammalian steady state densities will be realized primarily by smaller mammals (Fig. 2.3, Supplementary Materials Appendix II), and it is these size classes where traits such as caching and torpor are most commonly observed [44, 46, 47].

2.4.3 Predation mortality and the feasibility of megatrophic interactions

Predators introduce an external source of mortality on prey populations, fueling their own population growth in whole (trophic specialists) or in part (trophic generalists), by the rate at which prey are consumed. We account for the effects of an implicit predator density P with body size M_P on the herbivore consumer density C with body size M_C. The mortality

rate of the herbivore consumer from an external predator is given by

$$\beta(C,P) = f\frac{\lambda_P(C)P}{CY_P}, \tag{2.8}$$

where $\lambda_P(C)$ is the growth rate of the predator and Y_P is the predator yield coefficient, describing the grams of predator produced per gram of prey consumed (see Supplementary Materials Appendix III), and f is the degree of specialization of the predator on the consumer prey ($f = 1$ denotes specialization, whereas $f < 1$ denotes generalization). Assuming a linear functional response for predation mortality, $\lambda_P(C)$ is maximized when the consumer reaches its theoretical maximum population density, which we calculate by converting the resource carrying capacity directly to grams of consumer produced, or $C^{\max} = Y_C k$. While this is an ultimately unattainable theoretical bound, it allows for a direct calculation of the predator growth rate as a function of C, written as

$$\lambda_P(C) = \lambda_P^{\max}\frac{C}{C^{\max}} = \lambda_P^{\max}\frac{C}{Y_C k}, \tag{2.9}$$

where $\lambda_P^{\max}$ is the maximum predator growth rate. The theoretical boundary density for herbivore consumers $C^{\max}$ can similarly be used to calculate the boundary density for predators, $P^{\max} = Y_P C^{\max}$, both of which accurately capture the upper-bounds of herbivore and carnivore mass-density relationships (dashed lines in Fig. 2.4A). Because the effects of the predator are implicit, we assume that the predator population remains at empirically measured steady state densities for mammalian carnivores, where $P \equiv P^* = P_0 M_P^{-0.88}$ (Table 2.1) [40].

The predation mortality rate depends on both the body size of the herbivore consumer and its respective predator. Trophic interactions are constrained by body size [2, 9, 48], and large prey generally suffer mortality from large predators, though the nature of predator-prey mass ratios (PPMRs) varies across communities [49], organismal body size [48, 50–53], and is not well understood outside of aquatic gape-limited systems [54]. Because our framework is prey-centric, we require a prediction of the expected predator mass given an herbivore of body size M_C, which cannot be directly extrapolated from the expected prey mass for a given predator mass (see Supplementary Materials Appendix III). For larger predators and prey ($> 10^5$ g) [10, 55, 56], the expected predator mass given a particular herbivore consumer mass follows roughly $\mathrm{E}(M_P|M_C) = v_0 M_C^{v_1}$, where $v_0 = 1.18 \times 10^4$ g and $v_1 = 0.19$ (see Supplementary Materials Appendix III). Accordingly, larger terrestrial

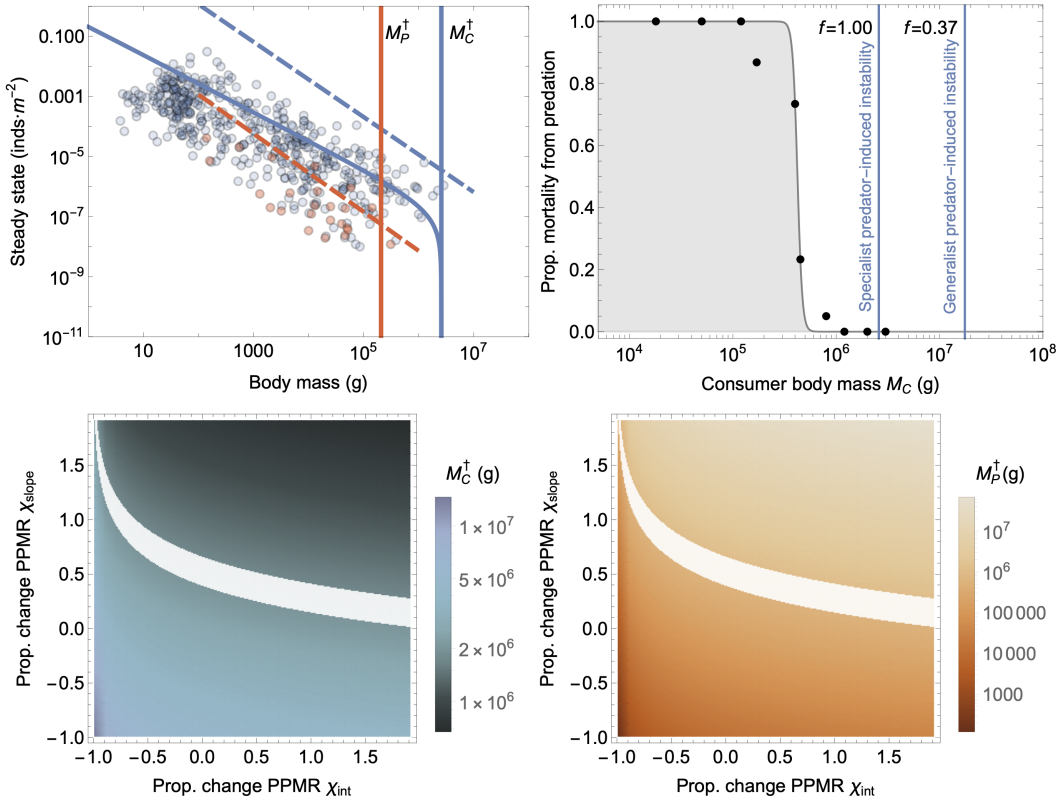

Figure 2.4: The feasibility of predation. (a) Empirical mammalian herbivore (blue points) and predator (red points) mass-densities shown alongside the theoretical maximum herbivore $C^{\max}$ and predator $P^{\max}$ densities as a function of body size. The solid blue curve denotes the predicted herbivore consumer steady state $C^*(M_C)$ with predation mortality. Predicted herbivore $M_C^\dagger$ and predator $M_P^\dagger$ size thresholds (blue and red vertical lines, respectively) resulting from a predation-induced instability. (b) Percent mortality from predation for Serengeti herbivores (redrawn from Sinclair et al. [2]) as a function of body mass M_C. Gray shaded region denotes a sigmoidal fit to the data with the inflection at 4.22×10^5 g. Vertical lines show herbivore size thresholds under the assumption of predator specialization ($f = 1.00$; $M_C^\dagger = 2.58 \times 10^6$) and generalization ($f = 0.37$; $M_C^\dagger = 1.75 \times 10^7$). (c) Threshold herbivore sizes $M_C^\dagger$ and (d) carnivore sizes $M_P^\dagger$ across changes to the predator-prey mass ratio (PPMR) intercept χ_{int} and slope χ_{slope} (see Eq. A.12). White shaded region denotes megatrophic threshold sizes, where both $(M_C^\dagger, M_P^\dagger) > 6 \times 10^5$ g.

herbivores tend to suffer mortality from proportionately smaller predators, an asymmetry that becomes more pronounced with increasing size [2]. We note that smaller terrestrial predator/prey size classes tend to follow different PPMR relationships, where predators tend to be much larger than prey (e.g. rodent- or insect-specialist mesocarnivores) [57, 58]. Here and throughout the prefix 'mega' is used to signify size classes $> 5 \times 10^5$ g [55].

Integrating the large-bodied PPMR relationship into the predation mortality rate reveals the emergence of a dynamic instability at megaherbivore size classes (Fig. 2.4A). An implicit predator population with body size $\mathrm{E}(M_P|M_C)$ is thus able to withdraw sufficient biomass from an herbivore prey population to sustain itself, without crashing the herbivore population, below a threshold herbivore size of $M_C^\dagger = 2.58 \times 10^6$ g (Fig. 2.4A). Above this critical size threshold, the herbivore population has such low densities that it is unable to sustain a specialist predator species large enough to consume it, introducing a strong upper-bound to mammalian carnivore body size driven by a trophic cascade. This boundary matches the herbivore maximum size limit observed in contemporary terrestrial systems, at roughly the size of an elephant [2] (Fig. 2.4B; Supplementary Materials Appendix III).

While $M_C^\dagger$ marks the threshold herbivore mass above which predation is unsustainable, Sinclair et al. [2] have shown contemporary herbivores to begin to escape predation at ca. 4.22×10^5 g (redrawn in Fig. 2.4B). This change-point reflects the limitations of contemporary carnivores, which reach a maximum body size of 1.15 to 2.60×10^5 g [2, 55], and have preferences for prey up to 5.50×10^5 g [55]. As such, the sole predators of contemporary giants are not megaherbivore specialists, instead opportunistically subsidizing their preferred prey base. While we have so far assumed a specialized predator-prey interaction, the largest predators in natural systems tend be dietary generalists [2, 59]. We observe that increasing the implicit dietary generality of the predator (such that $f < 1$) increases $M_C^\dagger$ to a larger threshold mass. For example, $f = 0.37$ means that a predator is supporting a little more than 1/3 of its growth rate by the targeted prey, increasing the herbivore body mass boundary to $M_C^\dagger = 1.75 \times 10^7$ grams (Fig. 2.4B; Supplementary Materials Appendix III), roughly the body mass attained by the largest terrestrial herbivores, the Oligocene paraceratheres and Miocene deinotheres [18,39]. That the threshold herbivore mass decreases with increasing predator specialization suggests that larger predators are dynamically constrained to be dietary generalists [2], while also pointing to an amplifying feedback mechanism [31] that may operate in diverse communities undergoing megafaunal extinctions. As megaherbivore species are lost, the largest predators must respond by increasing their reliance on those

remaining. Our results reveal that this energetic redirection will reduce the threshold herbivore mass $M_C^\dagger$ to lower size classes, thereby promoting additional extinctions and attendant predator specialization, a quantitative assessment of the previously proposed influence of top-down dietary ratcheting [60, 61].

While deinotheres and paraceratheres top the megaherbivore scale, the Eocene artiodactyl *Andrewsarchus* may have been the largest terrestrial mammalian predator at up to 1×10^6 g [62], while the Miocene Hyaenodontid *Megistotherium osteothlastes* ranged between 5 to 8×10^5 g and the early Eocene Oxyaenodont *Sarkastodon mongoliensis* weighed ca. 8×10^5 g [63] . A theoretical maximum mammalian carnivore size of 1.1×10^6 g has been proposed based on the intersection of daily energetic uptake requirements against metabolic expenditures [64], closely aligning with the largest known megapredators. While our consumer-resource framework provides a range of predicted megaherbivore body mass thresholds depending on the fraction of predator growth it fuels, we next ask under what conditions megatrophic relationships between megaherbivores and megapredators are dynamically feasible.

A principle relationship in our framework is the allometric PPMR observed for the largest contemporary herbivores and carnivores, however this PPMR cannot account for past megatrophic relationships (Supplementary Materials Appendix III). While it is not clear whether these super-sized carnivores were specialists on deinothere size-classes, our framework allows us to investigate whether and to what extent changes to the contemporary PPMR enable megatrophic interactions, where we allow the PPMR to vary as

$$\mathrm{E}(M_P|M_C) = v_0(1+\chi_{\mathrm{int}})M_C^{v_1(1+\chi_{\mathrm{slope}})}, \tag{2.10}$$

where the proportional changes in the PPMR intercept and slope are given by χ_{int} and $\chi_{\mathrm{slope}} \in (-0.99, 2)$. We find that the threshold herbivore body size $M_C^\dagger$ increases, while $M_P^\dagger$ decreases, with lower PPMR intercepts and shallower slopes (Fig. 2.4C,D). Lower PPMR intercepts and shallower slopes mean that predator sizes are generally smaller, and increase more slowly, with larger herbivore body sizes. So given a particular herbivore size, proportionately smaller predators elevate the threshold herbivore mass, while proportionately larger predators drive down the threshold herbivore mass. Importantly, only a small range of values for PPMR intercepts and slopes permit the existence of megatrophic interactions where megaherbivores ($1.72 - 2.01 \times 10^6$ g) serve as prey for megapredators

($6.11 \times 10^5 - 1.19 \times 10^6$ g; white band in Fig. 2.4C,D). While significantly larger PPMR intercepts ($\chi_{\text{int}} \gg 0$) are unlikely to be realized in natural systems, the megainteraction range does include very low intercepts with very high slopes, such that PPMRs are low at smaller masses, and much higher at large masses. Such a hypothesized PPMR does not stray far from contemporary large-mammal interactions (Supplementary Materials Appendix III) and may be a good candidate for megatrophic interactions.

Feasible megatrophic interactions increase substantially if a smaller percentage of the predator growth rate is fueled by the target herbivore population ($f < 1$). Setting $f = 0.37$ – which we observed increases $M_C^\dagger$ to deinothere/indricothere size classes – and allowing both χ_{int} and χ_{slope} to vary, results in megatrophic interactions spanning the largest megaherbivore ($1.27 - 1.48 \times 10^7$ g) and megapredator ($6.15 \times 10^5 - 1.20 \times 10^6$ g) sizes observed in the fossil record (Supplementary Materials Appendix III; Fig. A.3). That increased generality favors megatrophic feasibility agrees with previous conjectures that the largest mammalian terrestrial predators were likely dietary generalists [65]. Our framework highlights dynamic constraints existing between predators and prey that may serve to structure mammalian communities over evolutionary time, in particular revealing the tenuous positions of mega-sized herbivores and predators. As carnivorous clades acquire body sizes enabling megaherbivore predation over evolutionary time, their super-sized appetites may result in unsustainable megaherbivore densities where the risk of extinction becomes overwhelming – an evolutionary trap marking the final tooth in the hypercarnivore ratchet [66].

2.4.4 Harvesting to extinction

We last consider the effects of anthropogenic harvest-induced mortality on consumer populations. While the predation rate is naturally limited by the energetic needs of the predator, we consider harvest to be a comparatively unconstrained source of mortality. This may be the case if the human population(s) engaged in harvesting are subsidized by alternative resources [67]. Harvest pressure has potentially varying relationships with consumer (prey) body mass, a complex product of environment, climate, culture, and technology [68], where we can assume a general harvest rate is of the form $h = \xi M_C^w$. For example, hunting traditions specializing on mass-collecting, by way of trapping or netting [68, 69] are expected to exhibit harvest allometries biased towards smaller species (negative size-scaling, $w < 0$), whereas a purely opportunistic strategy may be expected to have very little allometric dependence (zero size-scaling, $w = 0$). Inclusion of negative size-scaling harvest reveals that

smaller-sized prey can withstand significant harvesting pressure before their populations are negatively impacted. While smaller mammals do not appear to offer a significant return on investment, the mass-collecting of invertebrates such as grasshoppers, and fish can offer significant returns [69]. The inclusion of zero size-scaling harvest reveals that it is the larger-bodied species that are negatively impacted, but only where $h(M_C) > \lambda_C(M_C)$ (Supplementary Materials Appendix IV). In contrast, the innovation of advanced projectiles is thought to have enabled harvest of terrestrial megafauna [68,70], while archeological evidence points to many Pleistocene human populations as potential megafaunal specialists (positive size-scaling, $w > 0$) [71].

Because harvest scaling may be difficult to measure and idiosyncratic, we instead calculate the harvest rate required to induce extinction, $h^\dagger$, as a function of body size M_C, and find a scaling relationship proportional to the mass-density relationship where $h^\dagger \propto M_C^{-1/4}$. This is a natural result, as the effort required to suppress a population is expected to be proportional to the consumer's abundance. As a proportion of the other sources of consumer mortality that we have considered (excluding predation; $f = 0$), extinction-level harvesting is lower for smaller consumers, saturating at close to unity for larger consumers, reflecting the elevated role of starvation mortality among smaller-sized organisms (Fig 2.5A). With predation mortality included from both generalist ($f = 0.37$) and specialist ($f = 1$) predators, extinction-level harvesting accounts for an increasingly smaller proportion of mortality for larger organisms (orange and red lines, Fig. 2.5A). This highlights the delicate nature of the megafaunal niche, where smaller changes in mortality rates can induce population collapse.

To examine how our estimate of extinction-level harvesting rates $h^\dagger$ compare to those estimated for human hunting of paleontological and historical mammalian populations, we converted $h^\dagger$ to harvest pressure $\psi^\dagger$, or the number of individuals harvested per year to reduce the population to a fraction of its steady state ϵC^* where we set $\epsilon = 0.01$. We calculate $\psi^\dagger$ for an arbitrary area (see Supplementary Materials Appendix IV), which we standardize as the area of California ($A_{\mathrm{CA}} = 4.24 \times 10^5$ km^2), such that

$$\psi^\dagger \propto -h^\dagger \frac{C^*(1-\epsilon)}{M_C \log(\epsilon)}. \tag{2.11}$$

Though the annual harvesting pressure is unrealistically high for smaller organisms, we observe that it is ca. 4.3×10^3 inds/yr/A_{CA} for elephant-sized organisms (ca. 2.5×10^6 g)

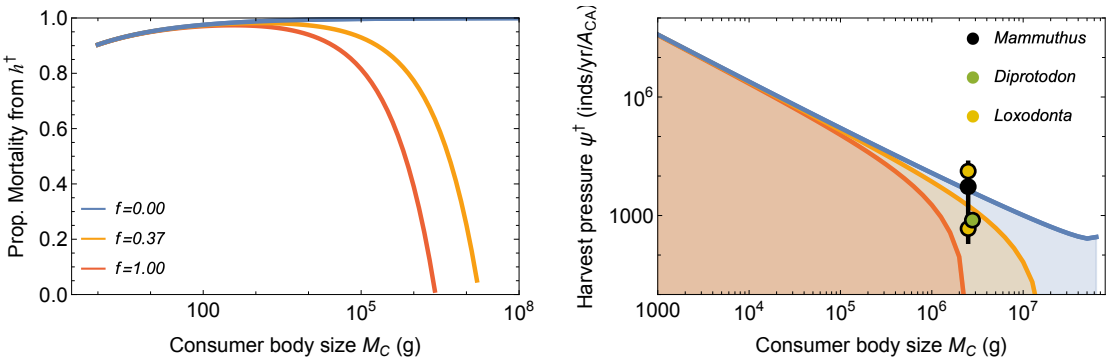

Figure 2.5: The effects of harvest mortality on herbivore consumers. (a) Proportion mortality due to an extinction-inducing harvest rate $\xi^\dagger$ without predation ($f = 0$; blue line), and with mortality from a generalist predator ($f = 0.37$; orange line) or a specialist predator ($f = 1$; red line), as a function of consumer body mass M_C. (b) Harvest pressure $\psi^\dagger$ resulting from extinction-inducing harvest (inds/year/A_{CA}) without predation ($f = 0$; blue line), with the inclusion of mortality from a generalist predator ($f = 0.37$; orange line), and with the inclusion of mortality from a specialist predator ($f = 1$; red line), as a function of consumer body mass M_C. Black point and line: median and range of estimated harvest rates for wooly mammoths (*Mammuthus primigenius*) [3]; Green point: estimated harvest pressure for the Australian *Diprotodon* [4]; Lower and upper yellow point: estimated harvest rates for contemporary *Loxodonta* during the early 1800s and just prior to 1987, respectively [5].

in the absence of predation mortality ($f = 0$). With the increasing pressures of generalist and specialist predation, the harvest pressure required to induce extinction is much less for these larger consumers (orange and red lines in Fig. 2.5B). We note that this calculation of harvest pressure should be viewed as a minimum estimate given that we do not account for demographic rebound. As such, this measure is appropriate only if the timescale of harvest is less than the generational timescale, which is the case for the megafauna considered here.

Our predictions of extinction-inducing harvest pressure compare well with paleontological and historical estimates of harvest pressure on mammalian megafauna (see Supplementary Materials Appendix IV for details). For example, Fordham et al.'s [3] estimate of the harvest pressure required to collapse mammoth (*Mammuthus primigenius*) populations (using a formulation similar to that of Alroy; [30]) reveals a range of values consistent with our expectation for similar size-classes (est. harvest pressure $= 1.24 \times 10^4$ inds/yr/A_{CA}), as did estimates of extinction-inducing harvest of the Australian *Diprotodon* (est. harvest pressure = ca. 763 inds/yr/A_{CA}; [4]). Within the historical record, elephant (*Loxodonta*) populations experienced comparatively lower harvest pressure through 1850 (ca. 466 inds/yr/A_{CA}, derived from the volume of ivory exports; [5]). While fluctuating over the next century, harvest pressure elevated to a maximum of ca. 13.3×10^5 inds/yr/A_{CA} just prior to 1987 (Fig. 2.5B). This level of harvest was not sustained, as ivory export volume plummeted following the implementation of trade restrictions in 1989 [5]. Both Fordham et al.'s [3] estimate for Pleistocene mammoths and the short-lived harvest maximum for African elephants in 1987 [5] achieved pressures greater than $\psi^{\dagger}$ under the conservative assumption of no natural predation. While estimates for *Diprotodon* harvest are considerably lower [4], it is important to note that our measure of harvest pressure is parameterized for eutherian rather than marsupial mammals. Nevertheless, the estimated *Diprotodon* $\psi^{\dagger}$ is well within range of extinction-inducing harvest rates if natural predation pressures are also included, and there is evidence to suggest that *Diprotodon* likely served as prey for marsupial lions [72, 73], and both giant crocodylians (*Pallimnarchus*) and varanid lizards (*Megalania*) [74].

2.5 Conclusion

We have shown that the inclusion of mass-specific energetic transfer between resources and consumers, combined with the unique timescales governing consumer mortality, both predict Damuth's Law [1] and provide insight into dynamic thresholds constraining populations.

While natural and starvation mortality primarily impact small-bodied species, trophic mortality primarily impacts large-bodied species with longer generational timescales. Moreover, while mass-specific predation gives rise to dynamic thresholds on herbivore populations, these effects are sensitive to both predator generality as well as the associated predator-prey mass ratio, which isn't well understood for terrestrial megafauna [54]. While assessment of particular communities and/or species requires more detailed approaches – integrating, for example, life history dynamics as in Bradshaw et al. [4] – we suggest that a general and lower-dimensional framework may be useful for extracting first-order energetic constraints that both shape and potentially limit the general nature of mammalian communities.

That extinction risk appears to increase with body size [75] is integral to our understanding of the Pleistocene extinctions [4,30,31,71,76] and anthropogenic effects throughout the Holocene [77]. Assessing which energetic walls close in and why, as body size increases, is fundamental for reconciling the nature of extinction [31], particularly when there is size-selectivity [71]. That we observe dynamically-feasible megatrophic interactions to occupy a narrow band of PPMR relationships points to a broader range of interaction structures than are realized in contemporary communities. As the threshold consumer mass decreases with predator specialization, how megafaunal trophic structure changes during extinction cascades may be central for understanding the dynamics of community disassembly [52]. And while these dynamics may arise naturally from the energetic limitations of mammalian interactions, it may be that the added pressures of subsidized harvest, particularly on megafauna, inevitably lead to collapse.

Chapter 3

Body Size and Competition Drive the Structure and Dynamics of Mammalian Herbivore Communities

3.1 Abstract

The fundamental constraints governing the flow of energy through consumer-resource systems ultimately determines the structure and dynamics of food webs. As this is true generally, it is also true for plant-herbivore systems, where herbivores must compete with each other to obtain sufficient caloric return. Because diverse herbivore communities are composed of species spanning a large range in body sizes, the different life histories imposed by these body sizes and the different effects these species have on their resources interact in complex ways, perhaps playing a role in determining the conditions for coexistence. Here we construct an n-dimensional plant-herbivore food web model where the vital rates determining life history attributes are established on process-based energetic trade-offs, and where foraging behaviors are adaptive. In addition, we explore three alternative relationships between body-mass and diet-breadth: that of increasing breadth with mass, decreasing breadth with mass, and a non-linear relationship with high diet breadth

for large and small herbivores. Our results demonstrate that our approach accurately captures macroecological patterns such as Damuth's Law, with weaker support for the noted invariance between mean body size and community biomass. Secondly, we observe that the negative mass-breadth relationship maximizes herbivore survival, while the competitive dynamics of plant-herbivore systems heavily favours larger consumers, with smaller consumers adaptively avoiding competitive overlap to enable persistence. Finally, communities with high levels of dietary overlap, where small consumers cannot escape predation, display consistently reduced richness.

3.2 Introduction

Competition for resources is a central driver shaping the structure and dynamics of communities [78, 79]. While the effects of competitive interactions can be direct, resulting in antagonistic interactions between species [80], it can be difficult to parse out the presence and impacts of indirect competition [81]. Competition for shared food resources among herbivorous mammals may drive the organization of local communities and play a central role in coexistence [82]. While competitive interactions sometimes result in local dominance by one species over another, often due to which competitor drives the limiting resource to lower densities [83, 84], consumer behaviors that can dynamically respond to changes in competition may promote increased species richness even when competitive loads are high. The intensity and outcome of these competitive interactions is, in part, a function of the composition of the consumer diets and how much of their resource base is shared [85, 86].

When resources are limited, the collective dietary breadth describing consumer diets ultimately determines the magnitude of diet overlap. The overlap of trophic niches across consumers is thus an effective measure of the competitive pressure on a set of resources [87]. This trophic niche overlap, in concert with the functional and nutritional diversity of shared resources, is likely an important driver of the behavioral responses consumers have to competition. A consumer that adapts its diet to increased competition with respect to a suite of resources must react to parallel demands: decreasing the competitive load while maintaining necessary caloric and nutritional requirements, all within the bounds of resources that are physically and biochemically available to the consumer. This emergent compromise often manifests as adaptive foraging behaviors [88, 89].

Access to the nutritional reserves of various foods depends on the physiology and

anatomy of both consumers and their resources, where increased food quality corresponds to greater nutritional or energetic rewards per gram available to the consumer. Both overall quality, as well as the abundance, of a consumer's potential resources determines the availability of the energy required to fuel the growth of its population over time. While many consumer characteristics influence this availability, perhaps none has as much influence as its body size. While the body mass of a consumer M_C determines its metabolic rate [90], it also scales the sizes of physiological storage compartments within the organism. For example, because fat storage among terrestrial mammals scales superlinearly with body size – such that larger mammals carry a larger proportion of their body weight as fat – larger organisms are less sensitive to resource scarcity, i.e. greater fasting endurance [43], lowering the risk of starvation [18]. In tandem, the potential risks inherent to consumers of different body sizes interact with their differing abilities to access and assimilate nutrients from resources that range from rare to common, from low quality to nutritionally replete [29].

The spectrum of needs and sensitivities of consumers ultimately determines to what extent patterns of resource interactions change with consumer body size. While larger consumers are, on average, able to tolerate lower-quality foods [91, 92] and are less averse to the effects of periodic resource scarcity [43], how these constraints impact the number and intensity of interactions with potential resources is less clear. Smaller mammalian herbivores above 4 kg generally have increased dietary breadth, which tends to decline with increasing body size [6–8]. The greater dietary breadth and preference for higher quality foods among smaller mammals may enable fast resource switching to reduce long intervals between acquisition, a potentially fatal event for these starvation-prone species. In contrast, larger consumers have greater fasting endurance [43], and can tolerate lower quality foods [92]. Such a relationship could be argued to result in a smaller dietary breadth in environments where quantity of a few hyper-abundant low-quality resources comprise the bulk of a consumer's diet. An argument could also be made for increased dietary breadth once consumers enter megaherbivore size classes (where the prefix 'mega' is used to describe consumers > 500 kg), resulting in a nonlinear relationship between body size and dietary breadth. For example, the broader trophic niche and 'mixed-feeder' classification of African elephants [93–95] is a deviation from the rest of the mass-generality pattern and may indicate second peak of trophic breadth among the mega-herbivores. Here, the increased tolerance for both low quality resources and temporal delays in resource acquisition may enable a diet where less common high quality resources are preferred, while abundant low

quality resources are integrated to ensure energetic demands are met, the combination of which serving to maximize dietary breadth. That megaherbivores may unlock this dietary potential is perhaps speculative; while contemporary megaherbivore species appear to support such a relationship [8, 96, 97], the limited representation of these size classes within Holocene ecosystems precludes a rigorous assessment.

It is the combined effect of herbivore diets across body sizes within a community that gives rise to the structure of plant-herbivore interactions. While the distribution of consumer body sizes within a community is understood to significantly impact its structure and function [98], it is less clear how the dynamics of competition feed back to reorganize this structure. Because similar-sized consumers are exposed to similar risks and dietary constraints [29, 92], it is expected that the effects of competition may also be elevated [85]. As competitive pressure for a particular resource is increased, the extent to which it produces energetic rewards decreases, such that herbivore consumers are likely to adaptively modify the proportional contribution of potential resources to their diet [88, 99]. Because smaller herbivores are more sensitive to the effects of resource scarcity [100, 101], increased dietary breadth at these sizes may enable adaptively dodging the competitive pressures of larger herbivores less prone to starvation-induced mortality. Through this capacity to adaptively modulate the strengths of resource interactions, the overlapping dietary niches of competitors (the potential niche) can be redirected into modified diets with reduced overlap (the realized niche).

This adaptive foraging dynamic has been shown to increase the stability of increasingly diverse and connected food webs [88,99] and mutualistic networks [89,102], by reducing competition and enabling the co-existence of species otherwise prone to exclusion. Despite the stabilizing effects of adaptive food webs, it is unknown how and to what extent these dietary dynamics interact with the body size distributions and allometric structures of mammalian communities. It is likely that these competitive dynamics have a direct impact on both the forces that permit coexistence of herbivores in diverse communities, as well as size-based extinction risks that may shape the structure of these communities over macroevolutionary timescales.

Here we establish a plant-herbivore network to examine mammalian community dynamics as a function of body-size distributions, the structural assumptions underlying species' diet breadth, and the inclusion of adaptive foraging that serves to minimize competitive

overlap. Building on prior efforts incorporating process-based metabolic relationships governing allometric timescales associated with growth and mortality into consumer-resource dynamics [18, 103], we expand these perspectives to an n-dimensional plant-herbivore community where we explore the effects of three relationships linking consumer body size to dietary breadth: *i*) increasing dietary breadth with body size, *ii*) decreasing dietary breadth with body size, and *iii*) nonlinear (decreasing and then increasing) dietary breadth with body size. By examining how these structural assumptions underlying herbivore-plant relationships impact the persistence of different body size ranges, we gain insight into the role that competition plays in shaping the composition of diverse herbivore communities.

Our results reveal four key insights into the structure of mammalian plant-herbivore communities. First, our framework is shown to reproduce large-scale macroecological patterns, such as Damuth's Law [1], while providing weaker support for the observed across-community mass-biomass equivalence [9]. Second, we show that adaptive foraging behavior facilitates niche partitioning and increases species persistence, though these effects are not evenly applied across herbivore body sizes. Third, we show that high levels of niche overlap lead to the size-based competitive exclusion of smaller herbivores. Finally, we find that the trophic structure associated with negative and nonlinear mass-breadth relationships increases both species persistence and community richness. We suggest that integrating process-based metabolic relationships into models of consumer-resource community dynamics is well-suited to provide insight into our developing understanding of the structure and function of diverse herbivore communities, and may be central to deciphering observed changes in the communities throughout the Cenozoic.

3.3 Model Framework

3.3.1 Consumer-resource dynamics

We construct a bipartite network of interacting herbivores and their plant resources, where the trophic structure of the network and the proportional contributions of resources to consumer diets are given by the weighted adjacency matrix A. As such, a given element of A, A_{ij}, is given a value > 0 if the herbivore i consumes resource j, and a value of zero otherwise, where the proportional contributions of resources j in the diet of consumer i is constrained by $\sum_j A_{ji} = 1$. The available resources R_j (g/m^2) grow logistically with intrinsic growth rate α_j to a carrying capacity k_j, and decline due to consumption by herbivore consumer

populations C_i (g/m^2) (Eq. 3.3). Consumed resources fuel both consumer growth and reproduction. The rate of consumption to fuel reproduction is proportional to resource density and is given by $\lambda_j(R_j)/Y_{ij}$, where $\lambda_i(R_j)$ is the consumer growth rate and Y_{ij} is the consumer yield coefficient, or the grams of consumer i produced per gram of resource j consumed. The consumer's growth rate with respect to a particular resource j, $\lambda_i(R_j)$, follows Michaelis-Menton (Type II) kinetics as a function of the resource density R_j, where the maximum growth is $\lambda_i^{\max}$ and the resource half-saturation density is $\hat{k}_j = k_j/2$, such that

$$\lambda_i(R_j) = \lambda_i^{\max}\left(\frac{R_j}{\hat{k}_j + R_j}\right). \tag{3.1}$$

While the consumer population density grows as the sum of rates $\lambda_i(R_j)$ taken across consumed resources, we assume for now that consumer mortality is a function of starvation, where the rate of starvation for consumer i on resource j

$$\sigma_i(R_j) = \sigma_i^{\max}\left(1 - \frac{R_j}{k_j}\right). \tag{3.2}$$

As such, the rate of starvation increases as a consumer's suite of resources become scarce. In this context, $\sigma_i^{\max}$ is the maximal rate of starvation for consumer i that occurs when the environment is devoid of resources. See Table 3.1 for a description of parameters.

The full system describing n consumers interacting with m resources, such that species richness $S = n + m$, is given by

$$\begin{aligned}\frac{\mathrm{d}}{\mathrm{dt}}C_i &= \sum_{j=1}^{n} A_{ij}\lambda_i(R_j)C_i - \sum_{j=1}^{m} A_{ij}\sigma_i(R_j)C_i,\\ \frac{\mathrm{d}}{\mathrm{dt}}R_j &= \alpha_j R_j\left(1 - \frac{R_j}{k_j}\right) - \sum_{i=1}^{n} A_{ij}\frac{\lambda_i(R_j)}{Y_{ij}}C_i.\end{aligned} \tag{3.3}$$

The rate laws describing resource consumption as well as consumer growth and mortality all vary as a function of consumer body mass M_i, where the consumer is assumed to be a mammalian herbivore, and the resource j is an unspecified plant functional group with characteristic growth rate α_j, carrying capacity k_j, and energy density E_{dj}. E_{dj} then interacts with consumer mass to determine the consumer yield coefficient, Y_{ij}. To examine the dynamics for a particular system, we set the constraints governing resource growth and the body size distribution of the herbivore community (see Supplementary Appendix

I). Values of resource reproduction rate α_j and energy densities E_{dj} are drawn uniformly from the rates found in browse and graze plants [104,105] (see Supplementary Appendix I). Resource carrying capacities are established by first assuming a community-level carrying capacity K, where a subset of resource-specific carrying capacities are randomly chosen such that $\sum_j k_j = K$ for resources $j = 1...m$. Because we assume that consumer densities that fall below $C_i = 10^{-10}$ are functionally extinct and excluded from the system, the final body mass distribution may not reflect that used to initiate community dynamics.

Table 3.1: Model parameters and values/units

Definition	Parameter	Value/Units
Resource j		
density	R_j	g/m^2
reproduction rate	α_j	1/s
carrying capacity	k_j	g/m^2
Consumer i		
density	C	g/m^2
max reproduction rate	$\lambda_C^{\max}$	1/s
yield coefficient	Y_{ij}	none
natural mortality rate	μ_i	1/s
starvation rate	σ_i	1/s
foraging effort	A_{ij}	$(0, 1)$
learning rate	G_i	1/s

Given the assumption of adaptive dynamics, consumer species dynamically adjust the effort associated with a particular plant resource to maximize profitability, defined as the net reproductive output produced by a particular diet. This means that the proportional contribution of a given resource increases if the profitability associated with a focal resource j if

$$\lambda_i(R_j)C_i > \sum_{l=1}^{m} A_{il}\lambda_i(R_l)C_i, \tag{3.4}$$

and decreases otherwise [88, 89]. For consumer i, the rate at which this adaptation occurs is governed by the learning rate G_i, where together

$$\frac{\mathrm{d}}{\mathrm{dt}}A_{ij} = G_i A_{ij}\left(\lambda_{\mathrm{i}}(R_j)C_i - \sum_{j=1}^{m} A_{ij}\lambda_i(R_j)C_i\right). \tag{3.5}$$

As consumer and resource densities change over time, the diets of consumers change as

well. Because resources that become heavily consumed by a diversity of consumer species will suffer significant mortality, reducing their densities, this adaptive foraging dynamic will tend to result in consumers with steady state diets that minimize competitive loads. Throughout, we examine the outcome of community dynamics when adaptive foraging alters diets in response to competitive pressures ($G_i > 0$ for consumers $i = 1 : n$), as well as the case where diets are not assumed to change adaptively ($G_i = 0$ for consumers $i = 1 : n$).

3.3.2 Community structure from alternative mass-breadth relationships

The structure of a food web determines the direction and strength of biomass flow through trophic interactions between species, and is captured by the weighted adjacency matrix A. The structure of food webs is perhaps the most widely examined aspect of ecological networks [106], and understanding how body size constrains this structure has received much attention, particularly in gape-limited aquatic systems [98]. Along these lines, the role of body size in driving patterns of interaction among terrestrial mammalian herbivore communities and their plant resources is less well understood [107], though recent efforts utilizing metabarcoding have made significant progress [6,7]. Yet how dietary breadth varies as a function of herbivore body mass is unclear, the empirical data suggesting multiple alternative and plausible relationships [6–8]. Both the limited number of contemporary diverse herbivore communities and the loss of megaherbivore size classes during the end-Pleistocene [108] may limit a general understanding of the role of body size in structuring Cenozoic communities writ large.

We examine the dynamic consequences four potential herbivore-plant structures that establish general relationships between body mass and diet breadth, which we refer to as mass-breadth. We first examine a fully connected plant-herbivore network, where there is no assumed mass-breadth relationship, and every herbivore is trophically lined to every resource. Second, we examine a plant-herbivore network with a positive mass-breadth relationship, where dietary breadth increases with body size (Fig. 3.1A). This captures a well-known relationship that is integrated into the Niche model food web framework [109], and is particularly relevant for gape-limited aquatic systems. Third, we examine a negative mass-breadth relationship, where dietary breadth decreases with body size (Fig. 3.1B). This relationship is integrated into the Inverse Niche model that has been proposed for parasitic interactions [110], and while this particular approach has not been applied to plant-herbivore systems, may be appropriate for capturing the allometric effects of diet quality

[92]. Fourth, we introduce a nonlinear mass-breadth relationship, where dietary breadth is assumed to be high for small herbivores, decreasing to a minimum for intermediate-sized herbivores, and increasing to a second maximum at megaherbivore size classes (Fig. 3.1C). See Supplementary Appendix III for details.

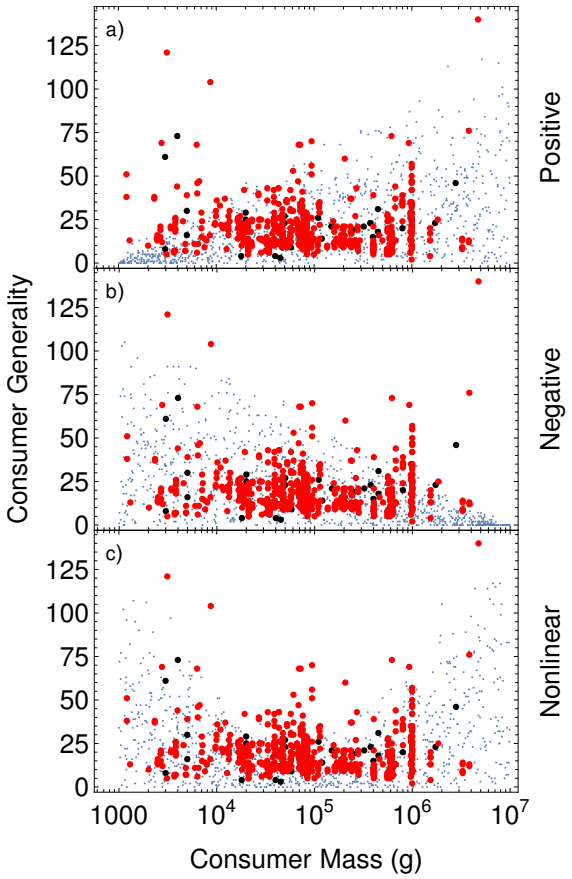

Figure 3.1: A comparison of mass-breadth relationships between observed data (red points [6] and black points [7, 8]) and three structural models (blue points), where Consumer Generality refers to the number of plant species in a herbivores's diet. The positive mass-breadth relationship a) does not well match the high generality of small herbivores. The negative b) and nonlinear c) mass-breadth relationships capture the generality of small consumers and present alternative hypothesis for the generality of megaherbivores.

3.4 Results and Discussion

3.4.1 Complex plant-herbivore food webs capture macroecological relationships

Our multi-species consumer-resource community (S-D) framework expands upon a single consumer-resource (2-D) model where the vital rates governing herbivore growth, mortality, and interaction with a plant resource, are derived from process-based metabolic relationships [18,103]. This 2-D perspective, where a specialist herbivore engages with single resource, has been shown to accurately capture the $-3/4$ scaling and documented variability of herbivore densities as a function of body mass, known as Damuth's Law [103]. In this community framework, we examined whether similar macroecological trends could be recovered with respect to both different mass-breadth relationships determining food web structure, as well as with respect to static ($G = 0$) versus adaptive ($G > 0$) foraging dynamics.

For each of our analyses, we simulated 250 herbivore communities to steady state where consumers enacted both non-adaptive ($G = 0$) and adaptive foraging ($G > 0$), under the four structural assumptions relating diet breadth to body mass: fully connected, and positive, negative, and nonlinear mass-breadth structures. We initiated each community with 10 resource groups, and 10 herbivore species with a body size distribution selected from a uniform distributions (in log space) from 10^1 to 10^7 g. For a given interaction structure, the initial proportional contribution of each resource j to a consumer i's diet was set by randomly selecting values between $A_{ij} = 0.0 : 1.0$ given the constraint $\sum_j A_{ij} = 1$. Allowing the system to change dynamically over time, an herbivore species was assumed to go extinct at time t if its density fell below $C_i(t) = 10^{-10}$, such that those species remaining defined the steady state community.

We observe that neither the choice of mass-breadth relationship underlying a particular food web structure nor the choice between static or adaptive foraging produces major deviations from Damuth's Law (Fig 3.2). Densities of herbivore species coexisting within steady state communities follow closely the -3/4 scaling relationship observed within natural systems. Despite this general agreement between theory and empirical data, there are some deviations from expectations. First, elevated population densities among the smallest herbivores, which create a slightly steeper slope than that known for Damuth's Law, have also been observed in 2-D models when the effects of explicit starvation are not included [41, 103]. Interestingly, these elevated densities are observed to align with the

$-3/4$ scaling of Damuth's Law when the effects of explicit starvation are introduced [18], pointing to the asymmetrical effects of starvation mortality among smaller mammalian herbivore species [103]. Second, densities of herbivore populations at steady state within fully connected, adaptive communities reveal bias towards coexistence of only larger species at densities higher than expected (Fig. 3.2B). This points to a general phenomenon that we will discuss momentarily: that the largest body sizes appear to have strong competitive advantages when foraging is adaptive. Because only the opposing forces of reproduction and starvation-induced mortality drive competition between species, we infer that this effect is driven entirely by the enhanced ability of larger species to cope with limitations in resource availability. In fully connected consumer-resource systems, competition is maximized, such that this effect is highly exaggerated.

Mammalian herbivore communities vary widely in terms of their representative species, often reflecting the productivity and rainfall regimes of their constituent environments [111]. Despite the large differences in composition, a striking invariance is observed when one examines the mean body size of mammalian herbivore communities as a function of the total community biomass [9]. This invariance has a scaling relationship with an exponent roughly zero, though it varies among terrestrial communities as a function of trophic level (scaling exponent for trees: 0.25; herbivores: -0.02; carnivores: -0.04) [9]. This suggests that the mean body size-biomass invariance emerges due to the fact that differences between communities are largely a function of changes in density and/or diversity rather than changes in body size structure [9]. So a community of species with smaller densities or lower diversity is expected to have the same body size structure as a community with increased densities or greater diversity. In our framework, communities that emerge at steady state are the product of different competitive forces that vary with structure and static versus adaptive foraging dynamics.

Our framework reveals a range of scaling exponents describing the relationship between mean body size and community biomass, which ranges from 0.3 to 1.0 (Fig. 3.3). These scaling relationships are substantially steeper than those observed in natural systems, such that steady state communities derived from our framework with increased biomass also tend to be biased towards larger size-classes. Of potential interest is the observation that the shallowest slope – the slope most similar to that observed in natural systems – corresponds to the negative mass-breadth food web structure under the assumption of adaptive foraging conditions (Fig. 3.3F). Here we observe that diet breadth is primarily a trait confined to

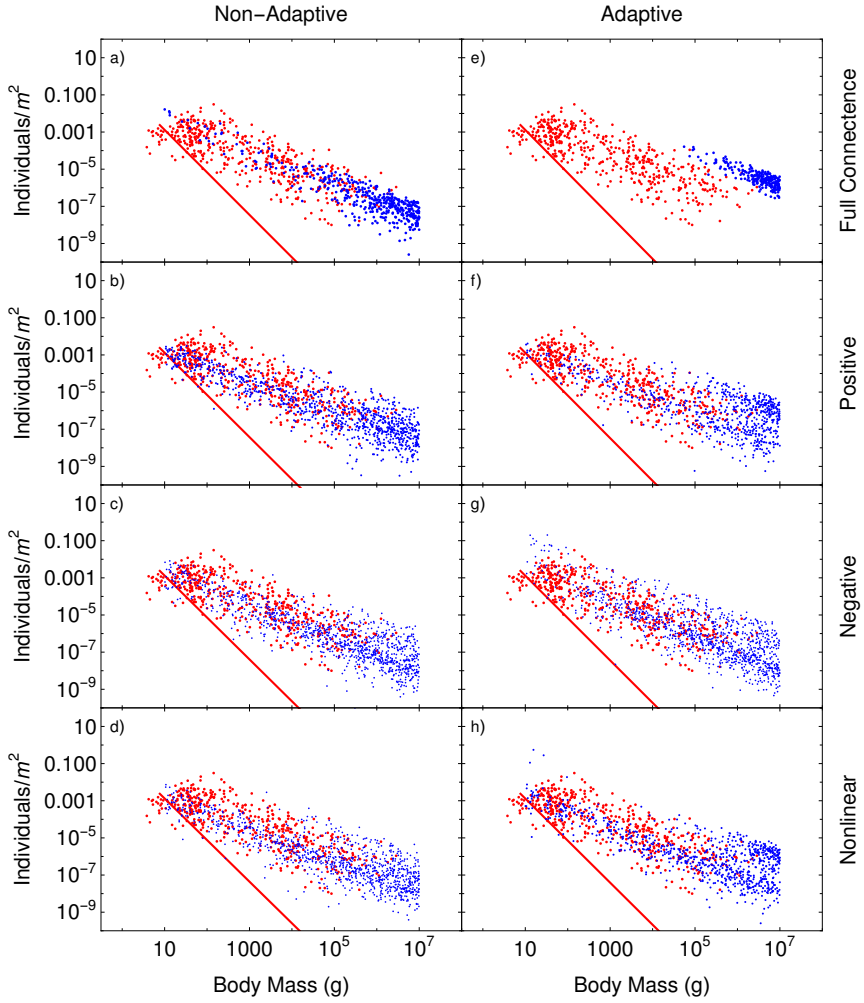

Figure 3.2: Model predictions of mammalian steady states (inds $\cdot$ m^{-2}) as a function of herbivore consumer body mass M_C (blue points) compared to observational data and best-fit from empirical observations [1] (red points and line). a) Non-adaptive foraging and e) adaptive foraging in a fully connected plant-herbivore system. b) Non-adaptive foraging and f) adaptive foraging in a plant-herbivore system with a positive mass-breadth structure. c) Non-adaptive foraging and g) adaptive foraging in a plant-herbivore system with a negative mass-breadth structure. d) Non-adaptive foraging and h) adaptive foraging in a plant-herbivore system with a nonlinear mass-breadth structure.

smaller size classes, and that the largest species have the narrowest diets. Because the largest size classes are not well represented in contemporary ecosystems, we suggest that whether or not megaherbivores had increased diet breadth, such a relationship will not be reflected in Anthropocene communities. Accordingly, a negative mass-breadth structure,

which more accurately captures the diets of smaller and intermediate-sized consumers, is more appropriate for comparisons with contemporary communities. Given these conditions, the correspondence of our model results with the mean body size versus biomass invariance relationship is weak, but suggests that a negative mass-breadth food web structure may be the best candidate for reproducing this observed pattern. It is tempting to speculate that mean body size-biomass invariance relationship may be a product of systems that have been stripped of their megafaunal ancestry, and it is worth considering in future efforts how a diverse megafaunal community might alter this expectation.

3.4.2 Patterns of coexistence and survival among herbivore communities

The processes that allow for the coexistence of species that overlap in their resource and habitat needs is fundamental to much of community ecology [112]. While competition is often expected to result in the exclusion of lesser competitors, we observe that in many cases diverse herbivore communities co-exist while drawing from very similar resource pools [113]. The processes and mechanisms facilitating coexistence are likely numerous and varied [114, 115]. On the one hand, spatial heterogeneity distributes resources, species, and ultimately competitive pressure across an equally diverse and varied landscape, ensuring that competitive effects serve to redistribute rather than exclude [116, 117]. On the other hand, a shared suite of resources between two similar species may conceal an adaptive dynamic whereby both species adjust the proportional contribution of individual resources to minimize the overlap of their realized dietary strategies [7]. As such, the inclusion of adaptive foraging into food-web models has been shown to stabilize what would otherwise be unstable communities [118, 119]. Among diverse mutualistic systems, the stabilizing dynamic has been directly linked to the dynamic partitioning of resource niches to minimize trophic overlap [89]. What remains unclear is how adaptive niche partitioning interacts with diverse size-structured herbivore communities. Whether and to what extent adaptive foraging enables or precludes coexistence of differently-sized herbivore species that must partition a shared resource base may provide insight into the macroevolutionary constraints structuring mammalian communities across the Cenozoic.

We next examine coexistence of mammalian communities simulated to steady state, where we assess mass-specific survival probabilities. Consumer survival is defined as retaining densities $C_i(t) > 10^{-10}$ g/m^2 over time t and until the system reaches steady state. The largest signal that emerges from our findings is that larger-sized herbivores have a clear

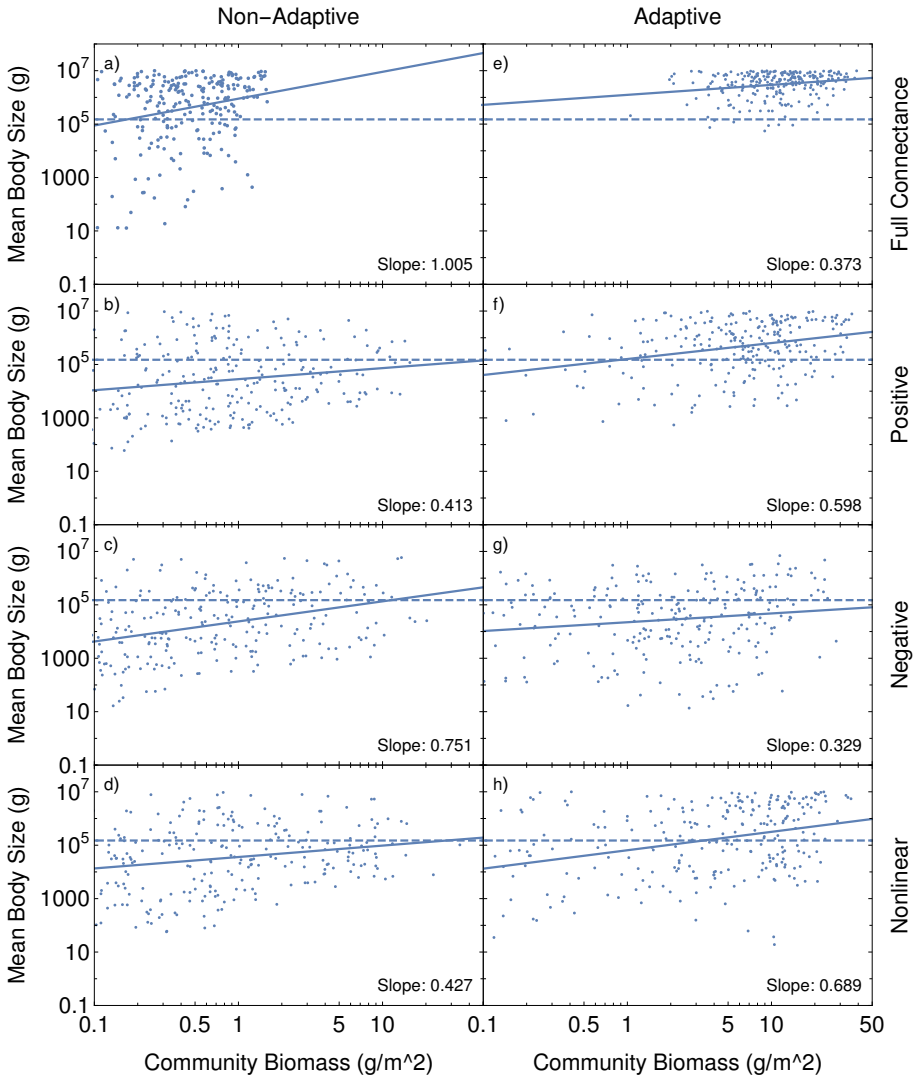

Figure 3.3: Model predictions of mean consumer body-mass (g) as a function of consumer community biomass (blue points and solid line) compared to the observed relationship (dotted line) [9]. a) Non-adaptive foraging and e) adaptive foraging in a fully connected plant-herbivore system. b) Non-adaptive foraging and f) adaptive foraging in a plant-herbivore system with a positive mass-breadth structure. c) Non-adaptive foraging and g) adaptive foraging in a plant-herbivore system with a negative mass-breadth structure. d) Non-adaptive foraging and h) adaptive foraging in a plant-herbivore system with a nonlinear mass-breadth structure.

competitive advantage over a smaller herbivores, and this pattern is consistent across all structural models and regardless of adaptive foraging (Fig. 3.4). While this pattern emerges

unilaterally, it is most stark when all consumers are trophically connected to all resource groups. In this case, and when foraging is adaptive, herbivores of the largest size-class outcompete every other (Fig. 3.4B). This effectively recapitulates classic expectations from non-spatial models of Lotka-Volterra competition dynamics [120–122], where the stronger competitor excludes the weaker competitors. When foraging effort is constant rather than dynamic, set differences in the proportional contribution of resources among herbivores enable enough differences in resource requirements to slightly increase the survival rates of smaller species (Fig. 3.4A).

While larger consumers have greater overall caloric needs, they are more efficient per-gram [15]. Moreover, larger species also have greater starvation tolerance [18, 103] due to the superlinear relationship between endogenous fat stores with body size [43], decreasing their sensitivity to resource limitation. In our framework, resource limitation is driven exclusively by competitive pressure exerted by species sharing similar diets, such that larger consumers are able to maintain higher growth rates relative to mortality when resource access is constricted, resulting in competitive dominance. In natural systems, there are many other factors that prevent direct competition between the very small and the very large. For example, smaller herbivores, mediated by mouth- and gut-size allometries, may focus on different parts of the same plants compared to larger herbivores, potentially driving herbivorous phenologies [82, 123], reducing competitive load. Moreover, herbivores of different sizes have different spatio-temporal distributions, such that competitive overlap is distributed across both space and time [114, 115]. As we assume co-occurring herbivores are described only by differences in body size in a spatially implicit landscape, it is the allometric differences in rates controlling growth, reproduction, and mortality alone that determine the outcome of competition and ultimately coexistence. We emphasize that these mass-specific survival probabilities should be evaluated in light of the dynamics included in our model framework. Because we have only included those vital rates described above, our results reflect the influence of those rates alone on the probability that a consumer is not competitively excluded.

In an adaptive herbivore community where species are fully connected to the potential resource base, only the largest survive (Fig. 3.4B). The ability for smaller herbivores to coexist emerges when patterns of resource use among consumers incorporate more complex structures (Fig. 3.4C-H). While all mass-breadth structural models increase the survival probabilities for smaller herbivores, each results in slightly different effects across the body

size continuum. A positive mass-breadth structure results in survival probabilities with a long tail towards smaller herbivores when foraging is non-adaptive, with reduced probabilities when foraging is adaptive (Fig. 3.4C,D). A positive mass-breadth structure is commonly used to simulate food web structures, such as in the Niche model [109], where the niche-axis that is used to establish diet breadth and overlap is often interpreted as body size [98]. While a positive mass-breadth relationship results in model structures with statistical features similar to empirical food webs, both the allometric relationships and structural comparisons are most successful when applied to aquatic systems where consumer-resources relationships are generally gape-limited [54, 98].

Both the negative and nonlinear mass-breadth structure result in elevated survival probabilities for larger consumers (relative to the positive mass-breadth structure) when foraging is both non-adaptive and adaptive (Fig. 3.4E-H). Overall, when foraging is adaptive, we observe that an increased dietary breadth among smaller herbivores – which is present in both the negative and nonlinear mass-breadth structural models – slightly increases the probability of survival associated with these species. As the differences in mass-specific survival probabilities among the three mass-breadth models considered here are slight, it is primarily the presence of structural complexity that allows some competitors an increased ability to adjust their diets in an effort to minimize competitive pressure, while the exact nature of structure appears to be less important. A negative mass-breadth relationship has been successfully applied to model the structure of parasitic interactions in food webs [110], but may also reflect important constraints of herbivore communities. Specifically, such a structure may capture increased selectivity for a broader range of energy-rich plants or plant-parts among smaller browsers [124, 125], in contrast to the lower selectivity and more uniform diets of larger grazers [7].

The nonlinear mass-breadth relationship generates a structure similar to the negative mass-breadth relationship at smaller to intermediate body size classes, while additionally including an increase in breadth at megaherbivore size classes, reflecting their distinct dietary generality [94,126]. We observe that when consumers adaptively forage under the conditions of a nonlinear mass-breadth relationship, the dietary generality of megaherbivores appears to erode the probability of survival at intermediate size-classes ($10^4 - 10^6$ g; Fig. 3.4H). This effect occurs because it is these size classes with the greatest dietary constraints, reducing their ability to avoid overlap with the more starvation-resistant megaherbivores. While contemporary sub-Saharan African mammalian communities have retained a size-diversity

similar to Pleistocene systems, the diversity of megaherbivores is now understood to have steadily declined after the end of the Miocene ca. 5 Myrs BP [127, 128], correlating with an increase in atmospheric pCO_2 and the spread of C_4-photosynthetic grasslands [128, 129]. With elevated Pliocene megaherbivore diversity, intermediate-sized ungulates had diets that were more mixed along the browser-grazer spectrum than they are today [128, 130].

The results of our approach point to potentially important changes in competitive forces during this transition from a community with diverse megaherbivores and intermediate-sized mixed-feeders to one with fewer megaherbivores and intermediate-sized mixed-feeders [128]. Specifically, if there are plentiful megaherbivores with broader diets, the more constricted diets of intermediate-sized herbivores (Fig. 3.4H) results in lower survival, building a case for increased selection pressures for mixed-feeding foraging strategies at these intermediate size-classes prior to 5 Myrs BP. In contrast, if megaherbivores are rare, such that the negative mass-breadth relationship better approximates the realized structure of the food web, the more constrained diets of intermediate-sized herbivores can achieve higher survival, lowering selective pressures on mixed-feeding strategies, potentially explaining their decline alongside decreases in megaherbivore diversity [130].

3.4.3 Lesser competitors escape competition through adaptive foraging and structural insulation

When foraging is adaptive, trophic overlap is itself a dynamic quantity that changes with time and context. As the competitive pressure experienced by consumers changes, consumers in turn alter their foraging behaviors, which alters the competitive pressure for shared resources and the resulting resource and consumer population densities. If a consumer is a non-specialist with more than one potential resource, the profitability of one resource may exceed the average profitability such that its proportional contribution will increase (see Eq. 4.5). In contrast, a specialist consumer with one resource cannot alter its proportional contribution regardless of competitive pressure. We evaluate the dynamic nature of diet overlap by calculating the Pianka Index [131] over time (Eq. 3.6). This measure provides a symmetric pairwise comparison of resource utilization and returns an overlap measure between 0 (no overlap) and 1 (complete overlap) for consumers in the community with respect to their shared resources. The dietary overlap between species i and k across

m resources, O_{ik}, is therefore measured as

$$O_{ik}(t) = O_{ki}(t) = \frac{\sum_j^m p_{ij}(t)p_{kj}(t)}{\sqrt{\sum_j^m p_{ij}(t)^2 \sum_j^m p_{kj}(t)^2}}, \tag{3.6}$$

where p_{ij} and p_{kj} are the proportional contribution of resource j in the diets of consumers i and k, respectively. An increase in this overlap index, $O_{ik} \to 1$, therefore means that consumers i and k have diets that are more similar – in terms of shared foods and in terms of the proportional contribution of shared foods – whereas an overlap index, $O_{ik} \to 0$, implies less overlap. As such, dietary overlap provides insight into the level of competitive pressure a species faces at a given moment in time, though it does not contain information regarding which species has a competitive advantage or which species altered their diet to reduce or promote overlap.

We examine changes in dietary overlap by evaluating to what extent consumers share their resources with competitors at both the beginning of a simulation and after the system reaches steady state. This comparison allows us to determine whether an herbivore population increases or decreases its dietary overlap relative to the initial state. We observe a range of mass-specific differences in overlap dynamics, depending on the mass-breadth structure of the food web (Fig. 3.5). When herbivores are fully connected, nearly all consumers face increases in dietary overlap and are then extirpated from the system, except for the largest size-class, which decreases its overlap and survives (Fig. 3.5A). As complex trophic structures are integrated, smaller body size classes avoid extirpation by altering their dietary overlap. When structure follows a positive mass-breadth relationship, we observe that only small consumers experience an increase in their niche overlap (Fig. 3.5B). This occurs because a positive mass-breadth relationship requires that smaller consumers have lower dietary breadth. The increased specialization of these size classes therefore limits the opportunities of these species to alter their diets in order to escape competition from larger consumers.

Structures that follow both negative and nonlinear mass-breadth relationships assume that the diet breadth of the smallest herbivores is large (Fig. 3.5C,D). Smaller species are thus imbued with an increased range of potential dietary adaptation, able to alter their diets across a larger combination of potential dietary strategies in order to minimize overlap with competitors, promoting coexistence. As such, the increased plasticity of small herbivore diets introduces 'dietary refugia', enabling them to escape the exclusionary effects

of competing with larger, stronger competitors. While larger species tend to dominate their resource base, if smaller species retain enough plasticity in their potential diets, they are able to consolidate their foraging efforts to those resources of lesser importance to superior competitors. A positive change in dietary overlap thus corresponds with lower a lower probability of survival (Fig. 3.4). This allows us to dissect the effect of increased megaherbivore dietary breadth on intermediate-sized herbivores: while these starvation-resistant giants alter their diets to avoid overlap, intermediate-sized herbivores are more constrained, such that the change in overlap attains concave-down geometry across log body mass (Fig. 3.4D).

3.4.4 Dietary overlap reduces community richness

If niche overlap drives competition among herbivores, it follows that reductions in dietary overlap via adaptive foraging are expected to increase species persistence generally, promoting community richness. By measuring community-wide dietary overlap, or the average steady state overlap across species as a function of the proportion of the community that survives, we can assess community-scale effects of both adaptive foraging and positive, negative, and nonlinear mass-breadth structures. Previous investigations have shown that size-structured adaptive food webs have reduced robustness with increased connectivity between species [132]. Similarly, we observe that in a fully connected system, because the largest consumer monopolizes the resource landscape, all other species are driven extinct (Fig. 3.6A). With the introduction of structural complexity, we observe a strong negative relationship between community richness and average steady state overlap, the slope of which depends on the mass-breadth relationship. When the mass-breadth relationship is positive, small increases in average dietary overlap drive smaller decreases in steady state community richness, resulting in a shallower slope (Fig. 3.6B).

If structure is assumed to result from either negative or nonlinear mass-breadth relationships, we observe two effects: *i*) the overall steady state community richness increases, and *ii*) increases in average overlap drive larger decreases in richness, resulting in a steeper slope (Fig. 3.6C,D). Interestingly, it is the negative mass-breadth relationship that appears to enable richer steady state communities, regardless of overlap (Fig. 3.6C). We suggest that it is the increased ability of smaller consumers to find dietary refugia from their larger competitors that results in increased richness, especially when average dietary overlap is

low. While these benefits are also realized when the mass-breadth relationship is nonlinear, the increased dietary breadth of megaherbivores lowers the diversity of intermediate size-classes, such that community richness ultimately suffers.

The steepening of the negative relationship between mean trophic niche overlap and species persistence is important for our understanding of how structural assumptions facilitate community richness. As seen in Fig 3.6, the negative and nonlinear mass-breadth structural assumptions produce richer communities than does the a positive mass-breadth that is often assumed in food web models. The negative mass-breadth relationship in particular, with it's assumption of low trophic breadth for large herbivores, most consistently produces rich communities. The addition of high trophic breadth for megaherbivores for the nonlinear mass-breadth relationship, in contrast, produces a wider range of outcomes (Fig. 3.6D). The richness of a plant-herbivore system, where competitive exclusion is often the outcome of those with the most constrained yet overlapping diets, is observed to depend on the presence of trophic refugia, particularly for less competitive species.

3.5 Conclusion

Complex ecological systems emerge from networks of interconnected species competing for shared resources and adapting in the face of competitive pressures [88] that are themselves changing through time. While it is well understood how complex ecological systems react to small perturbations [133], how larger disturbances, such as species extinctions, feed back to influence these complex adaptive systems is largely less well understood [89, 99]. Ultimately, ecologists seek to understand the forces that result in diverse communities, where competitive exclusion would be assumed to drive systems towards fewer species and simpler structures – an assumption that of course clearly contrasts with what is observed in nature.

Diverse assemblages of mammalian herbivores have been a defining feature of the Cenozoic, yet how these species operate across a shared resource base is not well understood. We have shown that allometric differences in the processes governing growth, reproduction, and mortality from starvation among competing consumers predicts both macroecological relationships and a strong sized-based competitive gradient, with the largest species generally having a competitive advantage. Our theoretical framework shows that the inclusion of structural complexity that introduces the potential for 'dietary refugia' increases

the potential for coexistence and community richness. The power of these general models is their potential to inform larger-scale trends observed across systems, both past and present. We suggest that our approach may shed light on how megaherbivore dietary generality can influence competition that may shape the selective pressures experienced by intermediate-sized herbivores, and this may have particular relevance for observed changes in sub-Saharan African mammalian communities across the Pliocene [127, 128, 130]. By incorporating process-based energetic constraints regulating plant-resource interactions, our approach may be useful for understanding the governing forces shaping and reshaping mammalian communities across the Cenozoic.

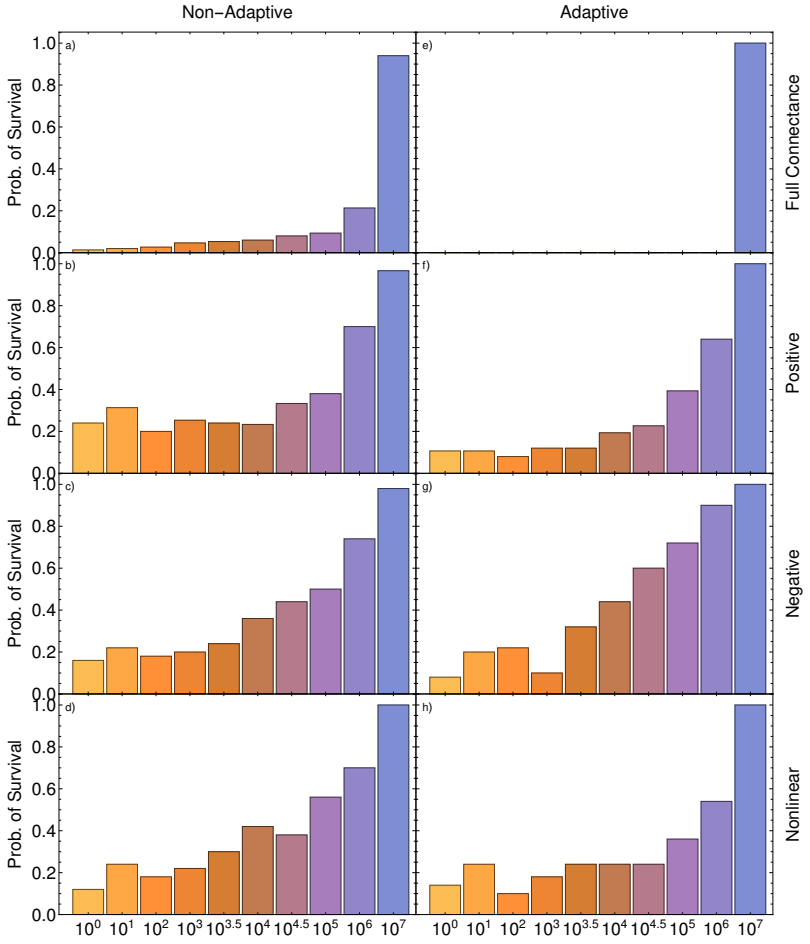

Figure 3.4: The probability of survival as a function of consumer body size. a) Non-adaptive foraging and e) adaptive foraging in a fully connected plant-herbivore system. b) Non-adaptive foraging and f) adaptive foraging in a plant-herbivore system with a positive mass-breadth structure. c) Non-adaptive foraging and g) adaptive foraging in a plant-herbivore system with a negative mass-breadth structure. d) Non-adaptive foraging and h) adaptive foraging in a plant-herbivore system with a nonlinear mass-breadth structure.

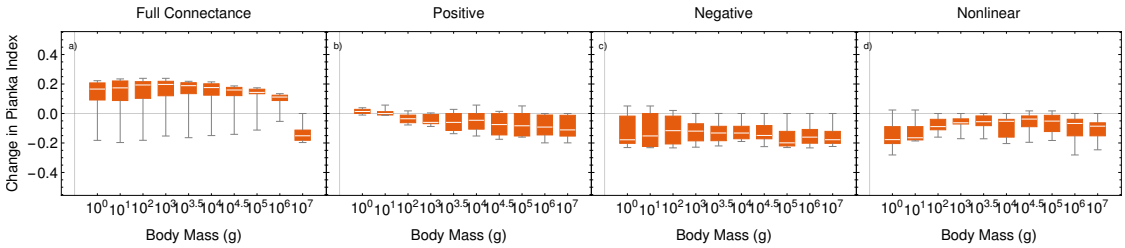

Figure 3.5: The change in the mean Pianka Index value of dietary overlap within community at the beginning of a simulation and steady state, for a a) fully connected plant-herbivore network, and plant-herbivore networks with b) positive, c) negative, and d) nonlinear mass-breadth structures. A change in Pianka Index > 0 denotes an increase in the average level of dietary overlap in a community from the initial state to steady state, whereas a value < 0 denotes a decrease.

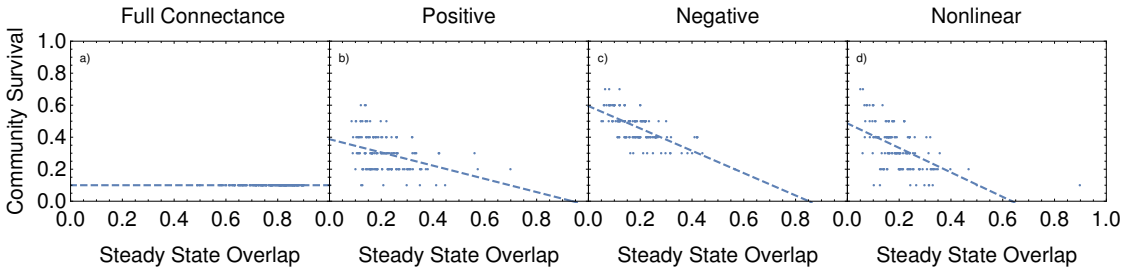

Figure 3.6: The proportion of the herbivore community surviving at system equilibrium as a function of the terminal mean trophic-niche overlap for a a) fully connected plant-herbivore network, and plant-herbivore networks with b) positive, c) negative, and d) nonlinear mass-breadth structures. The negative relationships indicate that higher levels of trophic niche overlap are associated with lower levels of community survival. The flat relationship seen under Full Connectance arises because only the largest herbivores survive in that scenario.

Chapter 4

The Dynamics of Competition Constrain and Explain Macroevolutionary Trends Among Mammalian Communities Across the Cenozoic

4.1 Abstract

Patterns in the distributions of body-mass heavily influence the structure and outcome of competitive dynamics. The herbivore communities of the Cenozoic provide a diverse range of body-mass distributions that allow us to explore the impact of different distributions on competition. Here we investigate mammalian herbivore body-mass distributions through allometric, adaptive, plant-herbivore food-webs over two broad environmental axes: closed vs open environments and humid vs arid environments.

The incorporation of diverse mass-distributions with environmental scenarios provides insight into the relationship between distribution structure and community stability. Our framework demonstrates that broad separation in body-mass increases community stability. It shows that very large gaps in body-size can reverse the normally positive mass-fitness relationship. The distinction between humid and arid environments does not alter the

patterns of herbivore competition that govern community stability. Finally, the distinction between closed and open environments can substantially alter competitive outcomes as closed environments can provide more opportunties for niche partitioning.

4.2 Introduction

Herbivore community dynamics are heavily influenced by competition for resources [82]. The nature and outcomes of these competitive interactions are an important component of the fitness landscape driving long term trends in the composition and functioning of communities over time [134]. Because mammalian vital rates governing population-level processes largely scale with body size [24], the fitness differences that emerge from competitive interactions between species may also retain a certain size-dependency [135]. Importantly, if the effects of competition vary with organismal body mass, the selective potential of the emergent fitness landscape may have particular influence on the forces that constrain the evolution of mammalian size distributions.

Mammalian herbivore communities spanning the Cenozoic (66-0 Myrs BP) provide a diverse set of experiments that test the structure and functioning of these systems across variable climate regimes and environmental conditions that cannot be replicated by looking at modern systems alone [136]. The long timescales by which changes in paleo-communities can be evaluated is particularly important for understanding the conditions and consequences under which diverse assemblages of species coexist, as well as long-term trends in their compositions. A defining trend characterizing the evolution of Cenozoic mammalian communities is the shifting nature of body size distributions, a consequence of both morphological niche expansion following the K-Pg extinction [137], as well as from changing resource environments driven by climate change [29, 138]. The evolution of mammalian body size during this period can be characterized by a rapid expansion in maximal sizes throughout the Paleocene and Eocene, followed by a more gradual increase during initial coolhouse conditions (35-40 Myrs BP) [137,139,140]. The tendency for lineages to increase in body size, known as Cope's Rule [141], is a well-known macroevolutionary trend in both terrestrial and aquatic systems [137,142,143]. The underlying forces governing Cope's Rule, however, from the physiological rates that constrain organismal life-histories, to the changing fitness landscapes associated with different body sizes, are not well understood. Because

body size scales metabolism, growth, energetic storage, and species interactions [144], deciphering the population-level consequences of body size may shed light on the constraints shaping the structure and functioning of mammalian communities over macroevolutionary timescales.

The factors underlying patterns of body-mass distribution in mammalian communities have undergone considerable debate [145]. Explanations range from constraints due to the energetic limitations of resource assimilation and reproduction [90], differences in dispersal abilities [146], different pressures from inter-species interactions [147], and discontinuities in landscape geometry and disturbance regimes [148]. While there is supporting evidence for all of these explanations to play contributing roles in the evolution and maintenance of the size-structure of communities [145], we lack a coherent framework for assessing the general role of population-level energetic constraints and interspecific interactions. By leveraging process-based models that capture the energetic trade-offs contributing to population growth and regulation, combined with a macroevolutionary perspective of mammalian community change over time, a deeper understanding of the mechanistic forces governing the structure of mammalian communities stands to be gained.

Here we examine the relationship between changing body-mass distributions and the resulting stability of associated body size classes within a single locality, across a range of environmental and ecological conditions throughout the Cenozoic. We build upon the integration of an n-dimensional plant-herbivore food-web model [135] with process-based allometric energetic constraints [103] to examine the influence of mammalian body mass distributions from the Linxia Basin in Gansu, China [149], as they evolved and assembled from the Oligocene to the Pleistocene. This time span witnessed significant uplift of the Tibetan Plateau resulting in dramatic shifts in climate and a vegetative environment transitioning from closed to open, to downstream effects on the structure of local mammalian communities. By understanding how these mammalian body size distributions impact the dynamic outcomes that emerge from competition between co-occurring herbivorous species, may provide general insight into the forces that give rise the distinctive body size distributions of mammalian communities.

Our results reveal four key insights into the role of competition dynamics in driving the nature of mammalian body mass distributions across the Cenozoic. First, we demonstrate that sufficiently large gaps in body-mass distributions can provide fitness advantages to smaller consumers, allowing these gaps to be maintained once created. Second, we show

that the distinction between arid and humid environments alone, as represented by changes in plant biomass, are not expected to significantly influence the outcomes of herbivore competition. Third, we show that the distinction between closed and open environments, as represented by changes in the resolution of resource partitioning, significantly alters the outcomes of herbivore competition. Finally, we demonstrate that the average mass gap between consumers directly influences the survival of herbivore communities. We suggest that understanding the energetic constraints of species' populations in the context of competition within a shared resource environment, provide direct insight into the macroevolutionary forces constraining mammalian size distributions across the Cenozoic.

4.3 Model Framework

4.3.1 Consumer-resource dynamics

We construct a bipartite network of interacting herbivores and their plant resources, where the trophic structure of the network and the proportional contributions of resources to consumer diets are given by the weighted adjacency matrix A. As such, a given element of A, A_{ij}, is given a value > 0 if the herbivore i consumes resource j, and a value of zero otherwise, where the proportional contributions of resources j in the diet of consumer i is constrained by $\sum_j A_{ji} = 1$. The available resources R_j (g/m^2) grow logistically with intrinsic growth rate α_j to a carrying capacity k_j, and decline due to consumption by herbivore consumer populations C_i (g/m^2) (Eq. 4.3). Consumed resources fuel both consumer growth and reproduction. The rate of consumption to fuel reproduction is proportional to resource density and is given by $\lambda_j(R_j)/Y_{ij}$, where $\lambda_i(R_j)$ is the consumer growth rate and Y_{ij} is the consumer yield coefficient, or the grams of consumer i produced per gram of resource j consumed. The consumer's growth rate with respect to a particular resource j, $\lambda_i(R_j)$, follows Michaelis-Menton (Type II) kinetics as a function of the resource density R_j, where the maximum growth is $\lambda_i^{\max}$ and the resource half-saturation density is $\hat{k}_j = k_j/2$, such that

$$\lambda_i(R_j) = \lambda_i^{\max}\left(\frac{R_j}{\hat{k}_j + R_j}\right). \tag{4.1}$$

While the consumer population density grows as the sum of rates $\lambda_i(R_j)$ taken across consumed resources, we assume for now that consumer mortality is a function of starvation, where the rate of starvation for consumer i on resource j

$$\sigma_i(R_j) = \sigma_i^{\max}\left(1 - \frac{R_j}{k_j}\right). \tag{4.2}$$

As such, the rate of starvation increases as a consumer's suite of resources become scarce. In this context, $\sigma_i^{\max}$ is the maximal rate of starvation for consumer i that occurs when the environment is devoid of resources. See Table 4.1 for a description of parameters.

The full system describing n consumers interacting with m resources, such that species richness $S = n + m$, is given by

$$\begin{aligned}\frac{\mathrm{d}}{\mathrm{dt}}C_i &= \sum_{j=1}^{n} A_{ij}\lambda_i(R_j)C_i - \sum_{j=1}^{m} A_{ij}\sigma_i(R_j)C_i,\\ \frac{\mathrm{d}}{\mathrm{dt}}R_j &= \alpha_j R_j\left(1 - \frac{R_j}{k_j}\right) - \sum_{i=1}^{n} A_{ij}\frac{\lambda_i(R_j)}{Y_{ij}}C_i.\end{aligned} \tag{4.3}$$

The rate laws describing resource consumption as well as consumer growth and mortality all vary as a function of consumer body mass M_i, where the consumer is assumed to be a mammalian herbivore, and the resource j is an unspecified plant functional group with characteristic growth rate α_j, carrying capacity k_j, and energy density E_{dj}. E_{dj} then interacts with consumer mass to determine the consumer yield coefficient, Y_{ij}. To examine the dynamics for a particular system, we set the constraints governing resource growth and the body size distribution of the herbivore community (see Supplementary Appendix II). Values of resource reproduction rate α_j and energy densities E_{dj} are drawn uniformly from the rates found in browse and graze plants [104, 105] (see Supplementary Appendix II). Resource carrying capacities are established by first assuming a community-level carrying capacity K, where a subset of resource-specific carrying capacities are randomly chosen such that $\sum_j k_j = K$ for resources $j = 1...m$. Because we assume that consumer densities that fall below $C_i = 10^{-10}$ are functionally extinct and excluded from the system, the final body mass distribution may not reflect that used to initiate community dynamics.

Given the assumption of adaptive dynamics, consumer species dynamically adjust the effort associated with a particular plant resource to maximize profitability, defined as the net reproductive output produced by a particular diet. This means that the proportional contribution of a given resource increases if the profitability associated with a focal resource

Table 4.1: Model parameters and values/units

Definition	Parameter	Value/Units
Resource j		
density	R_j	g/m^2
reproduction rate	α_j	1/s
carrying capacity	k_j	g/m^2
energy density	E_{dj}	J/g
Consumer i		
density	C	g/m^2
body mass	M_i	g
max reproduction rate	$\lambda^{\max}$	1/s
yield coefficient	Y_{ij}	none
natural mortality rate	μ_i	1/s
starvation rate	σ_i	1/s
foraging effort	A_{ij}	$(0, 1)$
learning rate	G_i	1/s

j if

$$\lambda_i(R_j)C_i > \sum_{l=1}^{m} A_{il}\lambda_i(R_l)C_i, \tag{4.4}$$

and decreases otherwise [88, 89]. For consumer i, the rate at which this adaptation occurs is governed by the learning rate G_i, where the dietary contribution of resource j changes as

$$\frac{\mathrm{d}}{\mathrm{dt}}A_{ij} = G_i A_{ij}\left(\lambda_{\mathrm{i}}(R_j)C_i - \sum_{j=1}^{m} A_{ij}\lambda_i(R_j)C_i\right). \tag{4.5}$$

As consumer and resource densities change over time, the diets of consumers change as well. Because resources that become heavily consumed by a diversity of consumer species will suffer significant mortality, reducing their densities, this adaptive foraging dynamic will tend to result in consumers with steady state diets that minimize competitive loads. Throughout, we examine the outcome of community dynamics when adaptive foraging alters diets in response to competitive pressures ($G_i > 0$ for consumers $i = 1 : n$), as well as the case where diets are not assumed to change adaptively ($G_i = 0$ for consumers $i = 1 : n$).

4.3.2 Cenozoic size distributions

Specific body mass distributions are integrated into our modeling framework by initiating a simulated community with the same number and size-classes of species represented by

a particular empirical community, where, with respect to the Linxia Basin fauna, are obtained from Ref. 149 (see Table C.2). Because organismal vital rates in our framework are allometric and purely a function of body mass M_i, the dynamical equations for consumers within the community are almost entirely set by size-distributions alone. We assess the body size distributions of six mammalian faunas from the Linxia Basin: the late Oligocene (25 Myrs BP), the mid-Miocene (14.5 Myrs BP), two communities from the late-Miocene (9.5 Myrs BP; 8.3 Myrs BP;), the early Pliocene (5.3 Myrs BP) [150], and the early Pleistocene (2.5-2.2 Myrs BP) [151]. Altogether, mammalian body sizes across these assemblages range from 17 g to 24,030,124 g [149]. The rank-ordered size distributions (cenograms) for each of these communities is shown in Fig. 4.1.

Throughout, we include m resource groups equal to the number of consumers, where a particular resource group is one that may be assumed to include multiple species with similar growth rates, carrying capacities, and energy densities. Resource dynamics require three specific inputs, which we draw from Uniform Distributions about known mean values: those for individual resource carrying capacities k_j, growth rates α_j, and energy densities E_{dj} (see Supplementary Appendix II. These resource traits are altered systematically to account for alternative environmental conditions: open vs. closed, arid vs. humid. Aridity is assumed to determine system carrying capacity k_{system} for plant resources. An 'arid' environment sets carrying capacity to 15000 g/m^2. A 'humid' environment sets carrying capacity to 30000 g/m^2. Openness is assumed to determine potential diet partitioning, as represented by the number of distinct plant resources present in the system. An 'open' environment sets the number of resources to 2/3 the number of consumers. A 'closed' environment sets the number of resources to 4/3 the number of consumers. We assume an interaction structure between herbivores and resources that follows a negative mass-breadth relationship, meaning that the number of resources consumed by a particular herbivore decreases with body size [135] (see Supplementary Appendix V), an assumption closely matching empirical observations of contemporary communities [7,8]. Because the contribution of each resource to the diet of each consumer is dynamic over time (see Eq. 4.5), initial proportional contributions are drawn from a uniform distribution between $[0, 1]$, where they are then normalized to sum to 1 for each consumer. For all analyses, we run 250 replicates. To calculate the probability of survival, W_i, for a particular species i, we evaluate the proportion of replicate communities where the density of that species $C_i(t) > 10^{-10}$ inds/m^2 for all t.

4.4 Results and Discussion

4.4.1 Ecological insights into macroevolutionary trends among mammalian communities

The Cenozoic represents a time of considerable experimentation across diverse mammalian communities evolving under unique environmental conditions [140]. Following the explosion in mammalian diversity and morphologies after the extinction of non-Avian dinosaurs 66 Myrs BP, communities of interacting mammalian species emerged, forming their own unique assemblages over space and time [152, 153]. A number of macroevolutionary trends influenced the nature of these communities, particularly during the first 20 Myrs following the K-Pg extinction [39]. The expansion of maximum body size among both herbivores and carnivores dramatically increased by four orders of magnitude by the mid-Eocene ca. 40 Myrs BP [39]. This trend towards increasing body size over macroevolutionary timescales, known as Cope's Rule [141], diffused across vacant niches left behind by larger dinosaurian clades [137,154], potentially fueled by the increasing competitive advantages associated with starvation tolerance among larger mammalian species [18, 103, 135].

We first evaluate the dynamic properties of mammalian systems from body mass distributions of communities located in the Linxia Basin, Gansu, China [149]. The Linxia Basin assemblages represent seven distinct communities, including the late Oligocene, the mid-Miocene, three from the late-Miocene, the Pliocene, and the early Pleistocene. While understanding temporal dynamics across these systems is clearly of interest, we first evaluate these communities without respect to temporal trends, treating each community as a separate experiment in mammalian community organization. In this way, we aim to investigate whether there are general properties characterizing the dynamics of mammalian communities writ-large, across the diversity of environmental, ecological, and evolutionary conditions that led to their assembly over the course of the Cenozoic.

Our community-scale consumer-resource model allows us to evaluate the dynamic outcomes that emerge across a suite of herbivorous species representing a particular body mass distribution competing for resources [135]. These body mass distributions reconstructed from communities within the Linxia Basin represent snapshots of the community from the Oligocene to the Pleistocene, and can depicted by their cenograms, or rank-ordered size distributions. By using the different body mass distributions of species in the Linxia Basin to parameterize our food web framework [149], we can directly evaluate how the effects of

competition impact species falling into different body size classes, and to what extent this might influence the macroevolutionary forces at work in the community.

Our food web framework combines process-based energetic relationships (see [103]) to parameterize rates of herbivore reproduction, consumption, and mortality as a function of consumer mass M_i in a shared resource environment [135]. As consumers compete for a set of shared resources, we evaluate survival probabilities for each consumer i, W_i, defined as the probability that a species in a given size class maintains a steady state population density above the minimum threshold over time (see Methods), evaluated across a series of independent trials ($x = 250$). This survival probability describes the robustness of a species' population with respect to its competitive environment, and can therefore be understood as a component of fitness. Because species are described only by their body mass, the probability of survival can be directly equated with a particular size class, over which community-level patterns are evaluated.

We observe that the Linxia Basin communities across the Cenozoic, regardless of time period, reveal strong competitive advantages associated with larger body sizes (Fig. 4.1). The competitive advantage associated with increasing size is apparent even when community body size distributions are randomly generated [135], and emerges from the increased ability of larger organisms to withstand periods of resource scarcity. This starvation tolerance, or fasting endurance [43], has long been thought to influence mammalian macroevolution, and may directly contribute to the forces governing Cope's Rule [18]. Because the per-capita growth of each consumer is due solely to the competing effects of population growth and mortality from senescence and starvation, the increase in survival associated with larger sizes observed here originates entirely from the competitive advantages provided by increased starvation tolerance [135].

While the survival advantages associated with larger body sizes effectively cloud smaller-scale patterns, we can examine such patterns by calculating the change in expected survival of a consumer i associated with small changes in body mass, which is a measure of the relative strength of selection $\psi_i(M_i) = \partial W_i/\partial M_i$. As such, we would expect selection to favor larger body sizes if $\psi(M_i) > 0$ and smaller body sizes if $\psi(M_i) < 0$ with respect to a particular mass M_i, where the relative magnitude of ψ provides a measure of the steepness of the selection gradient. We observe that, for all of the Linxia Basin communities (Fig. 4.2A), the strength of selection is more often positive but can also assume negative values across the range of mass classes. In other words, while the selection surface is generally

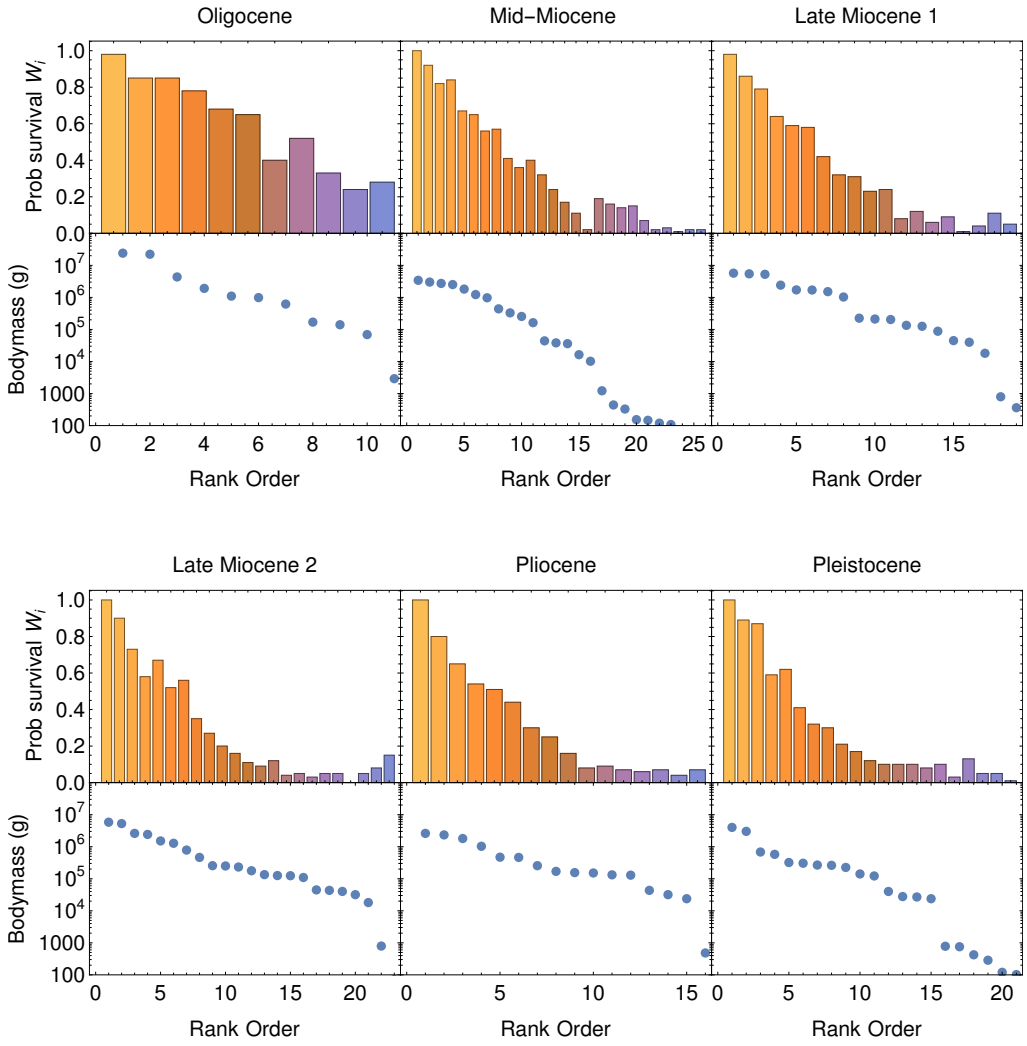

Figure 4.1: Mammalian communities from the Oligocene to the Pleistocene. Top rows: Survival probabilities W_i as a function of rank-ordered body-size, where larger sizes species generally have increased W_i. Bottom rows: Herbivore mass as a function of rank-order (cenograms).

biased towards the fitness advantages associated with larger body sizes, it is not always the case.

To understand under what conditions smaller body sizes are favored, such that $\psi(M_i) < 0$, we examine the strength of selection as a function of the body size gap separating each mammal from its nearest-sized neighbor. Specifically, we evaluate the strength of selection

with respect to the smaller-sized organism for each pair of mass-adjacent species, where larger gaps correlate with larger vertical spacings within a cenogram. When examined in this way, we observe that when the body size gap is small to intermediate in size, $\psi(M_i)$ is typically positive with respect to the smaller species of the pair (blue points in Fig. 4.2B) and occasionally negative (red points in Fig. 4.2B). In contrast, for large gaps in body size, $\psi(M_i)$ is always negative with respect to the smaller species of the pair. In other words, while the general tendency of the fitness surface inferred from our consumer-resource model favors larger body size, if the gap between body sizes in the community is very large, the fitness surface exclusively favors smaller body sizes. Within our framework, dietary overlap decreases with differences in body-mass, such that the competitive pressure between two mass-adjacent herbivores will be lower if the body size gap between species is larger. This reduction in competitive pressure, in turn, promotes the probability of survival of the smaller species, resulting in a negative $\psi(M_i)$.

The expansion of body sizes throughout the Cenozoic is perhaps the largest-scale trend associated with mammalian evolution, however it is not the only emergent pattern. Alongside the expansion of body size, there is a less dramatic but prominent feature of Cenozoic mammalian body mass distributions, sometimes referred to as the 'hole in morphospace' first documented by Alroy (1998) [137]. This hole – describing body sizes ranging from $10^3 - 10^4$ grams – documents the appearance of strong bimodality in mammalian body size distributions that first appears at ca. 40 Myrs BP [137], and has been maintained since, apparent across multiple continents [39]. In contemporary sub-Saharan African systems, the presence of two modes separated by this gap is present across multiple spatial scales [155]. One can either view this body size gap as the product of two body size optima – one at a 100 g mode and one at a larger-sized mode – or as a region of morphospace that is decidedly sub-optimal. The specific forces giving rise to this sub-optimality are unknown [155], but have been hypothesized to include decreased abilities of herbivores in this size class to hide or flee from predators [139], or perhaps represents a lower limit of digestive efficiencies, particularly for ruminants [156]. Importantly, the absence of a body size gap prior to 40 Myrs BP suggests that these body sizes were not always sub-optimal, though once the gap emerged, its maintenance became a defining characteristic of mammalian communities.

In the Linxia Basin, the body size gap is clearly evident across all temporal snapshots, from the Oligocene to the Pleistocene (Fig. 4.2A), and as observed in North American communities, ranges from 5×10^3 to 8×10^4 g Our finding of a negative $\psi(M_i)$ associated

with gaps of this size suggests that, when a gap is formed and regardless of its cause, if the size of the gap is above a particular threshold, the competitive forces captured by our consumer-resource framework will promote its maintenance. While our approach cannot provide insight into the cause of this 'hole in morphospace', we suggest that its maintenance over the 40 Myrs since its origination may be due to the relative fitness differences associated with smaller body sizes that arise when dietary overlap is lowered – that is, after the gap is formed. In diverse contemporary communities, smaller herbivores face maximal predation pressure at sizes near this morphospace gap [2], a product of the nested hierarchy of trophic interactions among mammalian predators [52]. Perhaps coincident with the hypothesized physiological limitations associated with fleeing and hiding [39] as well as digestive constraints [156], these factors create enough of a fitness disadvantage to generate a gap large enough that competitive interactions between species enable its maintenance by way of the selection differential observed here.

It is well known that the strength of selection for a particular trait is proportional to the rate of trait change within a population [157,158]. In the context of our analysis, this means that for a species of size M_i, the trajectory of its size evolution $\mathrm{d}M_i/\mathrm{d}t \propto \partial W_i/\partial M_i$. An additional observation pointed out by Alroy [137] from the body size trajectories of North American mammalian clades is the existence of two body size attractors that may give rise to the the small- and large-sized optima separating the noted hole in morphospace. These attractors are defined with respect to changes in mass over time across different mammalian lineages, as a function of the originating mass [137], resulting in body size modes at the lower end $M_i \approx 10^2$ g and at the higher end $M_i \approx 10^7$ g. Between these attractors, the maximal rate of body mass increase over evolutionary time is at $M_i \approx 7.53 \times 10^4$ g. Applying the proportional equivalence of observed rate of change in body sizes, $\mathrm{d}M_i/\mathrm{d}t$, with our estimated strength of selection $\psi(M_i)$, we next examine whether maximum average rates of within-lineage body size evolution correlate with predicted peak selective strengths.

Predicted selection strengths generally decline as a function of body mass, and as we have observed are a mixture of positive values associated with fitness advantages with increased size, and negative values associated with fitness advantages with decreased size. Accordingly, if we examine the average change in ψ over mass (accounting for only positive values), we obtain a negatively sloped function over mass $\bar{\psi}(M_i)$. Deviations above $\bar{\psi}(M_i)$ point to body sizes where the strength of selection is greater than expected for a given body mass. By examining $\psi(M_i) - \bar{\psi}(M_i)$, we observe two maxima on either side of the body

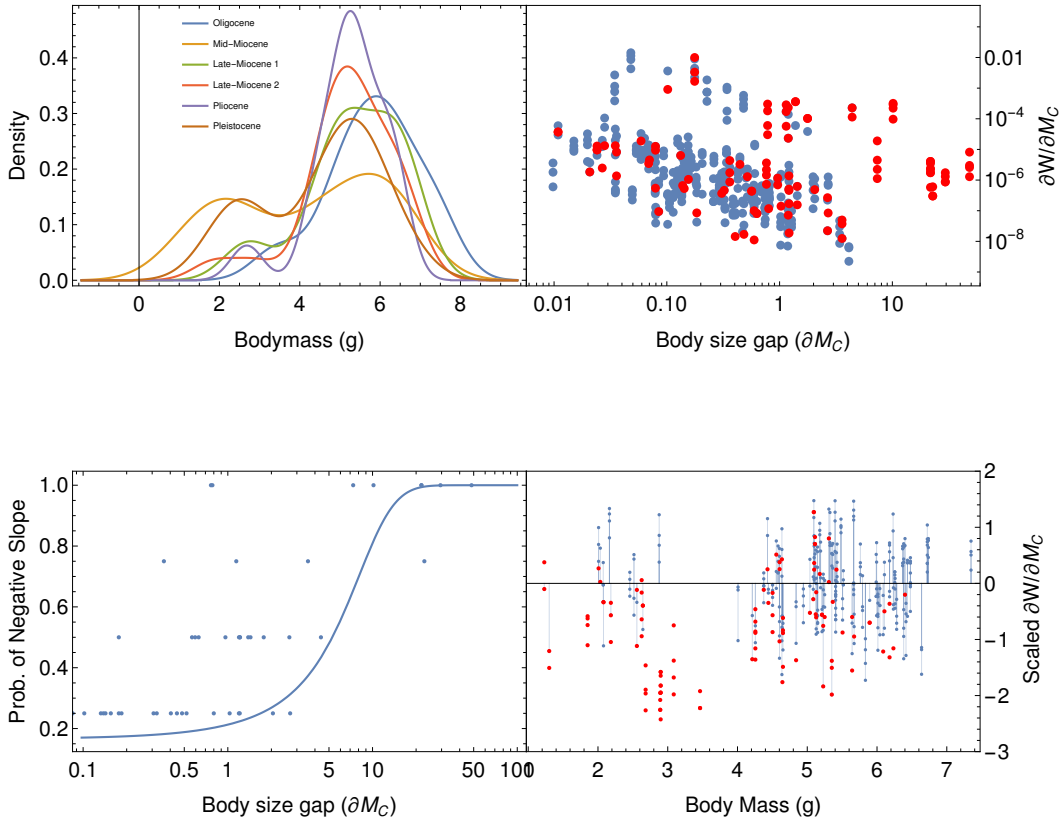

Figure 4.2: Top Left:The distribution of body masses in each era. The bimodal structure is consistent but the intensity varies by community. Top Right: The slope of the fitness surface as a function of the gap in body-mass between consumers. Blue dots show fitness increasing with mass. Red dots shoe fitness decreasing with mass. Bottom Let: The probability of fitness decreasing with body-mass (red dots from the top right panel) as a function of the body-mass gap between consumers. Bottom Right: Blue dots: Positive residuals from the slope of the fitness surface as a function of consumer body-mass. Red dots: Negative slopes.

size gap, occurring at $M_i^{\text{low}} \approx 160g$ and $M_i^{\text{high}} \approx 160,000g$ (Fig. 4.2D). That we obtain maximal relative selection strengths at body sizes where the rate of body size evolution is also maximized suggests that the dynamics of competition described in our framework may have played an important role in the evolutionary forces giving rise to mammalian communities across the Cenozoic.

The macroevolutionary dynamics that emerge from competitive interactions across body sizes also interact with environmental conditions. The 'hole in morphospace', for example,

is particularly associated with open environments [159]. Whether and to what extent environmental conditions influences the outcome these competitive interactions is important to understand.

4.4.2 Trends in the Linxia Basin across the Cenozoic

The Linxia Basin of China sits on the Northeastern edge of the Tibetan Plateau [149, 150]. The location is noted for its deposits of large mammal fossils from the Oligocene to the Pleistocene, particularly its diversity of fossil rhinoceros taxa, both from the True Rhinoceroses (*Rhinocerotidae*) and the relatives such as *Paraceratherium* [150]. The Tibetan Plateau saw substantial uplift over the course of the Cenozoic and this is thought to have driven environmental change in the region. The late Oligocene ecosystem is thought to have been an arid woodland, [149] which, by the Mid-Miocene, had become significantly more humid. After the Mid-Miocene, however, the region became colder and drier over time, giving rise to major expansions of grasses and grassland habitats [129]. By the early Pleistocene, the Linxia Basin had become an open steppe environment with some brush and occasional patches of woodland [149].

A distinct faunal procession accompanies the environmental change brought on by the uplift of the Tibetan Plateau [150]. The Oligocene fauna are dominated by Perissodactyls, notably Chalicothere taxa and the giants *Dzungariotherium orgosense*, *Paraceratherium yagouense*, as well as Creodont predators. Rhinoceros genera (*Rhinocerotidae*) remain abundant in the herbivore communities through most of the transition from Oligocene to Pleistocene. The diversity of Rhinoceros taxa is particularly noteworthy in the Late Miocene, where we also see the arrival of equids [150]. During the Pleistocene, there is an increase in carnivore diversity and abundance, as well as the arrival of more familiar forms including the giant horse (*Equus*) and ancestors of the woolly Rhinoceros (*Coelodonta*) [150]. The punctuated transition from woodland to arid steppe with its shifting herbivore community, dominated by Perissodactyls, provides a testing ground for examining the influence of environmental change on the effects of herbivore competition.

We address environmental change in the context of our model framework in two ways: we assume that *i*) the arid-humid gradient correlates with increased productivity, and *ii*) the open-closed vegetative gradient correlates with an increase in the functional diversity of resources. While the link between the arid-humid transition and productivity is well known and oft-assumed in environmental reconstructions of past climate [160], and we incorporate

these effects by lowering the carrying capacity in more arid environments by 50% (see Supplementary Appendix III). While we do not know the exact quantitative nature linking estimates of aridity in the paleorecord to estimates in carrying capacity used in our model, understanding the magnitude and direction of how a 50% change in the carrying capacity influences our results enables a qualitative understanding of the effects of environmental change on model results.

The increase in functional resource diversity along an open grassland to mixed woodland gradient is perhaps more ambiguous, though we emphasize that it is the effect of potential resource partitioning from the perspective of the herbivore community that is most relevant to our approach. Simply stated, our assumption here incorporates the idea that in increasingly segmented mixed woodlands, there exists a mosaic of micro-environments that distinguish the diets of co-occurring herbivores. This is supported, in part, by the association found between herbivore diversity and vegetation structural diversity prior to the terminal Pleistocene extinctions [161]. In contrast, we assume that open grassland environments – while potentially hosting a large diversity of plant species – enable less dietary segregation between co-occurring herbivores, supported by observations in the East Africa [7, 8]. We incorporate the increased functional diversity of closed woodlands by increasing the number of resource groups by 33%.

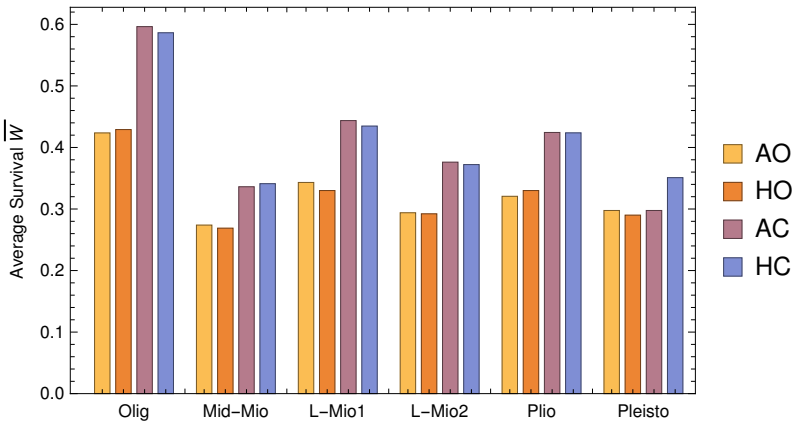

Figure 4.3: This shows the proportion of surviving species in a community over the four environmental scenarios. A-arid, H-humid, O-open, C-closed. The closed-open distinction drives differences in survival rates across communities.

Across all temporal snapshots of the Linxia Basin, we find that changes in productivity (by way of altering the carrying capacity) do not have significant effects on fitness averaged

across body size $\overline{W}$ (Fig. 4.3). This can be understood by observing that changes to both carrying capacity and plant resource growth rates scale linearly with changes in steady state densities across consumer body mass, as is observed 2-dimensional consumer-resource models [103]. Because changes in carrying capacity do not impact the dynamics of competition, the cumulative effect on survival across body mass is negligible. In contrast, the increased functional diversity of closed woodlands does have a significant effect, serving to increase $\overline{W}$ regardless of productivity (except for the Pleistocene Linxia community, where only the higher productivity associated with humid conditions enables increased $\overline{W}$ for closed environments (Fig. 4.3). Increasing the number of plant resources provides more opportunities for herbivores to partition resources into minimally overlapping diets, generally promoting the probability of survival.

By incorporating insights gained from paleoenvironmental reconstructions of the Linxia Basin community, we next apply the correct environmental conditions to each time period and evaluate temporal trends in community dynamics from the Oligocene through the Pleistocene. The Linxia Basin region maintained an approximately humid-closed environment until the late-Miocene, at which point the system transitioned to and maintained an arid-open environment up to and throughout the Pleistocene. [149]. Applying the effects of these environmental reconstructions (Fig. 4.4) consistently produces communities with $\overline{W} \approx 0.2-0.5$, with the exception of the Oligocene which has higher average survival. While it might be expected that closed environments would produce an increase in the average survival for both the Oligocene and Mid-Miocene, this does not occur due to differences in the size-structure of the Mid-Miocene community. These differences may also be due to the large difference in the number of species documented in the late Oligocene (11) versus the mid-Miocene (26), and in particular the representation of smaller size-classes. As such, the closed environmental conditions applied here is on par with open environments associated with other eras (Fig 4.3). At this very general scale of averaged fitness across body sizes, it is therefore clear that the Oligocene community stands in sharp contrast to those from the mid-Miocene through the Pleistocene.

The expansion of open habitats is one of the major transitions of the Cenozoic [129]. Open habitats begin to form globally in the late Paleogene but do not become a significant feature of landscapes until the early Miocene [162]. In China, open-habitats form first as *Ephedra*-dominated systems in the northwestern and central regions during the Paleogene while grasslands do not become widespread until the middle to late Miocene [163]. This

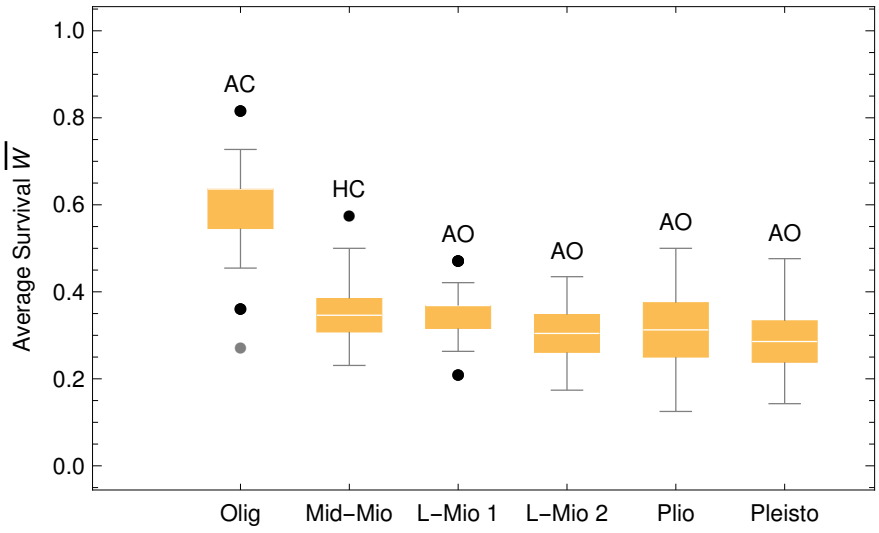

Figure 4.4: The average survival rate of each community in its historical environmental context through the transition to open environments. A-Arid, H-Humid, C-Closed, O-Open

transition from closed to open systems drives changes at the community and mass-specific levels. At the community level, the transition increases the overall competitive pressure experienced and, barring alternative mechanisms for diet partition, reduces average survival. At the mass-specific level, the loss of medium-sized herbivores reduces the competitive pressure felt by small sized herbivores, increasing survival probabilities for these size classes.

To assess the role of mass-dependent patterns differentiating Linxia Basin communities over time, we assess average fitness of the community as a function of the slope of each temporal cenogram. The cenogram slope describes the evenness or unevenness of the body size distribution of species within the community. A shallow slope means that there is a more even uniform distribution of species across body sizes, wheres a steep slope implies that there are large gaps between mass-adjacent species, such that the composition is uneven. When combined, we observe that the fitness-cenogram slope relationship across the entire span of body sizes (Fig. 4.5A) is roughly positive ($R^2 = 0.72$), with the Oligocene community as an outlier, driving the bulk of the relationship. The positive relationship between the cenogram slope and average fitness becomes more apparent when assessed across just large-bodied species ($M_i > 8000$ g), with the Oligocene community and to some extent the

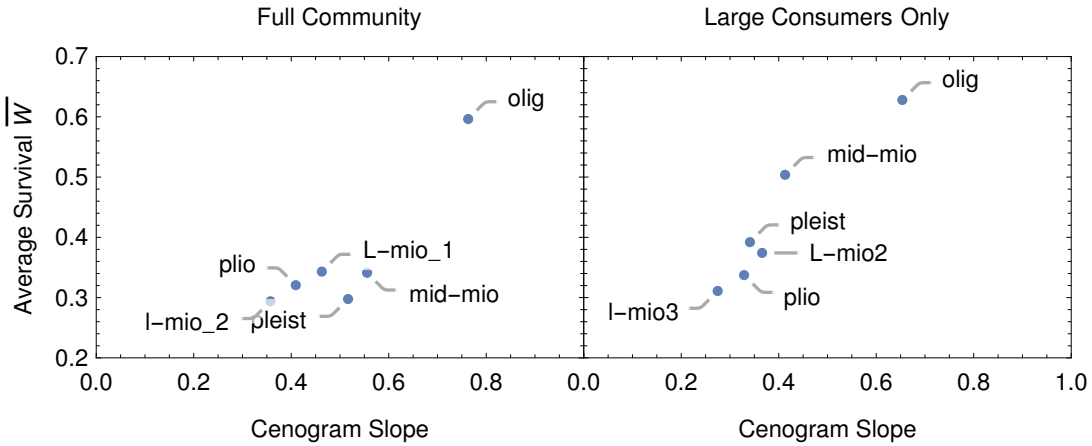

Figure 4.5: The relationship between cenogram slope and community survival rates. Left: Full cenogram slope and survival rate. Right: Large herbivore cenogram slope and survival rate. Steeper slopes, representing larger gaps in mass, are associated with higher rates of community survival.

mid-Miocene community, standing apart from the late Miocene to Pleistocene systems.

The Oligocene system is thought to have been and arid woodland, characterized by a general absence of smaller herbivores and the presence of two paracerathere megaherbivores [149]. These differences, and especially the extreme body sizes of the paraceratheres, serve to create a much steeper cenogram slope, documenting the uneven nature of the body size distribution of the Oligocene community. Additionally, the lack of small herbivores removes the least competitive members of the community, increasing the ability of those herbivores present to minimize competitive overlap, promoting fitness across the board. The faunal community shifts significantly through the transition to the mid-Miocene. Both paracerathere species are lost and the proboscidean community (particularly *Gomphotheriidae*) expands. Where the Oligocene fauna lacked small herbivores completely, the mid-Miocene fauna contain many such species [149]. Combined with the effects of higher diversity closed environments, and despite the fact that the Oligocene and mid-Miocene communities have very distinct body size distributions, the unevenness and average fitness of the large size classes in these communities set the Oligocene and mid-Miocene apart from those present in the Linxia Basin later in the Cenozoic.

The expansion of open environments through the Cenozoic, with their reduction in opportunities for dietary partitioning, may have motivated novel mechanisms for partitioning diets within those open habitats, such as foraging by sward height. These results may also help to explain the weak or non-scaling of body-mass with the grazer-browser continuum of herbivory [164]. Two competing herbivore species of similar masses will have similar needs for diet quality. In a mixed environment with access to both graze and browse resources, partitioning resources along the lines of graze and browse allows a reduction in competition without significant body-size evolution or compromising diet quality.

4.5 Conclusion

Plant-herbivore relationships emerge from a complex suite of trait interactions between consumers and their resources. While the central drivers of these relationships, such as nutritional content, plant secondary compounds, and consumer mouth morphology [12] and gut physiology [14], have received broad attention, how these traits influence interactions is poorly understood. The inability to predict dietary niche from traits and context also prevents the anticipation of food web structure from component species, an important goal of ecology and the future of conservation as well as our understanding of communities from the past.

To unravel the web of trait interactions governing plant-herbivore food-webs, we first need to understand herbivory at the broadest trait levels: herbivore mass, resource availability, and the resolution of diet partitioning made possible by the plant community. By exploring that base-layer of herbivore diet we gain insight into the mechanisms of coexistence of diverse herbivore communities throughout the Cenozoic and build a foundation towards a more predictive ecology. Moreover, understanding how food webs rewire and adapt under novel conditions is vital for predicting how consumer systems will respond to environmental change. In this sense, understanding how the internal mechanisms regulating competitive forces between species, and how these forces might influence evolutionary trajectories, is needed to anticipate how mammalian communities will respond to a changing world.

Appendix A

Supplementary Information: On the Dynamics of Mortality and the Ephemeral Nature of Mammalian Megafauna

A.1 Appendix I: Natural mortality

The natural mortality rate is obtained by first assuming that the number of surviving individuals in a cohort N follows a Gompertz relationship [33], where

$$N = N_0 \exp\left(\frac{q_0}{q_a}\Big(1 - \exp(-q_a t)\Big)\right), \tag{A.1}$$

given that q_0 is the initial cohort mortality rate, and q_a is the annual rate of increase in mortality, or the actuarial mortality rate. The change in the cohort's population over time then follows

$$\frac{\mathrm{d}}{\mathrm{dt}}N = -dN, \tag{A.2}$$

such that

$$d = -\frac{1}{N}\frac{\mathrm{d}}{\mathrm{dt}}N. \tag{A.3}$$

If t_ℓ is the expected lifetime of the organism, then the average rate of mortality over a lifetime t_ℓ is

$$\begin{aligned}\mu &= \frac{1}{t_\ell}\int_0^{t_\ell} q_0 \exp(q_a t_\ell) \\ &= \frac{q_0}{q_a t_\ell}\Big(\exp(q_a t_\ell) - 1\Big).\end{aligned} \tag{A.4}$$

The cohort mortality rate q_0, the actuarial mortality rate q_a and the expected lifetime t_ℓ of a mammal with mass M_C all follow allometric relationships, where $q_0 = 1.88\times10^{-8} M_C^{-0.56}$ (1/s) and $q_a = 1.45 \times 10^{-7} M_C^{-0.27}$ (1/s) where M_C is in grams. Together, we obtainn the allometric relationship

$$\mu(M_C) = \frac{3.21 \times 10^{-8}\left(\exp(0.586 M_C^{0.03}) - 1\right)}{M_C^{0.59}}. \tag{A.5}$$

A.2 Appendix II: Variations in model parameters and allometric rates

While our framework dictates that plant growth rates and carrying capacities are directly proportional to consumer steady states, we can gain insight into what drives the very large range of observed consumer densities by exploring the observed ranges of α and k in terrestrial systems. We assume an intrinsic growth rate roughly that of grass where $\alpha = 9.45 \times 10^{-9}$ (s^{-1}; [18]), whereas observations among terrestrial plants reveal a range in growth rates from 2.81×10^{-10} to 2.19×10^{-8} [104], according with a change in α of roughly 97% lower and 130% higher than the set value. By incorporating this range into our the estimated resource growth rate, we observe that we can account for a large portion of consumer steady state densities around the mean density (inner shaded region, Fig. 1, main text). If we additionally adjust the carrying capacity k of the resource to 90% less-than and 150% more-than the assumed value of 23×10^3 g/m^2, our framework accounts for nearly the full range of mammalian steady state densities (outer shaded region, Fig. 1, main text). In this context, the upper-boundary of k observed to capture most higher herbivore densities is ca. 34 kg/m^2, which is on the higher end of estimated live above-ground biomass densities in terrestrial forests such as in Isle Royal and the Allegheny National Forest [165].

Our model's ability to capture the bounds of mammalian densities at low and high

productivity invites some speculation into the actual steepness of the mass-density relationship. While the best-fit slope to Damuth's Law is -0.77 we also observe that the steeper relationship given by our framework better captures the boundaries of mass-density data, whereas varying the intercept of the statistical best-fit would not capture the lower-density outer-boundary of larger species. While within-clade mass-density relationships often reveal a shallower slope than if measured across clades [166], it is possible that the absence of data for larger mammals may bias estimates of the slope towards smaller (shallower) values. Mammalian communities have undergone significant anthropogenic restructuring throughout the Holocene [167], such that many larger species are excluded from the mass-density relationship by way of extinction [167], and the greater prevalence of smaller species may introduce size-dependent biases. For example, if species < 100 g are excluded, the empirical mass-density slope steepens from -0.77 to -0.85.

Considering how variations to the underlying energetic parameters driving consumer-resource dynamics alters the expected mass-density relationship may shed light on key constraints shaping mammalian communities. We next explore how variations in the vital rates included in the consumer-resource model modify the expected intercept and slope of the mammalian mass-density relationship. Different vital rates impact the mass-density relationship in three distinct ways, by either *i*) influencing only the mass-density slope, *ii*) influencing only the mass-density intercept, or *iii*) influencing both. Aside from the resource growth rate and carrying capacity, our framework also includes the intrinsic consumer reproductive rate $\lambda_C^{\max}$, the consumer yield coefficient Y_C, and the maximum rate of starvation σ. We introduce changes to these rates as, for example, $\lambda_C^{\max\prime} = \lambda_C^{\max}(1+\chi)$, where $\chi \in (-1, 2)$ represents the proportion increase or decrease of the altered parameter denoted by $'$. We note that the recovery rate ρ is sufficiently small that alterations do not have an influence on either the consumer mass-density intercept or slope.

Importantly, changes to the starvation rate have a large effect on both the consumer-density intercept and slope (Figs. A.1,A.2). We observe that decreasing σ from the expected value ($\chi < 0$) serves to increase the steady state intercept, while decreasing the mass-density slope. By comparison, increasing σ from the expected value ($\chi > 0$) has less effect on the mass-density relationship. In the consumer-resource model described in Eq. 2.3 (main text), starvation is the sole source of consumer mortality, and therefore plays an out-sized role in determining consumer steady states. As this mortality is reduced, consumer densities increase, raising the intercept. However, as consumer starvation rates decline we observe

a steeper mass-density slope. Reduced starvation rates therefore principally benefit the steady state densities of smaller species, with reduced effects observed for larger-bodied mammals. Because fat biomass scales super-linearly with body mass (see methods; [24]), the populations of larger consumers are more resilient to the effects of starvation, whereas those of smaller consumers are more prone.

The consumer's maximal rate of reproduction $\lambda_C^{\max}$ influences only the mass-density slope except for the case $\chi \to -1$, where growth becomes zero. Above this trivial limit, we observe the consumer growth rate to have a negative effect on the mass-density slope, such that as the growth rate increases, the mass-density relationship becomes steeper (Figs. A.1,A.2). As the intercept does not change, this means that the steady states of larger bodied consumers decline with increasing $\lambda_C^{\max}$, while those of smaller-bodied consumers remain unaltered, though the effect is slight. Of more interest is the effect of the yield coefficient Y_C and starvation rate σ (Figs. A.1,A.2). The yield coefficient represents the conversion of resources to consumer biomass, where an increase in χ correlates to large increases in consumer steady state without altering the mass-density slope. Here we observe that increased efficiency in converting resource to consumer biomass will have an effect similar to increasing resource productivity, as the effective abundance of the resource is greater when relatively fewer resources fuel a given unit of consumer biomass. Because $Y_C \propto E_d$ where E_d is the energy density of the resource (see methods), resource quality is therefore expected to translate directly to higher consumer steady state densities.

A.3 Appendix III: Mortality from predation

Per-capita mortality rate from predation The per-capita mortality rate from predation of the herbivore consumer with mass M_C and population density C by a mammalian predator with body mass M_P and population density P is given by

$$\beta(C, P) = f\frac{\lambda_P(C)P}{CY_P}, \tag{A.6}$$

where $\lambda_P(C)$ is the growth rate of the predator, Y_P is the predator yield coefficient, describing the grams of predator produced per gram of prey consumed, and f is the degree of specialization of the predator on the consumer prey ($f = 1$ denotes specialization, whereas

$f < 1$ denotes generalization). Assuming a linear functional response for predation mortality, $\lambda_P(C)$ is maximized to $\lambda_P^{\max}$ when the consumer reaches its theoretical maximum population density, which we calculate by converting the resource carrying capacity directly to grams of consumer produced, or $C^{\max} = Y_C k$. The growth rate of the predator is then given by

$$\lambda_P(C) = \lambda_P^{\max} \frac{C}{C^{\max}} = \lambda_P^{\max} \frac{C}{Y_C k}. \tag{A.7}$$

Together, we observe the per-capita mortality rate to be (as expected) independent of the consumer density C, and is simplified to

$$\beta(P) = f \frac{\lambda_P^{\max} P}{Y_P Y_C k}, \tag{A.8}$$

where we assume that the predator population remains at empirically measured steady state densities for mammalian carnivores, where $P \equiv P^* = P_0 M_P^{-0.88}$ [40]. This assumption is required because the effects of predation are implicit rather than explicit.

As described in the main text, consumer yield is calculated

$$Y_C = \frac{M_C E_d}{\int_0^{t_{\lambda_C}} B_0 m(t)^{\eta} \mathrm{dt}}, \tag{A.9}$$

where E_d is the energy density of the plant resource R (Joules/g) and the denominator is the lifetime energy use required by the herbivore consumer to reach maturity (Joules). The parameters t_{λ_C} and B_0 are the timescale associated with reaching reproductive maturity and the metabolic coefficient for herbivorous mammals, respectively, and $\eta = -3/4$ is the metabolic exponent. The predator yield is calculated similarly, where

$$Y_P = \frac{M_C E_C}{\int_0^{t_{\lambda_P}} B_{0P} m(t)^{\eta} \mathrm{dt}}, \tag{A.10}$$

where E_C is the energy density of the herbivore being consumed, and the denominator is the lifetime energy use required by the predator to reach maturity. The parameters t_{λ_P} and B_{0P} are the timescale associated with reaching reproductive maturity and the metabolic coefficient for predatory mammals, respectively, and $\eta = -3/4$ is the metabolic exponent. We note that the metabolic coefficient for predators is different than that for mammals [168].

Herbivore energy density The energy density of herbivore consumers changes with body

mass M_C. For example, small mammals have very low percent body fat, whereas very large mammals have high percent body fat. We assume that predators consume all non-skeletal mass of prey. Because the amount of consumable tissues with different energy densities within an herbivore varies allometrically, so too should the energy density E_C. We consider four primary tissue groups: a consumable set composed of muscle, fat, and *other* tissues, and an non-consumable set composed only of skeletal tissues. If the scalings associated with fat, muscle, and skeletal tissues are $M_C^{\text{fat}} = f_0 M_C^{1.19}$, $M_C^{\text{musc}} = g_0 M_C^{1.00}$, and $M_C^{\text{skel}} = h_0 M_C^{1.09}$, the scaling of the *other* tissue (gut tissue, organ tissue, etc) is given by $M_C^{\text{other}} = M_C - (M_C^{\text{fat}} + M_C^{\text{musc}} + M_C^{\text{skel}})$. The energy density of fat is $E_{\text{fat}} = 37700$ J/g, whereas the energy density of muscle is $E_{\text{musc}} = 17900$ J/g. If we assume that gut and organ tissues have roughly the same energy density as muscle, the attainable energy density for an herbivore of size M_C is given by

$$E_C(M_C) = E_{\text{fat}} \frac{M_C^{\text{fat}}}{M_C} + E_{\text{musc}} \left(\frac{M_C^{\text{musc}}}{M_C} + \frac{M_C^{\text{other}}}{M_C} \right). \tag{A.11}$$

Large-bodied Predator-Prey Mass Ratio (PPMR) The predator growth rate $\lambda_P^{\max}$, the time required for the predator to reach reproductive maturity t_{λ_P}, and the predator's steady state population density P^* are allometric relationships that depend on its body mass M_P. Accordingly, for an herbivore of a given mass M_C, we must anticipate the size of its likely predator M_P. This is very different than the more typical issue of anticipating the average prey size for a given predator. For example, the most preferred prey mass for an African lion is ca. 350 kg [55], where the inclusion of megaherbivores to diet is comparatively low. However from a megaherbivore's perspective, lions may represent the only potential predator. In other words, because the range of prey body mass increases for predators of larger body mass [2], it is the upper limit of the range that impacts the populations of larger herbivores.

To obtain an herbivore-centric measure of the expected predator mass given a particular herbivore mass $\mathrm{E}(M_P|M_C)$, we first compiled the known diets of large-bodied predators. Because smaller mammalian predators and prey have very different PPMR relationships than larger-bodied mammalian predators and prey, we here focus exclusively on the relationship between mammalian predators and prey $> 10^5$ g. From the dietary information

for large-bodied predators, we repeatedly sampled predator dietary distributions to reflect each predator's reliance as a function of prey mass. We introduced variability in predator and prey masses by assuming that body sizes were normally distributed about the expected value with a standard deviation of $\pm 10\%$, allowing us to obtain a distribution of expected predator diets as a function of prey mass. From this relationship, we then evaluated the expected predator mass for a given prey mass range to obtain $\mathrm{E}(M_P|M_C)$ shown in Fig. A.3 (the blue line denotes the best fit), demonstrating an allometric relationship for the herbivore-centric PPMR of $\mathrm{E}(M_P|M_C) = 1.18 \times 10^5 M_C^{0.19}$, which was robust to the particular sampling strategy. We emphasize that this relationship only pertains to large-bodied predators and prey $> 10^5$ g. Alterations to and variations from this relationship are explored in the main text.

As explored in the main text, the empirically-measured PPMR for large-bodied mammals results in a threshold body size for herbivore consumers $M_C^\dagger$. This size marks the point where the predator population, with a body mass derived from the PPMR, cannot sustain its own growth from the predated herbivore population, thereby driving the herbivore population to extinction. The size at which $M_C^\dagger$ occurs is both dependent on the nature of the PPMR, as well as predator specialization f. As f decreases such that the predator supports only a fraction of its growth from predation on the herbivore consumer, $M_C^\dagger$ increases (Fig. A.4.

By allowing the PPMR to vary as

$$\mathrm{E}(M_P|M_C) = v_0(1 + \chi_{\mathrm{int}}) M_C^{v_1(1+\chi_{\mathrm{slope}})}, \tag{A.12}$$

where the proportional changes in the PPMR intercept and slope are given by χ_{int} and $\chi_{\mathrm{slope}} \in (-0.99, 2)$, so does the threshold herbivore body mass $M_C^\dagger$ and, by extension, the related threshold predator body mass $M_P^\dagger$. From Fig. 4D (main text), we observe that changing the intercept and slope of the PPMR has a large influence on $M_C^\dagger$ and $M_P^\dagger$. Across this range of potential PPMR relationships, we highlight those values for the intercept and slope of the PPMR that permit megatrophic interactions, where both megapredators subsist on megaherbivores at the threshold body mass (highlighted region in Fig. 4D, main text). Fig. A.5 shows the relationship between megapredator and megaherbivore body masses highlighted within this region. Allowing both the PPMR to vary and assuming the megapredator is a generalist ($f = 0.37$) rather than a specialist enables much larger body

sizes for megaherbivores and their associated megapredators (Fig. A.6).

A.4 Appendix IV: Derivation of harvesting mortality

We first determined the harvest rate $h = h^\dagger$ required to drive an herbivore population to extinction, thereby satisfying the condition $C^*(M_C|h) = 0$ as a function of herbivore body mass M_C. This extinction-inducing harvest rate, itself now a function of consumer body mass $h^\dagger(M_C)$, defines the rate at which the population must be harvested to drive the steady state to zero. To compare this rate against measures of harvest both in nature and predicted from other mathematical or computational treatments of harvest-induced extinction, we calculated the harvest pressure $\psi^\dagger$, which we defined as the number of herbivore individuals per area harvested at this rate to reduce the population to some proportion ϵ of its steady state. This harvest pressure is thus defined by some number of individuals harvested per year over a certain number of years to reduce the population from C^* to its post-harvest density ϵC^*.

To calculate harvest pressure, we first assume that at the steady state, harvest is occurring on a shorter-than-generational timescale. For megaherbivores such as elephants, a generation is ca. 25 years [169], and for harvest pressures that must be applied beyond this period of time, we would expect population growth to counter the negative effects of harvest. Assuming harvest-only change, we simplify the dynamics to

$$\frac{\mathrm{d}}{\mathrm{dt}}C = -h^\dagger(M_C)C, \tag{A.13}$$

where the time to reduce C^* to ϵC^* is

$$\begin{aligned} C(t) &= C_0 \mathrm{e}^{-h^\dagger(M_C)t}, \\ \epsilon C^* &= C^* \mathrm{e}^{-h^\dagger(M_C)t} \\ t_\epsilon &= -\frac{\log(\epsilon)}{h^\dagger(M_C)}. \end{aligned} \tag{A.14}$$

We note that for elephant-sized herbivores and up, $t_\epsilon \leq 23$ years. While the time required to harvest the population to ϵC^* is only just approaching generational timescales, it should be treated as a minimum t_ϵ given the effects of population growth will prolong the imposed

harvest effort. Harvest pressure is then calculated as

$$\psi^{\dagger} = \frac{C^*(1-\epsilon)}{M_C t_\epsilon} c_0 = -h^{\dagger}(M_C) \frac{C^*(1-\epsilon)}{M_C \log(\epsilon)} c_0 \tag{A.15}$$

where the constant c_0 denotes the conversion from inds/m^2/second to inds/A_{CA}/year, where $A_{\mathrm{CA}} = 4.24 \times 10^{11}$ m^2 is the arbitrarily-chosen area of California. This conversion is particularly important for evaluating other harvest measures from the historical record and estimates from independent models and simulations for extinct species. As described in the main text, the extinction-inducing harvest pressure is calculated to be 4.3×10^3 inds/yr/A_{CA} for an elephant-sized organism of $M_C = 2.5 \times 10^6$ g (see Fig 5, main text).

Harvest pressure on Pleistocene mammoths We compare our measure of harvest pressure to that calculated for mammoths (*Mammuthus primigenius*) in Fordham et al. [3]. Because Fordham et al. employ a much more complex and detailed assessment of the effects of harvest specifically for mammoths over a spatially explicit landscape, we must make a few simplifications in order to derive a comparable estimate. First, the harvest interaction between mammoth populations and humans is modeled as a type 2 functional response, where, again isolating population-level effects to that of harvest we obtain

$$\frac{\mathrm{d}}{\mathrm{dt}} C = -\frac{sNFC}{G + \frac{C}{C_{\max} M_C}}, \tag{A.16}$$

where N is the normalized human population density maximized at unity, the constant $s = 7.884 \times 10^{-8}$ generations/second (where a generation is 25 years), F represents the effectiveness of human hunting, ranging from $(0.01, 0.34)$, $C_{\max} = 1.875 \times 10^{-6}$ g/m^2 is the maximum mammoth population density (converted from the average degree-by-degree grid cells in Siberia), $G = 0.4$ is the half-saturation constant, and $M_C = 2.5 \times 10^6$

Solving for the time required to reduce the population to ϵC^*, we obtain

$$t_\epsilon^{\mathrm{mammoth}} = \frac{C^* - C_{\max} G M_C \log\left[C^* \exp(\frac{C^* \epsilon}{C_{\max} G M_C})\epsilon\right]}{s C_{\max} F M_C N}. \tag{A.17}$$

We then calculate the harvest pressure as

$$\psi^{\mathrm{mammoth}} = c_0 \frac{s C_{\max} F N (C^* - C^* \epsilon)}{C^* - C_{\max} G M_C \log\left[C^* \exp(\frac{C^* \epsilon}{C_{\max} G M_C})\epsilon\right]}, \tag{A.18}$$

where the constant c_0 again denotes the conversion from inds/m^2/second to inds/A_{CA}/year, where A_{CA} is the arbitrarily-chosen area of California. Given a range in $F \in (0.01, 0.35$ and $N \in (0.01, 1)$, we obtain a distribution of values for mammoth harvest pressure with a median value of 1.24×10^4 inds/yr/A_{CA} over the course of 9.8 years. The bounds of the estimate range from 5×10^4 inds/yr/A_{CA} over the course of 2 years to 5×10^2 inds/yr/A_{CA} over the course of ca. 200 years (the range is plotted as the vertical black line in Fig. 5, main text). Again we emphasize that these calculations of harvest pressure are derived from an extinction timescale that should be viewed as a minimum estimate given that we do not account for demographic rebound.

Harvest pressure on Pleistocene *Diprotodon* The harvest rate needed to collapse *Diprotodon* populations was calculated by Bradshaw et al. [4], where a harvest pressure of between 400-500 inds/year/area of Australia was sufficient. Translating this to be relative to the area of California, we obtain between 678 to 848 inds/yr/A_{CA}, with a mean of 763.2 inds/yr/A_{CA}.

Harvest pressure on historical elephants *Loxodonta africana* Elephant harvest rates are estimated from historical documentation of the ivory trade detailed in Milner-Gulland & Beddington [5]. While the trade volume oscillates with changes in technology, access to habitats within Africa, and the feedbacks of trade on elephant population size, we compare our results against estimates taken at two points in time: early in the ivory trade (1810), and late in the ivory trade (1987). From [5] we assume that each elephant killed contributes 1.88 tusks, and that tusk mass begins at 15 kg per tusk early in trade to 5 kg per tusk in later years. While the area from which elephants were harvested is largely unknown, we assume the area harvested is that assessed to be suitable elephant habitat in sub-Saharan Africa, estimated at 3.22×10^{12} m^2 [170]. From rates of ca. 1×10^5 kg/yr of ivory harvested in 1810 to ca. 9.7×10^5 kg/yr of ivory harvested in 1987, normalized to habitat area and converted to the area of California, we obtain estimates of ca. 467 inds/yr/A_{CA} in 1810 to ca. 1.33×10^4 inds/yr/A_{CA} in 1987 (see Fig. 5, main text).

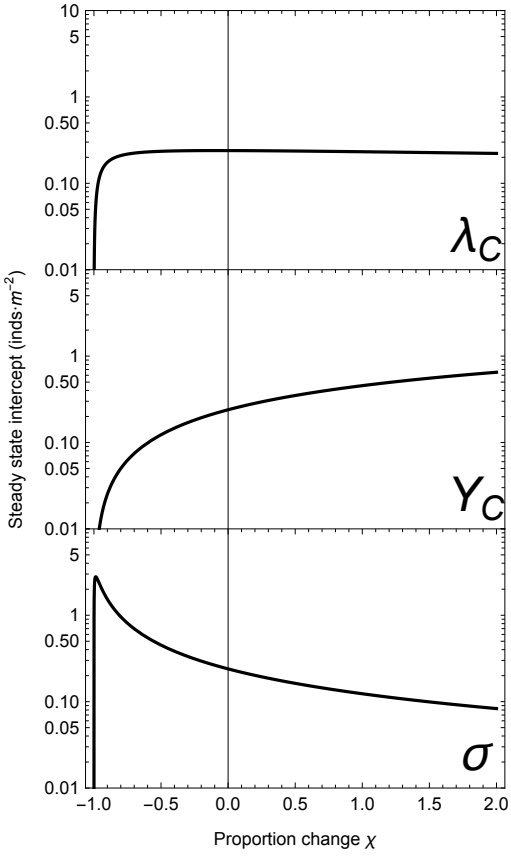

Figure A.1: The effects of changes to metabolic parameters on the prediction of the mass-density relationship.

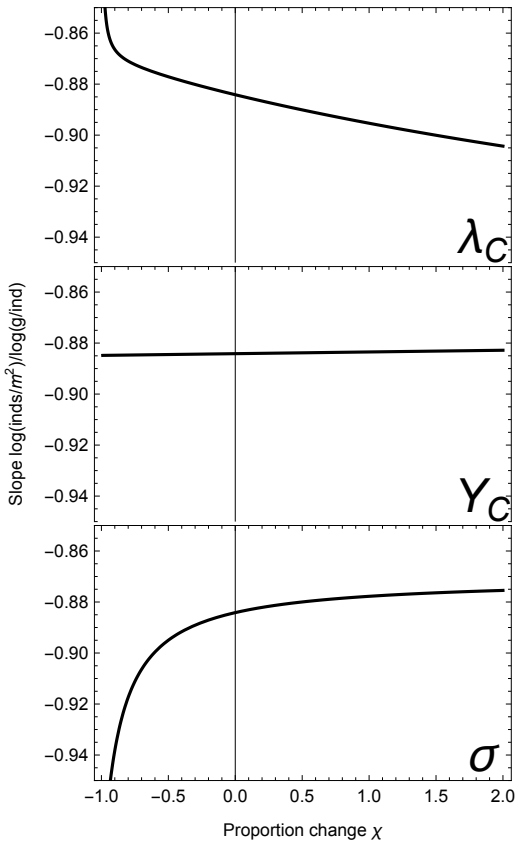

Figure A.2: The effects of changes to metabolic parameters on the prediction of the mass-density relationship.

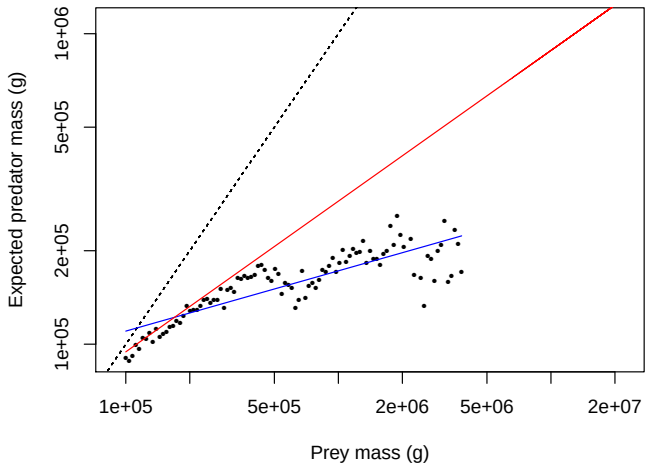

Figure A.3: Expected predator masses for contemporary large-bodied ($> 10^5$ g) terrestrial predators and prey. Expected predator sizes as a function of herbivore size class were determined by reconstructing dietary samples from observed trophic interactions for cheetah, wild dogs, dholes, leopards, hyenas, lions, and tigers from [10] (REF others), where masses for both predators and prey were allowed to vary ±20% from measured estimates. The blue line denotes the best fit relationship, given by $\mathrm{E}(M_P|M_C) = p_0 M_C^{p_1}$, where $p_0 = 11786.8$ g and $p_1 = 0.194$. The red line represents a modified PPMR where $p_0' = p_0(1 + \chi_{\text{int}})$ and $p_1' = p_1(1 + \chi_{\text{slope}})$ where $\chi_{\text{int}} = 0.97$ and $\chi_{\text{slope}} = 1.50$ that allows megatrophic interactions and resides within the white band displayed in Fig. 2.4C,D. This relationship is entirely hypothetical, but does not stray far from observations of contemporary species, describes megapredators that predate on megaherbivores, and results in threshold herbivore and carnivore size classes that permit dynamically feasible megatrophic interactions. The black line denotes the 1:1 line.

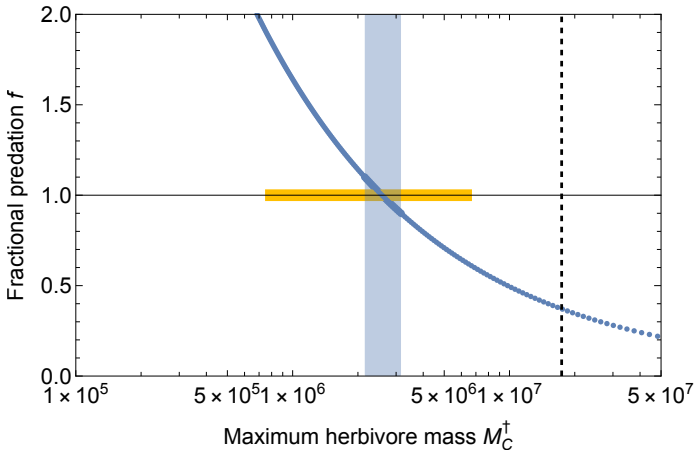

Figure A.4: The effect of changing the reliance of predator growth f on the single herbivore consumer population. If $f = 1$, the predator solely relies on the herbivore consumer. If $0 < f < 1$, the predator relies on the herbivore population to support a fraction of its growth. If $f > 1$, the predator is removing more biomass than is necessary to support its growth. Blue region denotes herbivore threshold mass range characterizing $f = 1 \pm 0.1$. Yellow line denotes the mass range of contemporary elephants. Vertical dashed line denotes the size of the largest terrestrial mammal (Deinotherium at ca. 1.74×10^7, corresponding to $f = 0.37$, such that a predator is supporting a little more than 1/3 of its growth from the herbivore consumer.

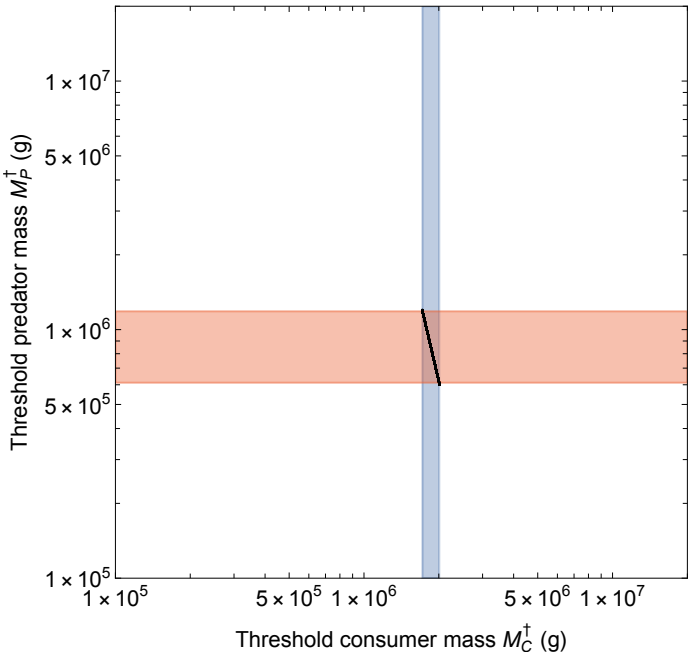

Figure A.5: Mass ranges corresponding to feasible megatrophic interactions (where herbivore and predator threshold masses are $> 6 \times 10^5$ g) across variations to the assumed predator-prey mass ratio (PPMR), demarcated by the white bands in Fig. 2.4C,D, and under the assumption specialist predation ($f = 1$).

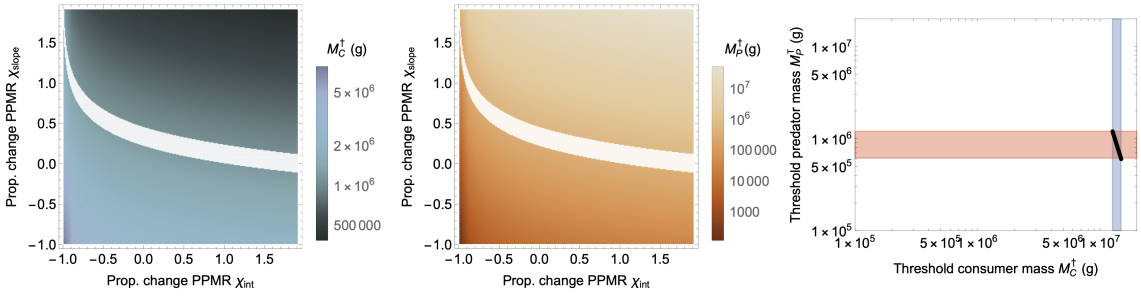

Figure A.6: The effects of predator generalization on A) threshold herbivore mass $M_C^\dagger$ and B) threshold predator mass $M_P^\dagger$ across variable PPMRs, where $\mathrm{E}(M_P|M_C) = p_0(1 + \chi_{\text{int}})M_C^{p_1(1+\chi_{\text{slope}})}$ and both χ_{int} and $\chi_{\text{slope}} \in (-0.99, 2)$. White bands denote regions of χ_{int} and χ_{slope} where megatrophic interactions are feasible (both perdator and herbivore threshold masses are $> 6 \times 10^5$ g). C) Mass ranges corresponding to feasible megatrophic interactions in the white bands in A and B.

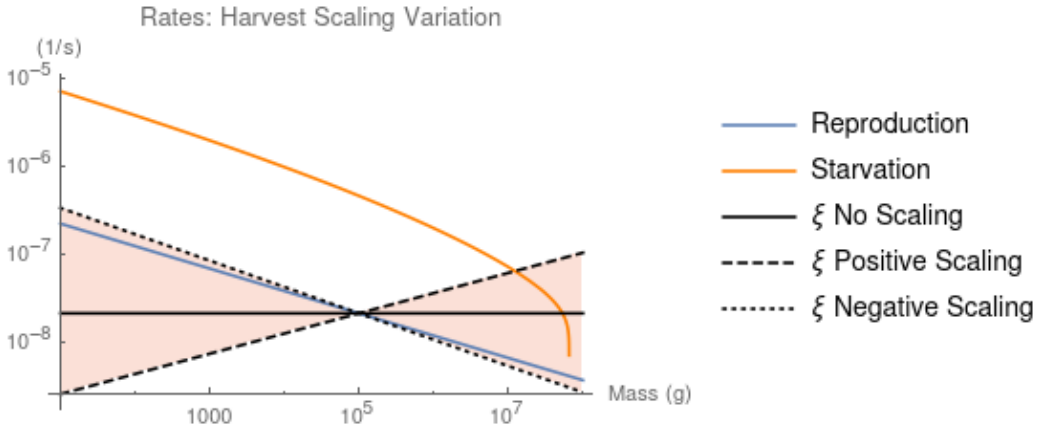
Rates: Harvest Scaling Variation
(1/s)
10^{-5}
10^{-6}
10^{-7}
10^{-8}
1000
10^5
10^7
Mass (g)
Reproduction
Starvation
ξ No Scaling
ξ Positive Scaling
ξ Negative Scaling

Figure A.7

Appendix B

Supplementary Information: Body Size and Competition Drive the Structure and Dynamics of Mammalian Herbivore Communities

B.1 Appendix I: Derivation of allometric rates

The rate laws describing resource consumption as well as consumer growth and mortality all vary as a function of consumer body mass M_i, where the consumer is assumed to be a mammalian herbivore, and the resource is an unspecified primary producer with characteristic growth rate α_j, carrying capacity k_j, and energy density E_{dj} for resource j. We approach the derivation of vital rates with respect to consumer mass by solving for multiple timescales associated with ontogenetic growth, maintenance, and expenditure. The growth of an individual consumer from birth mass $m = m_0$ to its reproductive size $m_i = 0.95M_i$ is given by the solution to the general balance condition $B_{0i}{m_i}^{\eta} = E_{mi}\dot{m}_i + B_m m_i$, where E_{mi} is the energy needed to synthesize a unit of biomass for consumer i, B_{mi} is the metabolic rate to support an existing unit of biomass for consumer i, and the metabolic exponent $\eta = 3/4$ [25]. From this balance condition, the time required for an organism starting from

mass m_{i1} to reach mass m_{i2} follows

$$\tau(m_{i1}, m_{i2}) = \ln\left(\frac{1-(m_{i1}/M_i)^{1-\eta}}{1-(m_{i2}/M_i)^{1-\eta}}\right)\frac{M_i^{1-\eta}}{a_i(1-\eta)} \tag{B.1}$$

where $a_i = B_{0i}/E_{mi}$. From this general equation, we calculate the timescale of reproduction for an herbivore consumer of mass M_i as $t_\lambda = \tau(m_{i0}, 0.95M_i)$, such that the reproductive rate is $\lambda_i^{\max} = \ln(\nu)/t_\lambda$, where $\nu = 2$ is the set number of offspring per reproductive cycle [18, 38]. The consumer yield coefficient is given by $Y_{ij} = M_i E_{dj}/B_{\lambda i}$ (g consumer per g resource), where $B_{\lambda i}$ is the lifetime energy use required to reach maturity $B_{\lambda i} = \int_0^{t_\lambda} B_{0i} m_i(t)^\eta \mathrm{d}t$.

Table B.1: Allometric parameters, values/units, and references.

Definition	Parameter	Value/Units	References
Resource j			
density	R_j	g/m^2	
reproduction rate	α_j	1/s	
carrying capacity	k_j	g/m^2	
Consumer i			
density	C_i	g/m^2	
body mass	M_i	g	
fat mass	${M_i}^{\text{fat}}$	$0.02M_i^{1.19}$ g	[24]
muscle mass	${M_i}^{\text{musc}}$	$0.38M_i^{1.00}$ g	[171]
initial body mass m_{0i}	g		
timescale of growth from m_{1i} to m_{2i}	$\tau(m_{1i}, m_{2i})$	s	
reproduction rate	$\lambda_i^{\max}$	1/s	
yield coefficient	Y_{ij}	(g/m^2 C_i)/(g/m^2 R_j)	
starvation rate	σ_i	1/s	
metabolic normalization constant	B_{0i}	0.047 Wg^{-1}	
Energy to synthesize a unit of mass	E_{mi}	5774 Jg^{-1}	[23, 41, 172]
Energy stored in a unit of mass	E_{mi}	7000 Jg^{-1}	[23, 41, 172]

To determine the rate of mortality from starvation, we calculate the time required for an organism to metabolize its endogenous energetic stores, estimated from its cumulative fat and muscle mass, where the remaining mass is given by $M_i^{\text{starve}} = M_i - (M_i^{\text{fat}} + M_i^{\text{musc}})$ (see Table B.1). During starvation, we assume that an organism burns its existing endogenous stores as its sole energy source, where the balance condition is altered to $\dot{m}_i E'_{mi} = -B_{mi} m_i$, where E'_{mi} is the amount of energy stored in a unit of biomass for consumer i (differing from the amount of energy used to synthesize a unit of biomass E_{mi}). The starvation timescale

is then given by

$$t(\sigma^{\max})_i = -\frac{M_i^{1-\eta}}{a'_i} \ln(M_i^{\text{starve}}/M_i), \tag{B.2}$$

where $a'_i = B_{0i}/E'_{mi}$, such that the starvation rate is the $\sigma_i^{\max} = 1/t(\sigma^{\max})_i$.

B.2 Appendix II: Parameterization of the dynamics model

Plants are randomly drawn and parameterized as graze or browse resources. The parameters that differ between graze and browse are digestibility and growth rate.

The growth rate parameters for browse are between $2.81 * 10^{-10}, 2.19 * 10^{-8}(1/s)$ [104]. The value of growth can be roughly estimated by the NPP divided by the corresponding biomass densities. Using grasslands from data from Nairobi [105] : $811/144.617 = 1.778 * 10^{-7}(1/s)$ (lit above ground NPP/ average above ground biomass). This is expanded to have a similar range as the browse growth rate $1.778 * 10^{-6} - 1.778 * 10^{-8}$.

The energy density parameter uses $E_{di} = 18200$ (J/g) [18] as the starting point for both graze and browse. This is then modified by graze and browse specific digestibilities. The measure of plant digestibility, cell wall digestibility (CWD), is a function of the acid detergent lignin (ADL) and neutral detergent fiber (NDF) of a plant species. It is calculated as $CWD = 100 - (ADL/NDF * 100)$ [173], providing a range of digestibility for graze: $91.27\% - 95.24\%$ and for browse: $58.2\% - 80.78\%$. CWD is cell wall digestibility. ADL is acid detergent lignin. NDF is neutral detergent fiber.

Herbivore body-masses, when randomly generated, are base-10, in grams, with a uniform random exponent between $1.0 - 7.0$. Adaptive consumer learning rate is set to 10 $1/s$.

B.3 Appendix III: Initial Conditions

Plant resource density, R_j is initialized at species specific carrying capacities, k_j. Consumer population density, C_i are initialized at their mass specific densities determined by Damuth's Law [1]. Foraging effort A_{ij} is initialized as a random proportion.

B.4 Appendix IV: Mass-breadth relationships

Four models of the relationship between herbivore mass and herbivore diet-breadth are explored. The full-connectance model refers to an interaction matrix where the herbivore

layer is full linked to the plant layer. That is, each herbivore is trophically connected to every plant in the system.

For the structural models of mass-breadth relationships, plants are randomly assigned values between $0 - 1$. Herbivore diet value is obtained by normalizing body-mass to be between $0 - 1$ based on minimum, 10^0, and maximum, 10^8, mass values. The diet value is then used to generate a diet range according the following equations: Positive Mass-Breadth: $value * B(\alpha, \beta)$, Negative Mass-Breadth: $(1 - value) * B(\alpha, \beta)$, Nonlinear Mass-Breadth. $(4 * (value - 0.5)^2 + 0.2) * B(\alpha, \beta)$, where B is a Beta distribution, $\beta = 2/3$, and $\alpha = 1$. A herbivore diet center is randomly generated from between $0.5 * value$ and the full diet value. From this center, the herbivore diet value minimum is set as the diet center +/- half the diet range. Any plants with values falling within this range are trophically linked to the herbivore. The positive and negative mass-breadth relationships replicates the dietary dynamics found in the niche model [109] and inverse niche model [110], respectively.

Appendix C

Supplementary Information: The Dynamics of Competition Constrain and Explain Macroevolutionary Trends Among Mammalian Communities Across the Cenozoic

C.1 Appendix I: Derivation of allometric rates

The rate laws describing resource consumption as well as consumer growth and mortality all vary as a function of consumer body mass M_i, where the consumer is assumed to be a mammalian herbivore, and the resource is an unspecified primary producer with characteristic growth rate α_j, carrying capacity k_j, and energy density E_{dj} for resource j. We approach the derivation of vital rates with respect to consumer mass by solving for multiple timescales associated with ontogenetic growth, maintenance, and expenditure. The growth of an individual consumer from birth mass $m = m_0$ to its reproductive size $m_i = 0.95M_i$ is given by the solution to the general balance condition $B_{0i}{m_i}^{\eta} = E_{mi}\dot{m}_i + B_m m_i$, where E_{mi} is the energy needed to synthesize a unit of biomass for consumer i, B_{mi} is the metabolic

rate to support an existing unit of biomass for consumer i, and the metabolic exponent $\eta = 3/4$ [25]. From this balance condition, the time required for an organism starting from mass m_{i1} to reach mass m_{i2} follows

$$\tau(m_{i1}, m_{i2}) = \ln\left(\frac{1-(m_{i1}/M_i)^{1-\eta}}{1-(m_{i2}/M_i)^{1-\eta}}\right)\frac{M_i^{1-\eta}}{a_i(1-\eta)} \tag{C.1}$$

where $a_i = B_{0i}/E_{mi}$. From this general equation, we calculate the timescale of reproduction for an herbivore consumer of mass M_i as $t_\lambda = \tau(m_{i0}, 0.95M_i)$, such that the reproductive rate is $\lambda_i^{\max} = \ln(\nu)/t_\lambda$, where $\nu = 2$ is the set number of offspring per reproductive cycle [18, 38]. The consumer yield coefficient is given by $Y_{ij} = M_i E_{dj}/B_{\lambda i}$ (g consumer per g resource), where $B_{\lambda i}$ is the lifetime energy use required to reach maturity $B_{\lambda i} = \int_0^{t_\lambda} B_{0i} m_i(t)^\eta \mathrm{d}t$.

Table C.1: Allometric parameters, values/units, and references.

Definition	Parameter	Value/Units	References
Resource j			
density	R_j	g/m^2	
reproduction rate	α_j	1/s	
carrying capacity	k_j	g/m^2	
Consumer i			
density	C_i	g/m^2	
body mass	M_i	g	
fat mass	M_i^{fat}	$0.02M_i^{1.19}$ g	[24]
muscle mass	M_i^{musc}	$0.38M_i^{1.00}$ g	[171]
initial body mass m_{0i}		g	
timescale of growth from m_{1i} to m_{2i}	$\tau(m_{1i}, m_{2i})$	s	
reproduction rate	$\lambda_i^{\max}$	1/s	
yield coefficient	Y_{ij}	(g/m^2 C_i)/(g/m^2 R_j)	
starvation rate	σ_i	1/s	
metabolic normalization constant	B_{0i}	0.047 Wg^{-1}	
Energy to synthesize a unit of mass	E_{mi}	5774 Jg^{-1}	[23, 41, 172]
Energy stored in a unit of mass	E_{mi}	7000 Jg^{-1}	[23, 41, 172]

To determine the rate of mortality from starvation, we calculate the time required for an organism to metabolize its endogenous energetic stores, estimated from its cumulative fat and muscle mass, where the remaining mass is given by $M_i^{\text{starve}} = M_i - (M_i^{\text{fat}} + M_i^{\text{musc}})$ (see Table C.1). During starvation, we assume that an organism burns its existing endogenous stores as its sole energy source, where the balance condition is altered to $\dot{m}_i E'_{mi} = -B_{mi} m_i$, where E'_{mi} is the amount of energy stored in a unit of biomass for consumer i (differing from

the amount of energy used to synthesize a unit of biomass E_{mi}). The starvation timescale is then given by

$$t(\sigma^{\max})_i = -\frac{M_i^{1-\eta}}{a_i'} \ln(M_i^{\text{starve}}/M_i), \tag{C.2}$$

where $a_i' = B_{0i}/E_{mi}'$, such that the starvation rate is the $\sigma_i^{\max} = 1/t(\sigma^{\max})_i$.

C.2 Appendix II: Parameterization of the dynamic model

Plants resources, of a number equalling the size of the consumer community or varying by environmental scenario (see Supplementary Appendix III), are randomly drawn and parameterized as graze or browse resources. The parameters that differ between graze and browse are digestibility and growth rate. The growth rate parameters for browse are between $2.81 * 10^{-10}, 2.19 * 10^{-8}(1/s)$ [104]. The value of growth can be roughly estimated by the NPP divided by the corresponding biomass densities. Using grasslands from data from Nairobi [105] : $811/144.617 = 1.778 * 10^{-7}(1/s)$ (lit above ground NPP/ average above ground biomass). This is expanded to have a similar range as the browse growth rate $1.778 * 10^{-6} - 1.778 * 10^{-8}$.

The energy density parameter uses $E_{di} = 18200$ (J/g) [18] as the starting point for both graze and browse. This is then modified by graze and browse specific digestibilities. The measure of plant digestibility, cell wall digestbility (CWD), is a function of the acid detergent lignin (ADL) and neutral detergent fiber (NDF) of a plant species. It is calculated as $CWD = 100 - (ADL/NDF * 100)$ [173], providing a range of digestibility for graze: $91.27\% - 95.24\%$ and for browse: $58.2\% - 80.78\%$. CWD is cell wall digestibility. ADL is acid detergent lignin. NDF is neutral detergent fiber. The adaptive consumer learning rate is set to $G_i = 10\ 1/s$

C.3 Appendix III: Environmental Scenarios

Environmental scenarios have two variables: aridity and openness. Aridity is assumed to determine system carrying capacity k_{system} for plants. An 'arid' environment sets carrying capacity to 15000 g/m^2. A 'humid' environment sets carrying capacity to 30000 g/m^2. Openness is assumed to determine potential diet partitioning, as represented by the number of distinct plant resources present in the system. An 'open' environment sets the number

of resources to 2/3 the number of consumers. A 'closed' environment sets the number of resources to 4/3 the number of consumers.

C.4 Appendix IV: Herbivore Body Mass Distributions

Table C.2: Body sizes (g) of mammalian fauna in the Linxia Basin

Period	Oligocene	M.Miocene	L.Miocene	L.Miocene	Pliocene	Pleistocene
Fuana	Jiaozigou	Laogou	Dashengou	Yangjiashan	Shilidun	Longdan
	24030124	3418146	5712059	5814225	2601720	3994735
Mass	22258121	3009953	5443095	5259194	2329010	3007620
(g)	4351615	2732138	5259194	2601720	1797143	682112
	1911407	2518920	2411613	2411613	1029299	577099
	1098237	1817159	1717728	1512330	469459	320645
	985935	1225585	1701080	1277050	462529	304320
	619804	973498	1512330	784185	255354	267465
	169248	439666	1029299	462529	169708	262032
	140359	328973	224749	255354	155171	225116
	69164	254695	211341	250402	151127	140916
	2905	162678	204038	232003	132252	121966
		44019	134376	177549	129147	40002
		38131	125567	134234	43320	27686
		36005	87985	125567	31815	26930
		16300	44833	124219	23777	23777
		10177	39863	109148	482	780
		1219	18033	44833		754
		440	792	43320		423
		328	361	40136		286
		153		31815		120
		146		18033		102
		119		792		
		108		71		
		20				
		20				
		17				

C.5 Appendix V: Initial Conditions

Plant resource density, R_j is initialized at species specific carrying capacities, k_j. Consumer population density, C_i are initialized at their mass specific densities determined by Damuth's Law [1]. Foraging effort A_{ij} is initialized as a random proportion.

C.6 Appendix VI: Mass-breadth relationship

For the structural model of mass-breadth relationships, plants are randomly assigned values between $0-1$. Herbivore diet value is obtained by normalizing body-mass to be between $0-1$ based on minimum, 10^0, and maximum, 10^8, mass values. The diet value is then used to generate a diet range according the following equation for Negative Mass-Breadth: $(1-value)*B(\alpha,\beta)$, where B is a Beta distribution, $\beta = 2/3$, and $\alpha = 1$. A herbivore diet center is randomly generated from between $0.5*value$ and the full diet value. From this center, the herbivore diet value minimum is set as the diet center +/- half the diet range. Any plants with values falling within this range are trophically linked to the herbivore. The negative mass-breadth relationship replicates the dietary dynamics found in the inverse niche model [110].

Bibliography

[1] John Damuth. Interspecific allometry of population density in mammals and other animals: the independence of body mass and population energy-use. *Biol. J. Linn. Soc.*, 31(3):193–246, jul 1987.

[2] Anthony R E Sinclair, S Mduma, and J S Brashares. Patterns of predation in a diverse predator-prey system. *Nature*, 425:288–290, 2003.

[3] Damien A Fordham, Stuart C Brown, H Re\csit Akçakaya, Barry W Brook, Sean Haythorne, Andrea Manica, Kevin T Shoemaker, Jeremy J Austin, Benjamin Blonder, Julia Pilowsky, and Others. Process-explicit models reveal pathway to extinction for woolly mammoth using pattern-oriented validation. *Ecology letters*, 25(1):125–137, 2022.

[4] Corey J A Bradshaw, Christopher N Johnson, John Llewelyn, Vera Weisbecker, Giovanni Strona, and Frédérik Saltré. Relative demographic susceptibility does not explain the extinction chronology of Sahul's megafauna. *Elife*, 10:e63870, 2021.

[5] E J Milner-Gulland and J R Beddington. The exploitation of elephants for the ivory trade: an historical perspective. *Proceedings of the Royal Society of London. Series B: Biological Sciences*, 252(1333):29–37, 1993.

[6] Matthew C. Hutchinson, Andrew P. Dobson, and Robert M. Pringle. Dietary abundance distributions: Dominance and diversity in vertebrate diets. *Ecology Letters*, 25(4):992–1008, 2022.

[7] Tyler R. Kartzinel, Patricia A. Chen, Tyler C. Coverdale, David L. Erickson, W. John Kress, Maria L. Kuzmina, Daniel I. Rubenstein, Wei Wang, and Robert M. Pringle.

DNA metabarcoding illuminates dietary niche partitioning by African large herbivores. *Proceedings of the National Academy of Sciences of the United States of America*, 112(26):8019–8024, 2015.

[8] Edward B. Baskerville, Andy P. Dobson, Trevor Bedford, Stefano Allesina, T. Michael Anderson, and Mercedes Pascual. Spatial guilds in the serengeti food web revealed by a bayesian group model. *PLoS Computational Biology*, 7(12), 2011.

[9] Ian A Hatton, Kevin S McCann, John M Fryxell, T Jonathan Davies, Matteo Smerlak, Anthony R E Sinclair, and Michel Loreau. The predator-prey power law: Biomass scaling across terrestrial and aquatic biomes. *Science*, 349(6252):aac6284, sep 2015.

[10] M W Hayward and G I H Kerley. Prey preferences and dietary overlap amongst Africa's large predators. *S. African J. Wild. Res.*, 38(2):93–108, 2008.

[11] Deron E. Burkepile and John D. Parker. Recent advances in plant-herbivore interactions. *F1000Research*, 6(0):119, 2017.

[12] Y. Pretorius, K. Kortekaas, Van M. Wijngaarden, De W.F. Boer, R. Slotow, and H.H.T. Prins. Why elephant have trunks, giraffe have long tongues and rhino have broad lips: mechanisms for how plants shape large herbivore mouth morphology. *Acta Zoologica (Stockholm)*, 254(April):1–9, 2015.

[13] Howard V Cornell, Bradford A Hawkins, Source The, American Naturalist, No April, Howard V Cornell, and Bradford A Hawkins. Herbivore Responses to Plant Secondary Compounds : A Test of Phytochemical Coevolution Theory. *The American Naturalist*, 161(4):507–522, 2014.

[14] William H. Karasov, Carlos Martínez del Rio, and Enrique Caviedes-Vidal. Ecological Physiology of Diet and Digestive Systems. *Annual Review of Physiology*, 73(1):69–93, 2011.

[15] Virginia Hayssen and Robert C. Lacy. Basal metabolic rates in mammals: Taxonomic differences in the allometry of BMR and body mass. *Comparative Biochemistry and Physiology – Part A: Physiology*, 81(4):741–754, 1985.

[16] Geoffry E. Gerstner AND Jonathan B. Gerstein. Chewing Rate Allometry Among Mammals. *Journal of Mammalogy*, 89(4):1020–1030, 2008.

[17] Marcus Clauss, Patrick Steuer, Kerstin Erlinghagen-Lückerath, Jacques Kaandorp, Julia Fritz, Karl Heinz Südekum, and Jürgen Hummel. Faecal particle size: Digestive physiology meets herbivore diversity. *Comparative Biochemistry and Physiology -Part A : Molecular and Integrative Physiology*, 179:182–191, 2015.

[18] Justin D. Yeakel, Christopher P. Kempes, and Sidney Redner. Dynamics of starvation and recovery predict extinction risk and both Damuth's law and Cope's rule. *Nature Communications*, 9(1):1–10, 2018.

[19] John F. Wilmshurst, John M. Fryxell, and Carita M. Bergman. The allometry of patch selection in ruminants. *Proceedings of the Royal Society B: Biological Sciences*, 267(1441):345–349, 2000.

[20] Michael B.J. Harfoot, Tim Newbold, Derek P. Tittensor, Stephen Emmott, Jon Hutton, Vassily Lyutsarev, Matthew J. Smith, Jörn P.W. Scharlemann, and Drew W. Purves. Emergent Global Patterns of Ecosystem Structure and Function from a Mechanistic General Ecosystem Model. *PLoS Biology*, 12(4), 2014.

[21] D L DeAngelis. Energy flow, nutrient cycling, and ecosystem resilience. *Ecology*, 61(4):764–771, 1980.

[22] P Yodzis and S Innes. Body Size and Consumer-Resource Dynamics. *Am. Nat.*, 139(6):1151–1175, 1992.

[23] Chen Hou, Wenyun Zuo, Melanie E Moses, William H Woodruff, James H Brown, and Geoffrey B West. Energy Uptake and Allocation During Ontogeny. *Science*, 322(5902):736–739, oct 2008.

[24] S L Lindstedt and P J Schaeffer. Use of allometry in predicting anatomical and physiological parameters of mammals. *Lab. Anim.*, 36(1):1–19, jan 2002.

[25] Geoffrey B West, James H Brown, and Brian J Enquist. A general model for ontogenetic growth. *Nature*, 413(6856):628–631, oct 2001.

[26] Willard W Hennemann. Relationship among body mass, metabolic rate and the intrinsic rate of natural increase in mammals. *Oecologia*, 56(1):104–108, 1983.

[27] Geoffrey B West, William H Woodruff, and James H Brown. Allometric scaling of metabolic rate from molecules and mitochondria to cells and mammals. *Proc. Natl. Acad. Sci. USA*, 99(Suppl 1):2473–2478, feb 2002.

[28] Christopher P Kempes, Stephanie Dutkiewicz, and Michael J Follows. Growth, metabolic partitioning, and the size of microorganisms. *PNAS*, 109(2):495–500, jan 2012.

[29] Uttam Bhat, Christopher P Kempes, and Justin D Yeakel. Scaling the risk landscape drives optimal life-history strategies and the evolution of grazing. *Proceedings of the National Academy of Sciences*, 117(3):1580–1586, 2020.

[30] John Alroy. A multispecies overkill simulation of the end-Pleistocene megafaunal mass extinction. *Science*, 292(5523):1893–1896, 2001.

[31] Barry W Brook, Navjot S Sodhi, and Corey J A Bradshaw. Synergies among extinction drivers under global change. *Trends in ecology & evolution*, 23(8):453–460, 2008.

[32] W W Murdoch, C J Briggs, and R M Nisbet. *Consumer-resource Dynamics*. Monographs in population biology. Princeton University Press, 2003.

[33] W A Calder III. An allometric approach to population cycles of mammals. *J. Theor. Biol.*, 100(2):275–282, jan 1983.

[34] Alexandre Robert, Stéphane Chantepie, Samuel Pavard, François Sarrazin, and Céline Teplitsky. Actuarial senescence can increase the risk of extinction of mammal populations. *Ecological Applications*, 25(1):116–124, 2015.

[35] Suzanne H Alonzo. State-dependent habitat selection games between predators and prey: the importance of behavioural interactions and expected lifetime reproductive success. *Evol. Ecol. Res.*, 4(5):759–778, 2002.

[36] Jennifer A Dunne, Herbert Maschner, Matthew W Betts, Nancy Huntly, Roly Russell, Richard J Williams, and Spencer A Wood. The roles and impacts of human hunter-gatherers in North Pacific marine food webs. *Sci. Rep.*, 6:1–9, jan 2016.

[37] John P DeLong and David A Vasseur. Size-density scaling in protists and the links between consumer{\textendash}resource interaction parameters. *J. Anim. Ecol.*, 81(6):1193–1201, nov 2012.

[38] Van M Savage, James F Gillooly, James H Brown, Geoffrey B West, and Eric L Charnov. Effects of Body Size and Temperature on Population Growth. *http://dx.doi.org.proxy.lib.sfu.ca/10.1086/679735*, 163(3):429–441, mar 2004.

[39] F Smith, A Boyer, J Brown, and D Costa. The Evolution of Maximum Body Size of Terrestrial Mammals. *Science*, jan 2010.

[40] Chris Carbone and John L Gittleman. A common rule for the scaling of carnivore density. *Science*, 295(5563):2273–2276, 2002.

[41] John P DeLong, Jordan G Okie, Melanie E Moses, Richard M Sibly, and James H Brown. Shifts in metabolic scaling, production, and efficiency across major evolutionary transitions of life. *PNAS*, 107(29):12941–12945, jul 2010.

[42] Owen R Jones, Jean-Michel Gaillard, Shripad Tuljapurkar, Jussi S Alho, Kenneth B Armitage, Peter H Becker, Pierre Bize, Jon Brommer, Anne Charmantier, Marie Charpentier, and Others. Senescence rates are determined by ranking on the fast–slow life-history continuum. *Ecology letters*, 11(7):664–673, 2008.

[43] J. S. Millar and G. J. Hickling. Fasting Endurance and the Evolution of Mammalian Body Size. *Functional Ecology*, 4(1):5, 1990.

[44] Justin D Yeakel, Uttam Bhat, and Seth D Newsome. Caching in or falling back at the Sevilleta: the effects of body size and seasonal uncertainty on desert rodent foraging. *The American Naturalist*, 196(2):241–256, 2020.

[45] Kristin A Schubert, Ate S Boerema, Lobke M Vaanholt, Sietse F de Boer, Arjen M Strijkstra, and Serge Daan. Daily torpor in mice: high foraging costs trigger energy-saving hypothermia. *Biology letters*, 6(1):132–135, 2010.

[46] Fritz Geiser. Evolution of daily torpor and hibernation in birds and mammals: importance of body size. *Clinical and experimental pharmacology and physiology*, 25(9):736–740, 1998.

[47] C C Smith and O J Reichman. The evolution of food caching by birds and mammals. *Annual Review of Ecology and Systematics*, 15(1):329–351, 1984.

[48] U Brose, L Cushing, E L Berlow, and T Jonsson. Body sizes of consumers and their resources. *Ecology*, 2005.

[49] Carolyn Barnes, David Maxwell, Daniel C Reuman, and Simon Jennings. Global patterns in predator–prey size relationships reveal size dependency of trophic transfer efficiency. *Ecology*, 91(1):222–232, 2010.

[50] Rudolf Philippe Rohr, Heike Scherer, Patrik Kehrli, Christian Mazza, and Louis-Félix Bersier. Modeling food webs: Exploring unexplained structure using latent traits. *Am. Nat.*, 176(2):170–177, aug 2010.

[51] Jens O Riede, Ulrich Brose, Bo Ebenman, Ute Jacob, Ross Thompson, Colin R Townsend, and Tomas Jonsson. Stepping in Elton's footprints: a general scaling model for body masses and trophic levels across ecosystems. *Ecology letters*, 14(2):169–178, 2011.

[52] Justin D Yeakel, M M Pires, L Rudolf, N J Dominy, P L Koch, Paulo R Guimarães Jr, and T Gross. Collapse of an ecological network in Ancient Egypt. *Proceedings of the National Academy of Sciences*, 111(40):14472–14477, sep 2014.

[53] Mathias M. Pires, Paul L. Koch, Richard A. Fariña, Marcus A.M. de Aguiar, Sérgio F. dos Reis, and Paulo R. Guimarães. Pleistocene megafaunal interaction networks became more vulnerable after human arrival. *Proceedings of the Royal Society B: Biological Sciences*, 282(1814):20151367, 2015.

[54] Takefumi Nakazawa. Individual interaction data are required in community ecology: a conceptual review of the predator–prey mass ratio and more. *Ecological Research*, 32(1):5–12, 2017.

[55] Graham I H Kerley. Prey preferences of the lion (Panthera leo). *J. Zoology*, 267(03):309, oct 2005.

[56] M W Hayward. Prey preferences of the spotted hyaena (Crocuta crocuta) and degree of dietary overlap with the lion (Panthera leo). *J. Zoology*, 270(4):606–614, dec 2006.

[57] L\'\ivia R Cruz, Renata L Muylaert, Mauro Galetti, and Mathias M Pires. The geography of diet variation in Neotropical Carnivora. *Mammal Review*, 52(1):112–128, 2022.

[58] Lívia R Cruz and Mathias M Pires. Body mass ratios determine dietary patterns and help predicting predator–prey interactions of Neotropical Carnivora. *Mammal Research*, mar 2022.

[59] Thilo Gross, Lars Rudolf, Simon A Levin, and Ulf Dieckmann. Generalized models reveal stabilizing factors in food webs. *Science*, 325(5941):747–750, 2009.

[60] Charles E Kay. False gods, ecological myths, and biological reality. *Wilderness and political ecology: aboriginal influences and the original state of nature. University of Utah Press, Salt Lake City*, pages 238–261, 2002.

[61] William J Ripple and Blaire Van Valkenburgh. Linking top-down forces to the Pleistocene megafaunal extinctions. *BioScience*, 60(7):516–526, 2010.

[62] Gary P Burness, Jared Diamond, and Timothy Flannery. Dinosaurs, dragons, and dwarfs: the evolution of maximal body size. *Proceedings of the National Academy of Sciences*, 98(25):14518–14523, 2001.

[63] Boris Sorkin. A biomechanical constraint on body mass in terrestrial mammalian predators. *Lethaia*, 41(4):333–347, 2008.

[64] Chris Carbone, Amber Teacher, and J Marcus Rowcliffe. The Costs of Carnivory. *PLoS Biol*, 5(2):e22, jan 2007.

[65] James O Farlow. On the rareness of big, fierce animals; speculations about the body sizes, population densities, and geographic ranges of predatory mammals and large carnivorous dinosaurs. *American Journal of Science*, 293(A):167, 1993.

[66] B van Valkenburgh, X Wang, and J Damuth. Cope's rule, hypercarnivory, and extinction in North American canids. *Science*, 306(5693):101, 2004.

[67] Barry W Brook and David M J S Bowman. One equation fits overkill: why allometry underpins both prehistoric and modern body size-biased extinctions. *Population Ecology*, 47(2):137–141, aug 2005.

[68] Steven E Churchill. Weapon technology, prey size selection, and hunting methods in modern hunter-gatherers: implications for hunting in the Palaeolithic and Mesolithic. *Archeological Papers of the American Anthropological Association*, 4(1):11–24, 1993.

[69] Andrew Ugan. Does size matter? Body size, mass collecting, and their implications for understanding prehistoric foraging behavior. *American Antiquity*, 70(1):75–89, 2005.

[70] Luciano Prates, Diego Rivero, and S Ivan Perez. Changes in Projectile design and size of prey reveals the role of Fishtail points in megafauna hunting in South America. 2022.

[71] Felisa A Smith, Rosemary E Elliott Smith, S Kathleen Lyons, and Jonathan L Payne. Body size downgrading of mammals over the late Quaternary. *Science*, 360(6386):310–313, apr 2018.

[72] David R Horton and Richard V S Wright. Cuts on Lancefield bones: carnivorous Thylacoleo, not humans, the cause. *Archaeology in Oceania*, 16(2):73–80, 1981.

[73] S Wroe, T J Myers, R T Wells, and A Gillespie. Estimating the weight of the Pleistocene marsupial lion, Thylacoleo carnifex (Thylacoleonidae: Marsupialia): implications for the ecomorphology of a marsupial super-predator and hypotheses of impoverishment of Australian marsupial carnivore faunas. *Australian Journal of Zoology*, 47(5):489–498, 1999.

[74] Steve Webb. Late Quaternary distribution and biogeography of the southern Lake Eyre basin (SLEB) megafauna, South Australia. *Boreas*, 38(1):25–38, 2009.

[75] Marcel Cardillo, Georgina M Mace, Kate E Jones, Jon Bielby, Olaf R P Bininda-Emonds, Wes Sechrest, C David L Orme, and Andy Purvis. Multiple causes of high extinction risk in large mammal species. *Science*, 309(5738):1239–1241, jan 2005.

[76] Chrisopher N Johnson. Determinants of loss of mammal species during the Late Quaternary 'megafauna' extinctions: life history and ecology, but not body size. *Proceedings of the Royal Society of London. Series B: Biological Sciences*, 269(1506):2221–2227, 2002.

[77] J A Estes, J Terborgh, J S Brashares, M E Power, J Berger, W J Bond, S R Carpenter, T E Essington, R D Holt, J B C Jackson, R J Marquis, L Oksanen, T Oksanen, R T Paine, E K Pikitch, W J Ripple, S A Sandin, M Scheffer, T W Schoener, J B Shurin, A R E Sinclair, M E Soulé, R Virtanen, and D A Wardle. Trophic downgrading of planet Earth. *Science*, 333(6040):301–306, jul 2011.

[78] J. Roughgarden. Competition and theory in community ecology. *American Naturalist*, 122(5):583–601, 1983.

[79] Nicolas Loeuille and Michel Loreau. Evolutionary emergence of size-structured food webs. *Proceedings of the National Academy of Sciences of the United States of America*, 102(16):5761–5766, apr 2005.

[80] T M Caro and C J Stoner. The potential for interspecific competition among African carnivores. *Biol. Conserv.*, 110:67–75, nov 2003.

[81] Inon Scharf, Ido Filin, and Ofer Ovadia. An experimental design and a statistical analysis separating interference from exploitation competition. *Population Ecology*, 50(3):319–324, 2008.

[82] A. W. Illius and I. J. Gordon. The Allometry of Food Intake in Grazing Ruminants. *The Journal of Animal Ecology*, 56(3):989, 1987.

[83] David Tilman. The Resource-Ratio Hypothesis of Plant Succession. *The American Naturalist*, 125(6):827–852, 1985.

[84] Martyn G Murray and David R Baird. Resource-ratio theory applied to large herbivores. *Ecology*, 89(5):1445–1456, 2008.

[85] Peter F Sale. Overlap in resource use, and interspecific competition. *Oecologia*, 17(3):245–256, 1974.

[86] Thomas S Jung, Shannon A Stotyn, and Sophie M Czetwertynski. Dietary overlap and potential competition in a dynamic ungulate community in northwestern Canada. *The Journal of Wildlife Management*, 79(8):1277–1285, 2015.

[87] Robert MacArthur and Richard Levins. Divergence of Coexisting Species. *The American Naturalist*, 101(921):377–385, 1967.

[88] Michio Kondoh. Foraging Adaptation and the Relationship Between Food-Web Complexity and Stability. *Science*, 299(February):1388–1391, 2003.

[89] Fernanda S. Valdovinos, Berry J. Brosi, Heather M. Briggs, Pablo Moisset de Espanés, Rodrigo Ramos-Jiliberto, and Neo D. Martinez. Niche partitioning due to adaptive foraging reverses effects of nestedness and connectance on pollination network stability. *Ecology letters*, 19(10):1277–1286, 2016.

[90] J H Brown, J F Gillooly, A P Allen, V M Savage, and G B West. Toward a metabolic theory of ecology. *Ecology*, 85(7):1771–1789, 2004.

[91] P.J. J Jarman. The Social Organisation of Antelope in Relation To Their Ecology. *Behavior*, 48(1-4):215–267, 1974.

[92] Dennis W H Müller, Daryl Codron, Carlo Meloro, Adam Munn, Angela Schwarm, Jürgen Hummel, and Marcus Clauss. Assessing the Jarman–Bell principle: scaling of intake, digestibility, retention time and gut fill with body mass in mammalian herbivores. *Comparative Biochemistry and Physiology Part A: Molecular & Integrative Physiology*, 164(1):129–140, 2013.

[93] Nikolaas J van der Merwe, Julia A Lee Thorp, and Richard H V Bell. Carbon isotopes as indicators of elephant diets and African environments. *African Journal of Ecology*, 26(2):163–172, 1988.

[94] Jacqui Codron, Julia A Lee-Thorp, Matt Sponheimer, Daryl Codron, Rina C Grant, and Darryl J de Ruiter. Elephant (Loxodonta africana) diets in Kruger National Park, South Africa: spatial and landscape differences. *Journal of mammalogy*, 87(1):27–34, 2006.

[95] K T Uno, T E Cerling, and et Al. Late Miocene to Pliocene carbon isotope record of differential diet change among East African herbivores. *Proc. Natl. Acad. Sci. USA*, 2011.

[96] E. H. Colbert. Feeding strategies and metabolism in elephants and sauropod dinosaurs. *American Journal of Science*, 293 A:1–19, 1993.

[97] J. M. Hatt and M. Clauss. Feeding Asian and African elephants Elephas maximus and Loxodonta africana in captivity. *International Zoo Yearbook*, 40(1):88–95, 2006.

[98] Ulrich Brose, Richard J. Williams, and Neo D. Martinez. Allometric scaling enhances stability in complex food webs. *Ecology Letters*, 9(11):1228–1236, nov 2006.

[99] Fernanda S Valdovinos, Rodrigo Ramos-Jiliberto, Leslie Garay-Narváez, Pasquinell Urbani, and Jennifer A Dunne. Consequences of adaptive behaviour for the structure and dynamics of food webs. *Ecology letters*, 13(12):1546–1559, 2010.

[100] Stan L Lindstedt and Mark S Boyce. Seasonality, Fasting Endurance, and Body Size in Mammals. *Am. Nat.*, 125(6):873–878, jun 1985.

[101] Robert L Dunbrack and Malcolm A Ramsay. The Allometry of Mammalian Adaptations to Seasonal Environments: A Critique of the Fasting Endurance Hypothesis. *Oikos*, 66(2):336–342, mar 1993.

[102] Fernanda S Valdovinos, Pablo de Espanés, José D Flores, and Rodrigo Ramos-Jiliberto. Adaptive foraging allows the maintenance of biodiversity of pollination networks. *Oikos*, 122(6):907–917, 2013.

[103] Taran Rallings, Christopher P Kempes, and Justin D Yeakel. No Title. *Thesis Chapter 1*, pages p1—-p2, 2022.

[104] Sean T. Michaletz, Dongliang Cheng, Andrew J. Kerkhoff, and Brian J. Enquist. Convergence of terrestrial plant production across global climate gradients. *Nature*, 512(1):39–43, 2014.

[105] J. M.O. O Scurlock, K. Johnson, and R. J. Olson. Estimating net primary productivity from grassland biomass dynamics measurements. *Global Change Biology*, 8(8):736–753, 2002.

[106] Mercedes Pascual and Jennifer A. Dunne. *Ecological Networks: Linking Structure to Dynamics in Food Webs*. 2005.

[107] Marcus Clauss, Angela Schwarm, Sylvia Ortmann, W Jürgen Streich, and Jürgen Hummel. A case of non-scaling in mammalian physiology? Body size, digestive capacity, food intake, and ingesta passage in mammalian herbivores. *Comparative Biochemistry and Physiology - A Molecular and Integrative Physiology*, 148(2):249–265, 2007.

[108] P L Koch and A D Barnosky. Late Quaternary extinctions: state of the debate. *Annu. Rev. Ecol. Evol. Syst.*, 37:215–250, 2006.

[109] Williams Richard J, , Neo D Martinez, Richard J Williams, Neo D Martinez, Williams Richard J, , Neo D Martinez, Richard J Williams, Neo D Martinez, Williams Richard J, , and Neo D Martinez. Simple rules yield complex food webs. *Nature*, 404:180–183, 2000.

[110] Christopher P Warren, Mercedes Pascual, Kevin D Lafferty, and Armand M Kuris. The inverse niche model for food webs with parasites. *Theoretical ecology*, 3(4):285–294, 2010.

[111] Gareth P Hempson, Sally Archibald, and William J Bond. A continent-wide assessment of the form and intensity of large mammal herbivory in Africa. *Science*, 350(6264):1056–1061, 2015.

[112] Peter Chesson. Mechanisms of Maintenance of Species Diversity. *Annual Review of Ecology and Systematics*, 31:343–366, 2000.

[113] K. D. Farnsworth, S. Focardi, and J. A. Beecham. Grassland-herbivore interactions: How do grazers coexist? *American Naturalist*, 159(1):24–39, 2002.

[114] Emilio A Laca, Susanne Sokolow, Julio R Galli, and Carlos A Cangiano. Allometry and spatial scales of foraging in mammalian herbivores. *Ecology letters*, 13(3):311–320, 2010.

[115] E Mori, S Bagnato, P Serroni, A Sangiuliano, F Rotondaro, V Marchianò, V Cascini, L Poerio, and F Ferretti. Spatiotemporal mechanisms of coexistence in an European mammal community in a protected area of southern Italy. *Journal of Zoology*, 310(3):232–245, 2020.

[116] Simon A. Levin. Population Dynamic Models in Heterogeneous Environments. *Annual Review of Ecology and Systematics*, 7(1):287–310, 1976.

[117] Jean P Gibert and Justin D Yeakel. Laplacian matrices and Turing bifurcations: revisiting Levin 1974 and the consequences of spatial structure and movement for ecological dynamics. *Theor. Ecol.*, 169(2):1–17, jan 2019.

[118] Michio Kondoh. Does foraging adaptation create the positive complexity-stability relationship in realistic food-web structure? *Journal of Theoretical Biology*, 238(3):646–651, 2006.

[119] Lotta Heckmann, Barbara Drossel, Ulrich Brose, and Christian Guill. Interactive effects of body-size structure and adaptive foraging on food-web stability. *Ecology Letters*, 15(3):243–250, 2012.

[120] Garrett Hardin. The Competitive Exclusion Principle: An idea that took a century to be born has implications in ecology, economics and genetics. *American Association for the Advencement of Science*, 131(3409):1292–1297, 1960.

[121] Pieter J. den Boer. The present status of the competitive exclusion principle. *Trends in Ecology and Evolution*, 1(1):25–28, 1986.

[122] Jean P. Gibert and Justin D. Yeakel. Eco-evolutionary origins of diverse abundance, biomass, and trophic structures in food webs. *Frontiers in Ecology and Evolution*, 7(FEB), 2019.

[123] Randal Arsenault and Norman Owen-Smith. Resource partitioning by grass height among grazing ungulates does not follow body size relation. *Oikos*, 117(11):1711–1717, 2008.

[124] Walter Leuthold. Ecological separation among browsing ungulates in Tsavo east National Park, Kenya. *Oecologia*, 35(2):241–252, 1978.

[125] Martine Kos, Arno J Hoetmer, Yolanda Pretorius, Willem Frederik de Boer, Henjo de Knegt, C C Grant, Edward Kohi, Bruce Page, Mike Peel, Rob Slotow, and Others. Seasonal diet changes in elephant and impala in mopane woodland. *European Journal of Wildlife Research*, 58(1):279–287, 2012.

[126] Norman Owen-Smith and Jonas Chafota. Selective feeding by a megaherbivore, the African elephant (Loxodonta africana). *Journal of mammalogy*, 93(3):698–705, 2012.

[127] J Tyler Faith, John Rowan, Andrew Du, and Paul L Koch. Plio-Pleistocene decline of African megaherbivores: No evidence for ancient hominin impacts. *Science*, 362(6417):938–941, 2018.

[128] J Tyler Faith, John Rowan, and Andrew Du. Early hominins evolved within non-analog ecosystems. *Proceedings of the National Academy of Sciences*, 2019.

[129] Caroline A E Strömberg. Evolution of Grasses and Grassland Ecosystems. *Annu. Rev. Earth. Pl. Sc.*, 39(1):517–544, may 2011.

[130] Thure E Cerling, Samuel A Andanje, Scott A Blumenthal, Francis H Brown, Kendra L Chritz, John M Harris, John A Hart, Francis M Kirera, Prince Kaleme, Louise N Leakey, Meave G Leakey, Naomi E Levin, Fredrick Kyalo Manthi, Benjamin H Passey, and Kevin T Uno. Dietary changes of large herbivores in the Turkana Basin, Kenya from 4 to 1 Ma. *PNAS*, 112(37):11467–11472, sep 2015.

[131] E. R. Pianka. Niche overlap and diffuse competition. *Proceedings of the National Academy of Sciences of the United States of America*, 71(5):2141–2145, 1974.

[132] Aaron Thierry, Andrew P Beckerman, Philip H Warren, Richard J Williams, Andrew J Cole, and Owen L Petchey. Adaptive foraging and the rewiring of size-structured food webs following extinctions. *Basic and Applied Ecology*, 12(7):562–570, 2011.

[133] Stefano Allesina and Si Tang. Stability criteria for complex ecosystems. *Nature*, 483(7388):205–208, 2012.

[134] Marjorie G Weber, Catherine E Wagner, Rebecca J Best, Luke J Harmon, and Blake Matthews. Evolution in a community context: on integrating ecological interactions and macroevolution. *Trends in ecology & evolution*, 32(4):291–304, 2017.

[135] Taran Rallings, Christopher P Kempes, and Justin D Yeakel. No Title. *Thesis Chapter 2*, pages p2—-p3, 2022.

[136] J Bret Bennington, William A Dimichele, Catherine Badgley, Richard K Bambach, Paul M Barrett, Anna K Behrensmeyer, René Bobe, Robyn J Burnham, Edward B Daeschler, Jan Van Dam, and Others. Critical issues of scale in paleoecology. *Palaios*, 24(1):1–4, 2009.

[137] J Alroy. Cope's rule and the dynamics of body mass evolution in North American fossil mammals. *Science*, 280(5364):731, 1998.

[138] Ross Secord, Jonathan I Bloch, Stephen G B Chester, Doug M Boyer, Aaron R Wood, Scott L Wing, Mary J Kraus, Francesca A McInerney, and John Krigbaum.

Evolution of the earliest horses driven by climate change in the Paleocene-Eocene Thermal Maximum. *Science*, 335(6071):959–962, feb 2012.

[139] Felisa A Smith and S Kathleen Lyons. How big should a mammal be? A macroecological look at mammalian body size over space and time. *Philos. T. Roy. Soc. B*, 366(1576):2364–2378, aug 2011.

[140] Thomas Westerhold, Norbert Marwan, Anna Joy Drury, Diederik Liebrand, Claudia Agnini, Eleni Anagnostou, James S K Barnet, Steven M Bohaty, David De Vleeschouwer, Fabio Florindo, Thomas Frederichs, David A Hodell, Ann E Holbourn, Dick Kroon, Vittoria Lauretano, Kate Littler, Lucas J Lourens, Mitchell Lyle, Heiko Pälike, Ursula Röhl, Jun Tian, Roy H Wilkens, Paul A Wilson, and James C Zachos. An astronomically dated record of Earth’s climate and its predictability over the last 66 million years. *Science*, 369(6509):1383–1387, 2020.

[141] John Damuth. Cope's rule, the island rule and the scaling of mammalian population density. *Nature*, 365(6448):748–750, oct 1993.

[142] Noel A Heim, Matthew L Knope, Ellen K Schaal, Steve C Wang, and Jonathan L Payne. Cope's rule in the evolution of marine animals. *Science*, 347(6224):867–870, 2015.

[143] Emily M Troyer, Ricardo Betancur-R, Lily C Hughes, Mark Westneat, Giorgio Carnevale, William T White, John J Pogonoski, James C Tyler, Carole C Baldwin, Guillermo Ort\'\i, and Others. The impact of paleoclimatic changes on body size evolution in marine fishes. *Proceedings of the National Academy of Sciences*, 119(29):e2122486119, 2022.

[144] Samraat Pawar, Anthony I Dell, and Van M Savage. Dimensionality of consumer search space drives trophic interaction strengths. *Nature*, may 2012.

[145] C R Allen, A S Garmestani, T D Havlicek, P A Marquet, G D Peterson, C Restrepo, C A Stow, and B E Weeks. Patterns in body mass distributions: Sifting among alternative hypotheses. *Ecol. Lett.*, 9(5):630–643, may 2006.

[146] Evan Siemann and James H Brown. Gaps in mammalian body size distributions reexamined. *Ecology*, 80(8):2788–2792, 1999.

[147] G E Hutchinson. Homage to Santa Rosalia or Why Are There So Many Kinds of Animals? *the American Naturalist*, 93(870):145–159, 1959.

[148] C S Holling. Cross-scale morphology, geometry, and dynamics of ecosystems. *Ecological Monographs*, 62(4):447–502, 1992.

[149] T Deng. Late Cenozoic environmental changes in the Linxia Basin (Gansu, China) as indicated by cenograms of fossil mammals. *Vertebrata PalAsiatica*, 47:282–298, 2009.

[150] T Deng. Linxia Basin: An Ancient Paradise for Late Cenozoic Rhinoceroses in North China. *Paleomammology*, 24(2):103–106, 2010.

[151] Jinbo Zan, Xiaomin Fang, Weilin Zhang, Maodu Yan, and Tao Zhang. Palaeoenvironmental and chronological constraints on the Early Pleistocene mammal fauna from loess deposits in the Linxia Basin , NE Tibetan Plateau. *Quaternary Science Reviews*, 148:234–242, 2016.

[152] Peter J Rose, David L Fox, Jonathan Marcot, and Catherine Badgley. Flat latitudinal gradient in Paleocene mammal richness suggests decoupling of climate and biodiversity. *Geology*, 39(2):163–166, 2011.

[153] Maureen A O'Leary, Jonathan I Bloch, John J Flynn, Timothy J Gaudin, Andres Giallombardo, Norberto P Giannini, Suzann L Goldberg, Brian P Kraatz, Zhe-Xi Luo, Jin Meng, Xijun Ni, Michael J Novacek, Fernando A Perini, Zachary S Randall, Guillermo W Rougier, Eric J Sargis, Mary T Silcox, Nancy B Simmons, Michelle Spaulding, Paúl M Velazco, Marcelo Weksler, John R Wible, and Andrea L Cirranello. The Placental Mammal Ancestor and the Post–K-Pg Radiation of Placentals. *Science*, 339(6120):662–667, 2013.

[154] A Clauset and S Redner. Evolutionary Model of Species Body Mass Diversification. *Phys. Rev. Lett.*, 102(3):38103, jan 2009.

[155] Douglas A Kelt. Body size frequency distributions in African mammals are bimodal at all spatial scales. *Global Ecol. Biogeogr.*, 18(1):19–29, jan 2009.

[156] Montague W Demment and Peter J Van Soest. A Nutritional Explanation for Body-Size Patterns of Ruminant and Nonruminant Herbivores. *The American naturalist*, 125(5):641–672, 1985.

[157] Sewall Wright and Others. Adaptation and selection. *Genetics, paleontology and evolution*, pages 365–389, 1949.

[158] Russell Lande. Natural selection and random genetic drift in phenotypic evolution. *Evolution*, 30(2):314–334, jun 1976.

[159] Serge Legendre. ANALYSIS OF MAMMALIAN COMMUNITIES FROM THE LATE EOCENE by Methods . *Palaeovertebrata*, 16(4):191–212, 1986.

[160] Yangyang Liu, Yue Yang, Qian Wang, Xiaolong Du, Jianlong Li, Chengcheng Gang, Wei Zhou, and Zhaoqi Wang. Evaluating the responses of net primary productivity and carbon use efficiency of global grassland to climate variability along an aridity gradient. *Science of the Total Environment*, 652:671–682, 2019.

[161] Christopher J Sandom, Rasmus Ejrnæs, Morten D D Hansen, and Jens-Christian Svenning. High herbivore density associated with vegetation diversity in interglacial ecosystems. *Proceedings of the National Academy of Sciences*, 111(11):4162–4167, 2014.

[162] Tobias Andermann, Caroline A E Strömberg, Alexandre Antonelli, and Daniele Silvestro. The origin and evolution of open habitats in North America inferred by Bayesian deep learning models. *Nature Communications*, 13(1):4833, aug 2022.

[163] Hanchao Jiang and Zhongli Ding. Spatial and temporal characteristics of Neogene palynoflora in China and its implication for the spread of steppe vegetation. *Journal of Arid Environments*, 73(9):765–772, 2009.

[164] M Gagnon and A E Chew. Dietary preferences in extant African Bovidae. *Journal of Mammalogy*, 81(2):490–511, 2000.

[165] Nathan R De Jager, Patrick J Drohan, Brian M Miranda, Brian R Sturtevant, Susan L Stout, Alejandro A Royo, Eric J Gustafson, and Mark C Romanski. Simulating ungulate herbivory across forest landscapes: A browsing extension for LANDIS-II. *Ecological Modelling*, 350:11–29, 2017.

[166] Rasmus Østergaard Pedersen, Søren Faurby, and Jens-Christian Svenning. Shallow size{\textendash}density relations within mammal clades suggest greater intra-guild ecological impact of large-bodied species. *J. Anim. Ecol.*, 86(5):1205–1213, sep 2017.

[167] Rodolfo Dirzo, Hillary S. Young, Mauro Galetti, Gerardo Ceballos, Nick J.B. Isaac, and Ben Collen. Defaunation in the Anthropocene. *Science*, 345(6195):401–406, 2014.

[168] Agustí Mu/˜noz-Garcia and Joseph B Williams. Basal Metabolic Rate in Carnivores Is Associated with Diet after Controlling for Phylogeny. *Physiological and Biochemical Zoology*, 78(6):1039–1056, 2005.

[169] Jordan G. Okie, Alison G. Boyer, James H. Brown, Daniel P. Costa, S. K. Morgan Ernest, Alistair R. Evans, Mikael Fortelius, John L. Gittleman, Marcus J. Hamilton, Larisa E. Harding, Kari Lintulaakso, S. Kathleen Lyons, Juha J. Saarinen, Felisa A. Smith, Patrick R. Stephens, Jessica Theodor, Mark D. Uhen, and Richard M. Sibly. Effects of allometry, productivity and lifestyle on rates and limits of body size evolution. *Proceedings of the Royal Society B: Biological Sciences*, 280(1764), 2013.

[170] Christopher Thouless, Holly T Dublin, Julian Blanc, D P Skinner, T E Daniel, Russell Taylor, Fiona Maisels, Howard Frederick, and Philipe Bouché. African elephant status report 2016. *An update from the African Elephant Database*, 2016.

[171] Beda L Estermann, Hans-Rudolf Wettstein, Franz Sutter, and Michael Kreuzer. Nutrient and energy conversion of grass-fed dairy and suckler beef cattle kept indoors and on high altitude pasture. *Anim. Res.*, 50(6):477–493, nov 2001.

[172] Melanie E Moses, Chen Hou, William H Woodruff, Geoffrey B West, Jeffery C Nekola, Wenyun Zuo, and James H Brown. Revisiting a Model of Ontogenetic Growth: Estimating Model Parameters from Theory and Data. *American Naturalist*, 171(5):632–645, may 2008.

[173] Daryl Codron, Julia A. Lee-Thorp, Matt Sponheimer, and Jacqui Codron. Nutritional content of savanna plant foods: Implications for browser/grazer models of ungulate diversification. *European Journal of Wildlife Research*, 53(2):100–111, 2007.